SYNTHESIS OF SILVER NANOPARTICLE VIA SOLVENT EXTRACTION ROUTE

A DISSERTATION

Submitted in partial fulfillment of the requirements for the award of the degree of

MASTER OF TECHNOLOGY

in

ADVANCED CHEMICAL ANALYSIS

By

ARVIND OLANIA

DEPARTMENT OF CHEMISTRY
INDIAN INSTITUTE OF TECHNOLOGY ROORKEE
ROORKEE-247 667 (INDIA)

NOVEMBER, 2010

CANDIDATE'S DECLARATION

I hereby declare that the work which is being presented in this thesis entitled **"Preparation of Silver Nanoparticles via Solvent Extraction Route "**, in partial fulfillment of the requirement for award of the degree of **Master of Technology in Advance Chemical Analysis**, submitted in Chemistry Department, Indian Institute of Technology, Roorkee, is an authentic record of my own work, carried out during the period from July 2009 to Oct. 2010 under the guidance and supervision of **Dr. Bina Gupta,** Associate Professor, Department of Chemistry, Indian Institute of Technology Roorkee, Roorkee.

I have not submitted the matter embodied in the dissertation for the award of any other degree or diploma.

Place : Roorkee
Date : 18/11/10

(Arvind Olania)

This is to certify that the above statement made by the candidate is correct to the best of my knowledge

Date 18th NOV. 2010

(Dr. Bina Gupta)

Associate Professor

Department of Chemistry

Indian Institute of Technology Roorkee

Roorkee-247667

ACKNOWLEDGEMENTS

I would like to express my gratitude to ***Dr. Bina Gupta*** *for her valuable guidance. I sincerely thank her for teaching me the skills of presenting and writing the technical matters. She has not just guided me in the scientific problems, but has always taken extra efforts to shape my approach towards research. She has always been a good critic to bring this thesis in its present form. I learnt a great deal from interacting with her.*

I am grateful to ***Prof. Kamaluddin****; head Department of chemistry, Indian Institute of Technology Roorkee, India, for providing the infrastructure and facilities for my research work.*

I am very much grateful to ***Dr. R. K. Dutta****, Co-ordinator of M.Tech in Department of chemistry, for providing me access to the facilities in the department. I am also very thankful to other professors in the department namely, Prof. R.N. Goyal, Dr. P.jeevanandam, Dr. Kausik Ghosh, for their timely help, fruitful discussions and support.*

I am also thankful my colleagues! Without their support, cooperation, discussions and timely help, my dissertation work could not have matured enough. So I extend my gratitude to my earlier and present lab-mates ***Mr.Rahul Dhaka, Mr. Bhawani, Ms. Manviri Rani, Ms. Indu Singh, Mr. Saubrah sahu and Mr. Ram Swaroop*** *. I also express my sincere thanks to my departmental colleagues* ***Abhishek pathak, Asheesh Kumar, Vijay khandelwal, Hement kumar, Harendra, Bhaskara Rao, shweta****, and all others for maintaining a warm and friendly atmosphere.*

Above all, I want to express my heartiest gratitude to all my family members for their love, faith and support for me, which has always been a constant source of inspiration

(Arvind Olania)

Abstract

Stable organic fluid containing silver nanoparticles have been prepared by the extraction – reduction method. Silver nitrate was extracted in n-Hexane or Toluene using different extractants namely Cyanex 923, Cyanex 471X and Aliquat 336. The Ag- extractant complex was reduced with sodium borohydride to get organic fluid containing silver nanoparticles. The obtained silver nanoparticles were stable and silver nanoparticles did not precipitate at room temperature. The molarity of $AgNO_3$, HNO_3 and extractants was varied to investigate the effect of variation on particle size, but no significant effect was observed.

The silver nanoparticles were separated from the organic fluid and characterized by FTIR, XRD, FESEM, AFM & TEM. Results indicate that silver nanoparticles are in the range of 20 to 70 nm and are well modified by the extractants.

TABLE OF CONTENTS

Table of contents

Table of contents

CHAPTER 1

Introduction

&

Literature Review

Introduction

1. General Introduction

In nanotechnology, a particle is defined as a small object that behaves as a whole unit in terms of its transport and properties. It is further classified according to size: in terms of diameter, fine particles cover a range between 100 and 2500 nanometers, while ultrafine particles, on the other hand, are sized between 1 and 100 nanometers. Similar to ultrafine particles, nanoparticles are sized between 1 and 100 nanometers. Nanoparticles may or may not exhibit size-related properties that differ significantly from those observed in fine particles or bulk materials [1,2]. Although the size of most molecules would fit into the above outline, individual molecules are usually not referred to as nanoparticles.

Nanoclusters have at least one dimension between 1 and 10 nanometers and a narrow size distribution. Nanopowders [3] are agglomerates of ultrafine particles, nanoparticles, or nanoclusters. Nanometer-sized single crystals, or single-domain ultrafine particles, are often referred to as nanocrystals. Nanoparticle research is currently an area of intense scientific interest due to a wide variety of potential applications in biomedical, optical and electronic fields.

Nanoparticles are of great scientific interest as they are effectively a bridge between bulk materials and atomic or molecular structures. A bulk material should have constant physical properties regardless of its size, but at the nanoscale size-dependent properties are often observed. Thus, the properties of materials change as their size approaches the nanoscale and as the percentage of atoms at the surface of a material becomes significant. For bulk materials larger than one micrometer (or micron), the percentage of atoms at the surface is insignificant in relation to the number of atoms in the bulk of the material. The interesting and sometimes unexpected properties of nanoparticles are therefore largely due to the large surface area of the material, which dominates the contributions made by the small bulk of the material [4].

An excellent example of this is the absorption of solar radiation in photovoltaic cells, which is much higher in materials composed of nanoparticles than it is in thin films of continuous sheets of material.

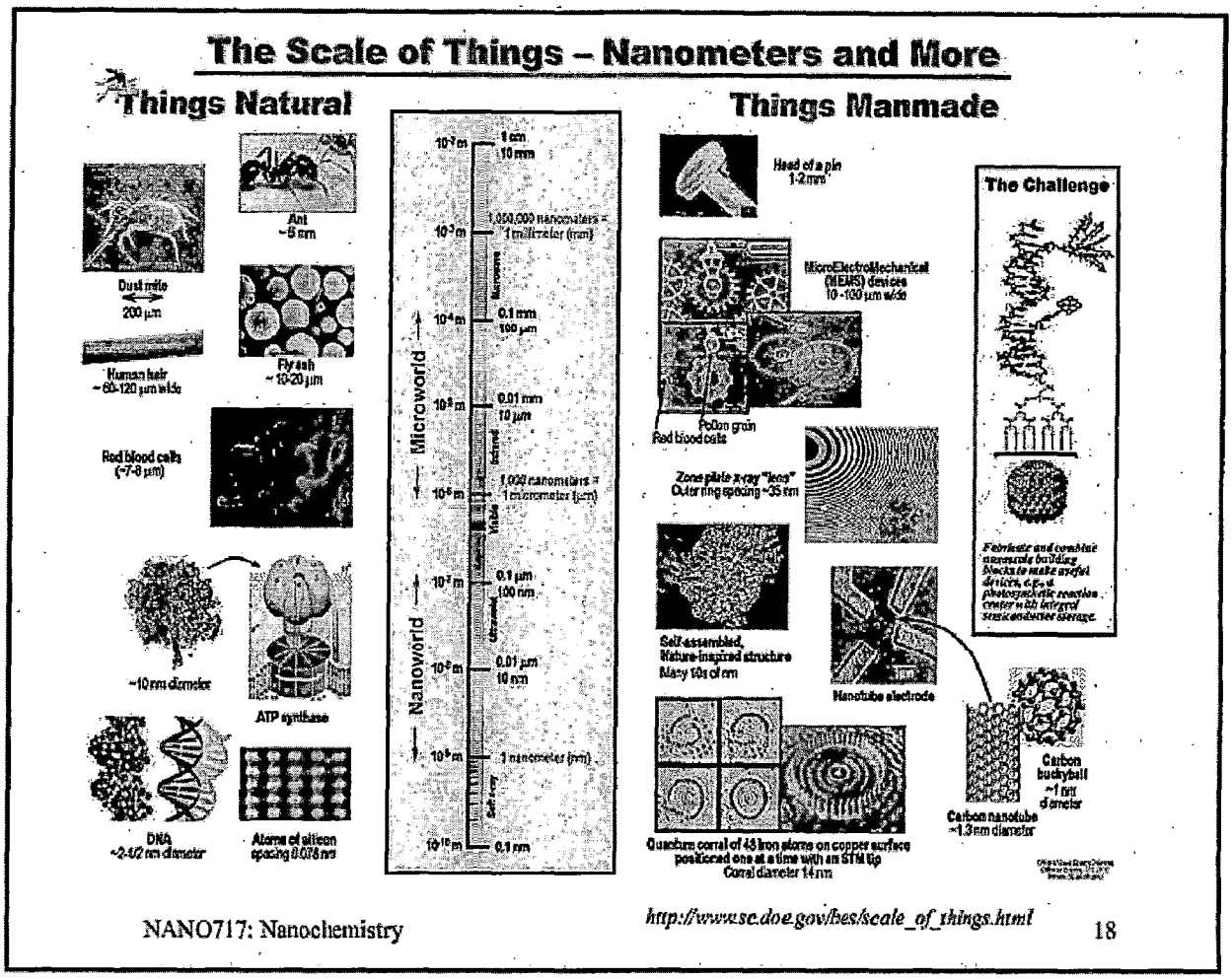

Figure 1. Various things of Nanometer scale and more

Other size-dependent changes include quantum confinement in semiconductor particles, Surface Plasmon Resonance in some metal particles and super paramagnetism in magnetic materials. Ironically, the changes in physical properties are not always desirable. Ferroelectric materials smaller than 10 nm can switch their magnetization direction using room temperature thermal energy, thus making them unsuitable for memory storage [5].

Suspensions of nanoparticles are possible since the interaction of the particle surface with the solvent is strong enough to overcome density differences, which otherwise usually result in a material either sinking or floating in a liquid. Nanoparticles also often possess unexpected optical

properties as they are small enough to confine their electrons and produce quantum effects. For example gold nanoparticles appear deep red to black in solution.

Nanoparticles have a very high surface area to volume ratio, which provides a tremendous driving force for diffusion, especially at elevated temperatures. Sintering can take place at lower temperatures, over shorter time scales than for larger particles. This theoretically does not affect the density of the final product, though flow difficulties and the tendency of nanoparticles to agglomerate complicates matters. The large surface area to volume ratio also reduces the incipient melting temperature of nanoparticles.

Moreover nanoparticles have been found to impart some extra properties to various day to day products. For example the presence of titanium dioxide nanoparticles imparts what we call the self-cleaning effect, and the size being nano range, the particles cannot be observed. Zinc oxide particles have been found to have superior UV blocking properties compared to its bulk substitute. This is one of the reasons why it is often used in the preparation of sunscreen lotions [6].

Nanoparticles can be classified in various ways, but we should first remember that some will have only one nanometric dimension (e.g., graphene sheets), two dimensions (e.g., nanofibers) or three dimensions (e.g., cubes, spheres...), while some processes are capable of directly applying surface coatings with only one nanometric dimension (thickness). Another way to classify nanoparticles is to divide them into two categories: particles that only exist in nanometric dimensions and particles that also exist in larger scales but are produced as nanoparticles to take advantage of their unique properties on this scale.

Carbon nanotubes, fullerenes, quantum dots and dendrimers are the main particles that exist only in nanometric dimensions. On the other hand, many inorganic products [metals (cobalt, copper, gold and iron), metal oxides (titanium dioxide, zinc oxides)], ceramics and organic products (polyvinyl chloride, latex) can be synthesized in these sizes. In fact, nearly every solid product can be reduced to nanometric dimensions, but not all would necessarily exhibit commercially interesting properties [7].

Chapter 1

1.1. Carbon Nanotubes

Carbon nanotubes (CNT) represent a new crystalline form of pure carbon, which only exists in these sizes. CNT are composed of cylinders of graphite sheets wound around themselves in one or more layers. Their synthesis normally requires the use of a metal catalyst, which will contaminate the end product. The diameter can be as small as 0.7 nm and the tubes can be as long as several millimeters. Since they are very stable chemically and thermally, CNT are good heat conductors, showing a strong molecular absorption capacity and metallic or semi conductive properties, depending on their mode of synthesis. CNT can be more than 60 times stronger than steel, while being six times lighter.

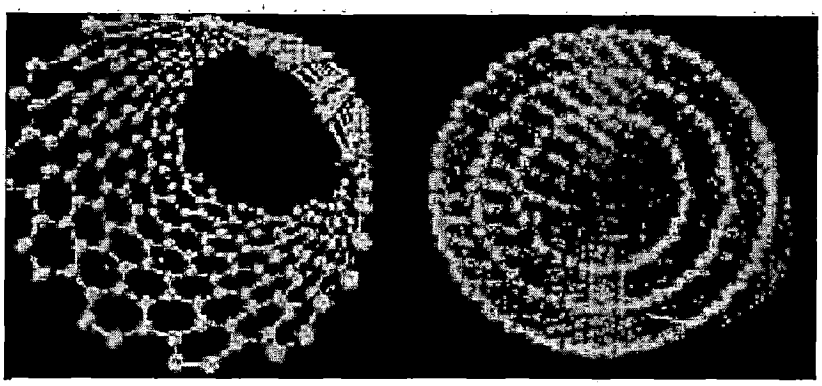

Figure 2 Schematic Illustration of single –walled and multi walled carbon nanotubes

1.2. Fullerenes

Pure fullerenes are another new crystalline form of carbon. They have a variable number of carbon atoms, which can range from 28 to more than 100 atoms, forming a hollow sphere. The best-known form, containing 60 carbon atoms, is C_{60}. Fullerenes, like CNT, can be modified in many ways by bonding organic or inorganic groups to them or incorporating various products. These modifications will have a major impact on their properties and toxicity. In current studies of the potential applications of fullerenes, the most attention seems to focus on solar and lithium batteries, electronics, storage of gases, such as methane and oxygen, additives to rubber and plastics, and treatment of various diseases, including AIDS and cancer.

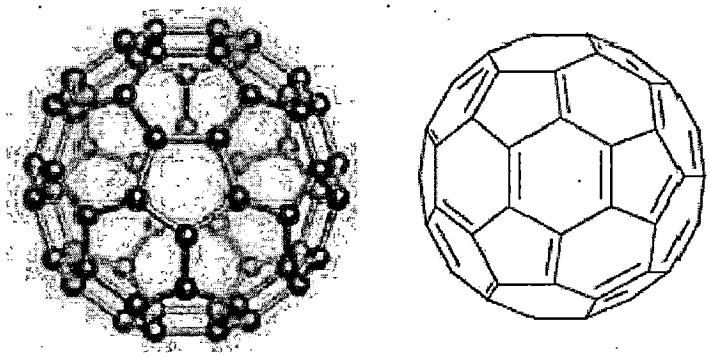

Figure 3. C_{60} fullerene, showing alternate cycles of 5 and 6 carbon atoms.

1.3. Quantum dots

Quantum dots typically are composed of combinations of chemical elements from Groups II and IV or Groups III and V of the periodic table. They have been developed in the form of semiconductors, insulators, metals, magnetic materials or metal oxides. In sizes of about 1 to 10 nm in diameter, they display unique optical and electronic properties. For example, quantum dots can absorb white or ultraviolet light and reemit it as a specific wavelength.

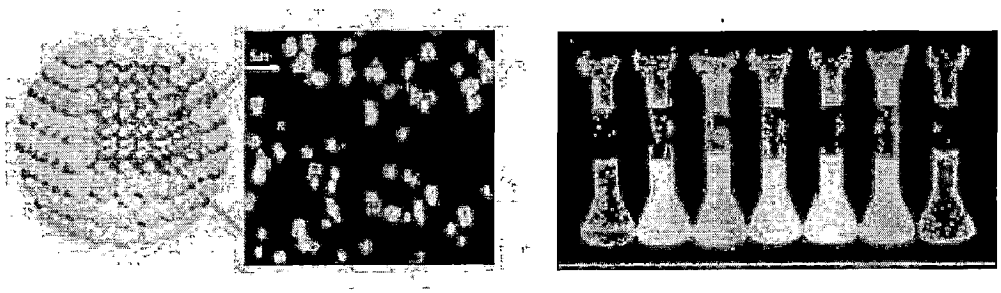

Figure 4. Quantum dot and its optical effects, depending on nanoparticles size

Depending on the composition and size of quantum dots the light emitted can range from blue to infrared. The flexibility of quantum dots and their associated optical properties allow applications to be envisioned in different fields, such as multicolor optical coding in the study of gene expression, high-resolution and high-speed screens, and medical imaging. Some quantum dots are modified chemically to produce drug vectors, diagnostic tools and solar batteries.

1.4. Dendrimers

New structures have also been synthesized in these sizes. This is particularly true of dendrimers, which represent a new class of nanoscaled polymers with controlled structure. These are synthetic three-dimensional macromolecules developed from a monomer, with new branches added, step by step, in successive tiers, until a symmetrical structure is synthesized. Dendrimers are considered to be basic building blocks for large-scale synthesis of organic and inorganic nanostructures ranging in size from 1 to 100 nm and displaying unique properties. They allow precise, atom-by-atom control of nanostructure synthesis, depending on the dimensions, shape and chemistry of the desired surface. In particular, it is anticipated that they will be used extensively in the medical and biomedical field.

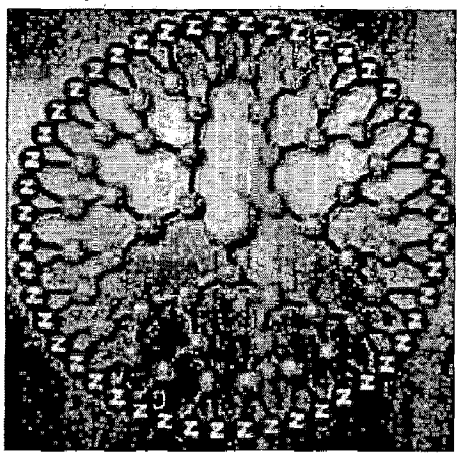

Figure 5. Dendimers

1.5. Applications of Nanomaterials

There is a wide variety of nanoparticles with organic or inorganic composition. Thus, most metals can be produced in nanometric dimensions. For example, gold nanoparticles reveal an optical resonance spectrum in the visible range, which is sensitive to environmental conditions and to nanoparticles size and shape. Their unique properties offer the prospect of a series of applications, particularly as optical markers or cancer treatment agents. Silver is currently used mainly for its antimicrobial properties. Metal nanowires of gold, copper, silicon and cobalt have

also been produced, which can serve as conductors or semiconductors and could be used in nanoelectronics.

There are many potential uses of nanoparticles such as in energy saving for vehicles, development of renewable energies, pollution reduction, water filtration, construction materials, medical applications, cosmetics, pharmaceuticals, textiles, electronics, paints, inks, etc. In recent years, the interest in the synthesis and preparations of metal nanoparticles in organic solvent has increased because of their potential application in the field of electronics and photonics due to their peculiar size dependent optical and electronic properties [8-12].

Several nanoscaled metal oxides have been fabricated, but the most common, because of their larger-scale production, are undoubtedly silica (SiO_2), titanium dioxide (TiO_2) and zinc oxide (ZnO). They are used in many fields, including rheology, as active agents and additives in the plastics and rubber industries (SiO_2), in sunscreens (TiO_2, ZnO) and in paints (TiO_2). Some structures display interesting properties, allowing potential applications to be envisioned in various fields: sensors, optoelectronics, transducers, medicine etc.

1.6. Health Effects of Nanoparticles

Several studies have been performed on different animal species to determine whether nanoparticles can have toxic health effects. Toxic effect of nanoparticles soluble in biological fluids are related to their different chemical components, independent of the particle's initial size. These effects are not specific to nanometric dimensions. The situation is completely different for nanoparticles that are insoluble or very weakly soluble in the organism. The data currently available on toxicity of insoluble nanoparticles are extremely limited and normally do not allow a quantitative risk assessment or an extrapolation to humans, possibly for TiO_2. However, they reveal some information, which, although fragmentary, gives reason to conclude that nanoparticles must be handled with care. This is because a product mass of the same chemical composition is normally more toxic if it is nanoscaled than if it is larger in size. The exposure of workers thus must be minimized, because several toxic effects have been documented, even though they are extremely variable from one product to another.

The nanoparticles reaching the blood system circulate throughout the body and there is clear evidence that they can be retained by different organs, depending on the nature of the nanoparticles. Several toxic effects have been documented for different organs and depend on the nature of the nanoparticles.

Toxicity of microscopic particles is normally well correlated to the mass of the toxic substance. However, the situation is totally different in the case of nanoparticles. The different studies showed clearly that toxicity, for a specific substance, varied substantially according to size for the same nanoparticle mass. In fact, toxicity is correlated to multiple parameters as mentioned in Table1. The most significant of these parameters seem to be chemical composition, specific surface area, concentration and size of the particles.

Table 1 Parameters capable of infulencing nanoparticle toxicity

The parameters most often reported	Other reported parameters
Specific surface area	Solubility
Number of particles	Shape, porosity
Size and granulometric distribution	Degree of agglomeration/aggregation
Concentration	Biopersistence
Chemical composition (purities and impurities)	Crystalline structure
Surface properties	Hydrophilicity/hydrophobicity
Zeta charge/potential, reactivity	Pulmonary deposition site
Functional groupings	Age of particles
Presence of metals/Redox potential	Producer, process and source of the material used
Potential to generate free radicals	
Surface coverage	

Different toxic effects have already been documented at the pulmonary, cardiac, reproductive, renal, cutaneous and cellular levels. Significant accumulations have been shown in the lungs, brain, liver, spleen and bones. However some authors consider that, most of the time, a comparison of published results between in vivo and in vitro tests indicates little correlation.

1.7. History

Although nanoparticles are generally considered an invention of modern science, they actually have a very long history. Nanoparticles were used by artisans as far back as the 9th century in Mesopotamia for generating a glittering effect on the surface of pots.

Even these days, pottery from the middle ages and renaissance often retains a distinct gold or copper colored metallic glitter. This so called luster is caused by a metallic film that was applied to the transparent surface. The luster can still be visible if the film has resisted atmospheric oxidation and other weathering.

The luster originated within the film itself, which contained silver and copper nanoparticles dispersed homogeneously in the glassy matrix of the ceramic glaze. These nanoparticles were created by the artisans by adding copper and silver salts and oxides together with vinegar, ochre and clay, on the surface of previously-glazed pottery. The object was then placed into a kiln and heated to about 600 °C in a reducing atmosphere. In the heat the glaze would soften, causing the copper and silver ions to migrate into the outer layers of the glaze. The reducing atmosphere reduced the ions back to metals, which then came together forming the nanoparticles that give the colour and optical effects.

Luster technique showed that ancient craftsmen had a rather sophisticated empirical knowledge of materials. The technique originated in the islamic world. As Muslims were not allowed to use gold in artistic representations, they had to find a way to create a similar effect without using real gold. The solution they found was using luster [13].

Michael Faraday provided the first description, in scientific terms, of the optical properties of nanometer-scale metals in his classic 1857 paper. In a subsequent paper, the author Turner points out that "when thin leaves of gold or silver are mounted upon glass and heated to a temperature which is well below a red heat (~500 °C), a remarkable change of properties takes place, whereby the continuity of the metallic film is destroyed. The result is that white light is now freely transmitted, reflection is correspondingly diminished, while the electrical resistivity is enormously increased." [14, 15, 16]

Recorded use of silver to prevent infection dates to ancient Greece and Rome, it was rediscovered in the Middle Ages, where it was used for several purposes, such as to disinfect

water and food during storage, and also for the treatment of burns and wounds as wound dressing. In the 19th century, sailors on long ocean voyages would put silver coins in barrels of water and wine to keep the liquid pure.

1.8. Silver Nanoparticles

Silver nanoparticles are the nanoparticles of silver within the range of 1 to 100 nm. It is most commonly used for hygienic and healing purposes [17]. However, over time, the use of silver compounds and ions has faded as an anti-infection agent due to the advent of antibiotics and other disinfectants and the poorly understood mechanisms of their toxic effects.

1.9. Synthesis of Silver nanoparticles

There are two approaches for the preparation of metal nanoparticle

1.9.1 Top down Approach

This method involves the continuous division of bulk matter into nanoparticles. A disadvantage of this method is the manipulation of small amounts of atoms at a time resulting in low fabrication throughput. The top-down approach takes a large-scaled substance and modifies it to nanometric dimensions. Etching, precision engineering, lithography and crushing are common approaches

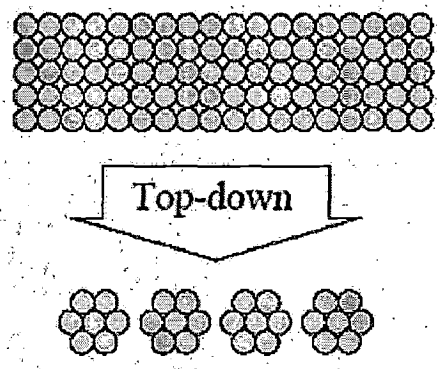

Top down Method for Nanofabrication.

Figure 6. Top down approch

1.9.2 Bottoms up Approach

This method involves the continuous building up of nanoparticles from molecular or atomic level. The bottom-up approach fabricates nanoparticles one atom or one molecule at a time, using processes such as chemical synthesis, auto assembly and assembly by individual positioning

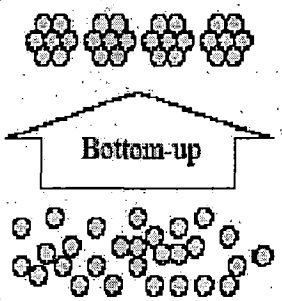

. Bottom Up Method for Nanofabrication.

Figure 7. Bottom Up approach

This technique includes evaporation under high vacuum [18]. Use of metal vapor techniques is limited because the operation of the apparatus is demanding and it is difficult to obtain a narrow particle size distribution. Among these are the solvated metal atom dispersion method (SMAD) [19], the laser ablation method in metal colloids [20] and electrochemical reductions methods [21]. The "bottom up" methods of wet chemical nanoparticle preparation rely on the chemical reduction of metal salts, electrochemical pathways, or the controlled decomposition of metastable organometallic compounds.

1.10. Optical Properties of Silver nanoparticles.

The distinctive colors of colloidal silver are due to a phenomenon known as plasmon absorbance. Incident light creates oscillations in conduction electrons on the surface of the nanoparticles and electromagnetic radiation is absorbed.

Of the three metals (Ag, Au, and Cu) that display plasmon resonances in the visible spectrum, Ag exhibits the highest efficiency of plasmon excitation [22]. Moreover, optical excitation of plasmon resonances in nanosized Ag particle is the most efficient mechanism by which light interacts with matter. A single Ag nanoparticle interacts with light more efficiently than a particle of the same dimension composed of any known organic or inorganic chromophore. The light-interaction cross-section for Ag can be about ten times that of the geometric cross-section, which indicates that the particles capture much more light than is physically incident on them [23].

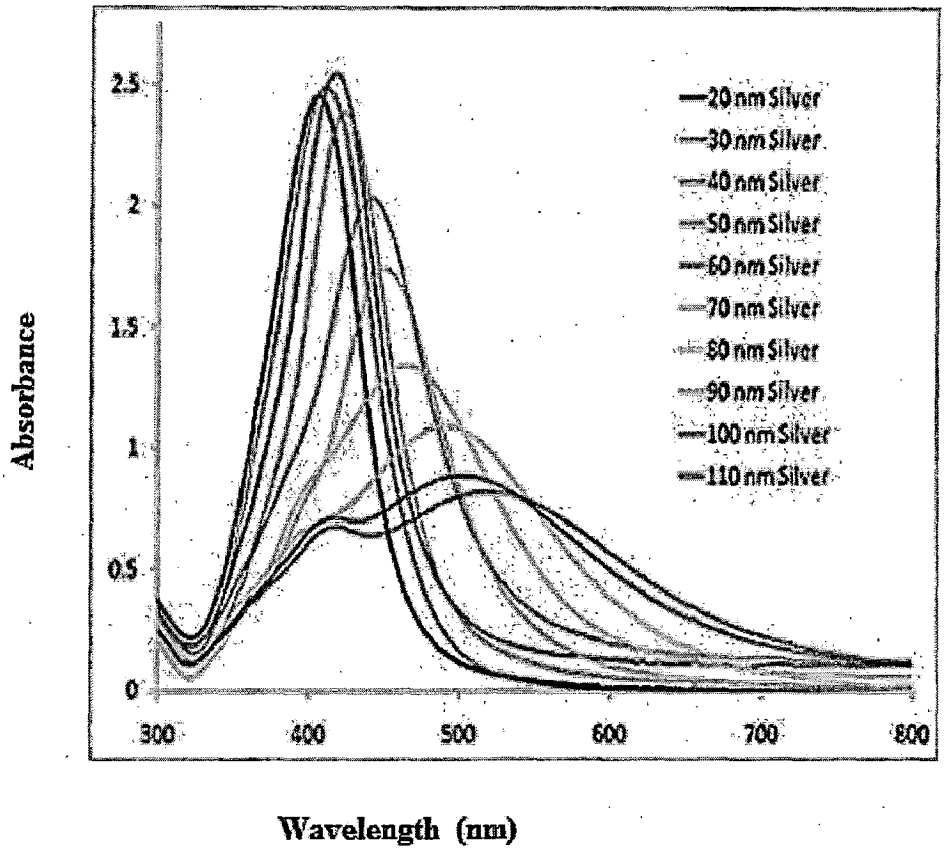

Figure 8. UV-Visible Graph of different Size of silver nanoparticles

The optical properties of spherical silver nanoparticles are highly dependent on the nanoparticle diameter. As the size of the silver particles increases, its unique plasmonic signature shifts towards the red region of the visible spectrum and both the dipole and quadrupole peaks are clearly expressed. The total optical extinction is comprised of absorption and scattering

Silver is also the only material whose plasmon resonance can be tuned to any wave length in the visible spectrum. Small Ag nanoparticles do not interact with light nearly as efficiently as particles that are in the 50–100 nm range and do so strictly through energy absorption. On the other hand, the plasmon resonances in larger Ag nanoparticles have a significant light-scattering component.

Table 2. Correlation between particle size, wave length and peak width half maximum

Particle Size/nm	λ_{max}/nm	PWHM/nm
10–14[a]	395–405	50–70
35–50[b]	420	100–110
60–80[c]	438	140–150

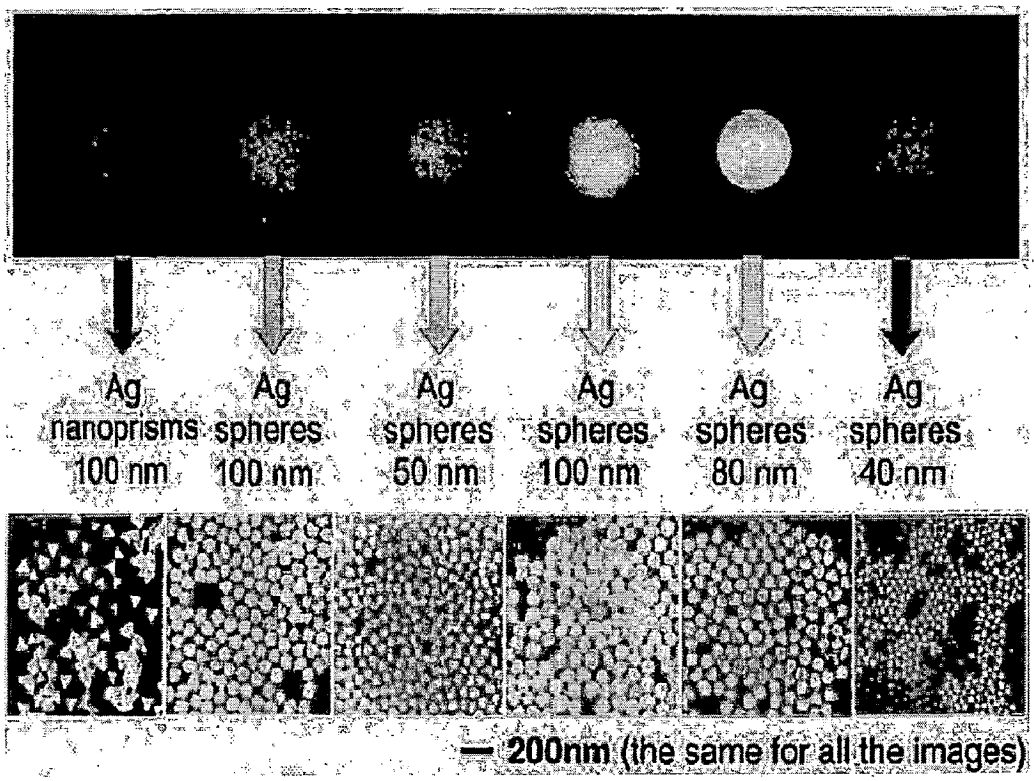

Figure 9. Different colours of silver solution and their particles size [24]

1.11. Application of silver Nanoparticles

Silver nanoparticles are known for their strong antibacterial effects for a wide array of organisms (e.g., viruses, bacteria, fungi) [25]. Therefore, silver nanoparticles are widely used in medical devices and supplies such as wound dressings, scaffold, skin donation, recipient sites, and sterilized materials in hospitals, medical catheters, contraceptive devices, surgical instruments, bone prostheses, artificial teeth, and bone coating.

One can also observe their wide use in consumer products such as cosmetics, lotions, creams, toothpastes, laundry detergents, soaps, surface cleaners, room sprays, toys, antimicrobial paints, home appliances (e.g., washing machines, air and water filters), automotive upholstery, shoe insoles, brooms, food storage containers, and textiles.

Silver nanoparticles can be used in sensing applications such as detection of DNA sequences, laser desorption/ionization mass spectrometry of peptides, colorimetric sensor for histidine, determination of fibrinogens in human plasma, real-time probing of membrane transport in living microbial cells.

Silver nanoparticles and silver nanocomposites have been used to catalyze many reactions such as CO oxidation, benzene oxidation for phenol, photo degradation of gaseous acetaldehyde, and reduction of p-nitrophenol to p-aminophenol.

In the present studies attempts have been made to synthesize silver nanoparticles via solvent extraction route using oxygen, sulphur and nitrogen containing extractants.

Literature Review

In the following few paragraphs literature on the synthesis of nanoparticles is reported.

Henglein [26] reduced $Ag(CN)_2^-$ at a low rate radiolytically and generated hydroxymethyl radicals. When colloidal silver seed particles are present in the solution, the reduction of $Ag(CN)_2^-$ is much faster, and larger silver particles with a narrow size distribution are produced. A mechanism was proposed, in which the $^{\bullet}CH_2OH$ radicals transfer electrons to the seed particles, and the stored electrons finally reduce $Ag(CN)_2^-$ directly on the surface of the seeds.

The limitations of radiolytic particle enlargement were discussed. Bimetallic particles of the Pt core Ag shell type with a non symmetric shape of the shell were also synthesized. Despite this irregular structure, the optical spectra agreed fairly well with the literature value calculated for symmetric bimetallic particles.

Nagasawa *et al.* [27] decomposed a silver-fatty acid complex at 250 °C in a nitrogen atmosphere to make stable, mono-disperse silver nanoparticles. The size distribution was measured using high-resolution transmission electron microscopy (HRTEM), the mean particle diameter was 4.7 nm and the standard deviation was 0.6 nm. This size distribution was verified by the measured surface-Plasmon absorption spectrum. Their X-ray diffraction pattern showed that they were metallic silver. The particles cross-sectional shapes were usually circular except some were hexagons or pentagons. Use of thermogravimetry and differential thermal analysis showed that their surface was coated by fatty acid. This coating stabilized the nanoparticles thus preventing their aggregation even after repeated dissolution and evaporating.

Xun *et al.* [28] prepared Stable fluids containing silver nanoparticles in kerosene by the extraction-reduction method. Silver nitrate was extracted in nonpolar solvent by thio-substituted phosphinic acid extractant Cyanex 302, and then Ag (I) was reduced by solid KBH_4. In order to enhance the loading content of silver nanoparticles in the fluids, a tri-block copolymer $(PEO)_{20}(PPO)_{70}(PEO)_{20}$ was added into the organic phase before the reduction of Ag(I). The results show that Cyanex 302 acts as both an extractant for Ag+ from aqueous solution to

kerosene and a stabilizer for silver nanoparticles, and the reverse micelles formed by copolymer $(PEO)_{20}(PPO)_{70}(PEO)_{20}$ can solubilize more silver nanoparticles modified by Cyanex 302 and prevent them from aggregating together. The highest stable concentration of silver nanoparticles in kerosene was up to 0.1 mol/L. The silver colloidal dispersions were analyzed by UV-Visible, FT-IR spectra, TEM, and X-ray diffraction techniques.

Shi *et al.* [29] prepared Stable organic fluid containing silver nanoparticles using the extractant Cyanex 301 (di-(2,4,4-trimethylpentyl) dithiophosphinic acid) in alkane by the solvent extraction-reduction method. Ag[I] is extracted into alkane by Cyanex 301, then the obtained Ag+ -Cyanex 301 complex is reduced with solid sodium borohydride to obtain the organic fluids containing Ag nanoparticles. The organic fluids were stable at room temperature for more than two months when the concentration of Ag nanoparticles was about 0.10 mol L^{-1}. The nanoparticles are characterized by XRD, TEM, IR, UV-Visible, and TG-DTG, showing that Ag nanoparticles are well modified by the extractant.

***Gao et al.* [30]** synthesized multi-dentate amphiphilic compound, 3,3'-(dodecylazanediyl)-bis-[*N*-(2-aminoethyl)propanamide] ($12C–2NH_2$) and was employed to stabilize silver nanoparticles. Surface properties and stability of silver nanoparticles were controlled by adjusting the $12C–2NH_2$ to silver (0) molar ratio. $12C–2NH_2$ was also applied to transfer silver nanoparticles from an aqueous to an organic phase. The transfer efficiency depends on $12C–2NH_2$ concentration. When $12C–2NH_2$ to silver (0) molar ratio was 2:1, the highest efficiency of phase transfer to toluene was obtained. The stabilized silver nanoparticles were stable up to four days in toluene.

Liu *et al.* [31] prepared Silver nanoparticles by the reduction of silver nitrate using $NaBH_4$ as reducing agent in water-in-oil reverse micelles system, in which Gemini surfactant 2-hydroxy-1, 3-bis(octadecyldimethylammonium) propane dibromide (18-3(OH)-18) was used as stabilizer. The results of TEM, AFM and UV–Visible absorption spectra show that the silver nanoparticles have a narrow size distribution. The results of UV–Visible absorption spectra and XPS reveal that the Gemini surfactant 18-3(OH)-18 can stabilize the silver nanoparticles for at least 2 months. The 18-3(OH)-18-capped silver nanoparticles exhibit visible luminescence at 448 nm upon photo excitation at 309 nm due to metal–ligand charge transfer absorption.

Yang et al **[32]** synthesized mercaptosuccinic acid (MSA)- modified Ag nanoparticles prepared using cetyltrimethylammonium bromide (CTAB). They observed that, at high CTAB concentration, some un bonded CTA^+ cations are physically adsorbed on particle surface and enter chloroform layer, which cannot be removed by simple water washing or centrifugation. By using β-cyclodextrin (CD) as a capturing agent, the unbound CTA^+ cations can be adequately removed due to the possible inclusion function of CD.

Hsu & Wu [33] synthesized silver nanoparticle suspensions by chemical reduction from silver nitrate in a formaldehyde reductant and PVP stabilizer using organic bases as the reaction promote. Two different organic bases of different basicity, triethylamine and pyridine were used in the reaction. The sizes of the silver particles prepared from the more basic triethylamine were around 20–30 nm. The particles made from the less basic pyridine had smaller sizes (10–20 nm).

Olenin *et al.* [34] studied the influence of experimental factors on particle size and surface hydrophilicity / hydrophobicity of silver nanoparticles. It is shown that silver nanoparticles with controlled mean size and surface hydrophilic– hydrophobic properties can be obtained through direct synthesis or successive transformations.

Seo et al. **[35]** prepared hydrophobic silver nanoparticles capped by oleic acid via solvent exchange method. $AgNO_3$ was reduced by $NaBH_4$ to produce Ag nanoparticles in aqueous solution with various pH conditions and oleic acid as stabilizer. By the addition of H_3PO_4, the carboxylate group was converted to carboxylic acid and this induced the reorientation of oleic acid and provided hydrophobic silver nanoparticles. The oleic acid-capped silver nanoparticles were characterized by UV–Visible spectroscopy and Fourier transfer infrared (FTIR) studies. Spherical silver particles with uniform size of 8 nm were obtained from silver nitrate under basic conditions.

Navaladian *et al.* [36] synthesized anisotropic silver nanoparticles using microwave irradiation by the decomposition of silver oxalate in a glycol medium using polyvinyl pyrolidone (PVP) as the capping agent. The obtained Ag nanoparticles have been characterized by UV–visible

spectroscopy, powder x-ray diffraction (XRD), transmission electron microscopy (TEM) and high-resolution TEM (HRTEM) studies. Anisotropic Ag nanoparticles of average size around 30 nm have been observed in the case of microwave irradiation for 75 s whereas spherical particles of a size around 5–6 nm are formed for 60 s of irradiation. The texture coefficient and particle size calculated from XRD patterns of anisotropic nanoparticles reveal the preferential orientation of (111) facets in the Ag sample. Ethylene glycol is found to be a more suitable medium than diethylene glycol. A plausible mechanism has been proposed for the formation of anisotropic Ag nanoparticles from silver oxalate.

Sarkar et al. **[37]** demonstrated simple method for either transfer of silver nanoparticles from formamide to chloroform or to form a film at their interface. The transfer of the particles is a two-step size dependent process. The size distribution of the colloidal hydrophobic silver particles in chloroform was almost the same as that before its transfer. Particles can be isolated by evaporation of chloroform. During evaporation, the hydrophobic particles become hydrophilic (charged) due to the formation of bi layer of CTAB over their surface. The isolated particles can be re-dispersed easily in polar solvents such as water and methanol. Nanocrystalline film of Ag is also prepared at the formamide–chloroform interface using suitable stabilizers in two immiscible layers. The nanocrystals have been characterized by various microscopic and spectroscopic techniques.

Guo *et al.* **[38]** synthesized NdF_3 and TbF_3 nanoparticles via a solvent extraction route using Cynex923. X-ray diffraction (XRD) study showed that pure hexagonal phase NdF_3 and pure orthorhombic phase TbF_3 could be obtained under the current synthetic conditions. Transmission electron microscopy (TEM) and scanning electron microscopy (SEM) observations indicated that NdF_3 nanoplates have a diameter of 50–80 nm and a thickness of 10–20 nm and TbF_3 products have sphere morphologies with diameter from 70 to 170 nm. The driving force for the growth of NdF_3 nanoplates could be attributed to the hexagonal crystal structure. The luminescence properties of NdF_3 and TbF_3 nanoparticles were investigated, which indicated that NdF3 nanoparticles showed typical emission at 888, 1064, and 1328 nm and TbF_3 nanoparticles showed characteristic emission of Tb^{3+} (f–f).

Shen & Yu [39] prepared silver nanoparticles in counter-current chromatography (CCC) based on a unique step-gradient extraction process. Carboxylate anions were modified on silver nanoparticles to produce water-dispersible nanoparticles. Then aqueous nanoparticles were readily transferred to the organic phase together with the phase transfer catalyst, tetraoctyl ammonium bromide (TOAB), owing to the ion-pair adduct formation between silver nanoparticles anions and tetraoctyl ammonium cations. Various concentrations of TOAB in the organic elution phase were used in the CCC extraction experiments. It appeared that a concentration of 0.02mM of TOAB was adequate to achieve optimum separation and recovery for the aqueous Ag nanoparticles sample (1.5 mg) in the CCC extraction experiments. Samples of 15.8±5.3nmwere separated; the distributions of four fractions collected were 13.7±1.9, 14.1±3.5, 19.2±4.3, and 22.2±4.9 nm. Results revealed that as compared to the stepwise extraction performed the step-gradient extractions using CCC provided much better size discrimination [14].

CHAPTER 2

Preparation and Characterization of Silver Nanoparticles

Chapter 2

Preparation and Characterization of Silver Nanoparticles using Cyanex 923,Cyanex 471X and Aliquat 336.

2.1 Materials and Reagents

The Cyanex 923 and Cyanex 471X were obtained as gift sample from CYTEC, Canada and were used as such. Aliquat 336 was purchased from Henkel corporation. The other chemicals and materials used are given in the table 3. along with their make and grade.

Table 3. Materials and Reagents used in synthesis

S.No.	Reagent / Material	Grade	Make
1	*n-Hexane*	AR	RENKEM
2	$AgNO_3$	-	-
3	*Acetone*	LR	RENKEM
4	$NaBH_4$	AR	MERCK
5	*Ethanol*	LR	RENKEM
6	HNO_3	LR	RENKEM
7	*Toluene*	LR	RENKEM

2.1.1 Cyanex 923

Cyanex 923 is a mixture of trialkyl phosphine oxide which has potential application as an extractant for the liquid-liquid extraction of metals.

The major advantage of Cyanex 923 extractant over similar extractants e.g. TOPO (tri octyl phosphine oxide), is that it is a liquid at room temperature completely miscible with all common hydrocarbon diluents even at low ambient temperatures.

The Composition and Structure:- The four trialkyl phosphine oxides are as follows

$R_3P(O)$ (~8%) $R_2R'P(O)$ (~32%) $RR'_2P(O)$ (~42%) $R'_3P(O)$ (~14%)

Where is R' = [$CH_3(CH_2)_7$] - - Normal Octyl

R = [$CH_3(CH_2)_6$] - - Normal Hexyl

Average Molecular Wt. is 348 approximately.

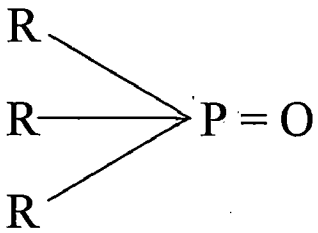

2.1.2 Cyanex 471X

Cyanex 471 X is aphosphine sulphide extractant and is used for the selective recovery of silver and in the separation of palladium and platinum. It is crystalline, off white solid having specific gravity 0.91 at 22 °C with average molecular Wt. 248 .

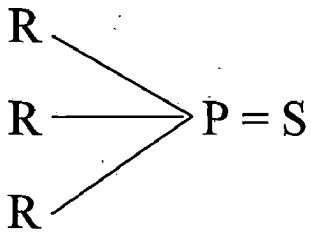

Where R is CH_3-CH_2-CH_2– with CH_3 on the second carbon

Triisobutylphosphine Sulfide (TIBPS)

2.1.3Aliquat 336

Aliquat 336 is a mixture of C_8 (octyl) and C_{10} (capryl) chains with C_8 predominating. It is a quaternary ammonium salt used as a phase transfer catalyst and metal extractant.

Aliquat 336 is composed of a large organic cation associated with a chloride ion, as shown below.

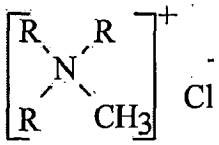

R = octyl and capryl

Because the ammonium structure has a permanent positive charge, it can form salts with anions over a wider pH range than primary, secondary or tertiary amines. For this reason, Aliquat 336 finds application in environments from acid to slightly alkaline pH.

2.2 Preparation of Silver Nanoparticles

The method includes extraction of metal ion from aqueous solution to organic solution and then the ions are reduced to metal. In this step the metal ion grows to nanometer size. After the reduction process these are separated, concentrated, washed and dried according to the process.

2.2.1 Stock Solutions

Calculated amounts of $AgNO_3$ were weighted and dissolved in HNO_3 (0.1 M) to make stock solutions of $AgNO_3$ (0.1M, 0.2M, 0.5M). The stock solutions of Cyanex 923 and Cyanex 471X (0.01M, 0.02M, 0.05M) were prepared in n-hexane. The solution of $NaBH_4$ (0.2 M) was prepared in 100 mL of water in measuring flask. A solution of HNO_3 (5M) was prepared separately to maintain the acidity.

2.2.2 Procedure for the preparation of Silver nanoparticles using Cyanex 923/Cyanex471X.

A solution of silver nitrate (0.01,0.02, 0.05) was prepared (25 mL) using stock solution of silver nitrate maintaining the acidity with 5M HNO_3. This was mixed thoroughly for some time. The aqueous solution was mixed slowly in an organic solution containing Cyanex 923/Cyanex 471X in a 100 mL conical flask under vigorous stirring using magnetic stirrer. The whole solution was stirred for one hour and allowed to settle for 1 hour. 2mL of $NaBH_4$ was added in the mixture

slowly under vigorous stirring. The resulting solution was again stirred for one hour and was allowed to settle for one hour. Organic and aqueous layers were separated using separating funnel. The organic layer containing metal nanoparticles was characterized by IR spectroscopy. The organic phase was evaporated in china dish slowly under high temperature using hot plate. After complete evaporation of organic phase the residue was dissolved in ethanol. The metal nanoparticles were separated by using whatman filter paper no. 41 and again washed by ethanol. After that the nanoparticles were washed 2 times by acetone. Then nanoparticles were dried in oven for at least 8 hours.

The resultant nanoparticles were characterized by XRD and SEM. The aqueous phase was analyzed by AAS before and after the extraction to calculate the % extraction.

Table 4. Working parameters of AAS for Ag determination

Element	Working range	Sensitivity (ppm)	Wavelength (nm)	Mode of analysis
Ag	1.5 -5.5 ppm	1.000 ppm	328.1 nm	Air-Acetylene

Some of the selected samples was treated in muffle furnace at 600°C for 3hours.

2.3 Stock solutions for Aliquat 336

Calculated amounts of $AgNO_3$ were weighted and dissolved in HNO_3 (0.1 M, 0.5M) to make stock solutions of $AgNO_3$ (0.1M). The stock solutions of Aliquat 336(0.1M, 0.3M) were prepared in n-hexane. But the final solution after mixing the solutions of $AgNO_3$ and Aliquat 336 was hazy so use of n-hexane was eliminated and another solvent toluene was introduced. The solution of $NaBH_4$ (0.2 M) was prepared in 100 mL of water in measuring flask. A solution of HNO_3 (5M) was prepared separately to maintain the acidity.

2.3.1. Procedure for the preparation of Silver nanoparticles using Aliquat 336

Aliquat 336 was dissolved in toluene to make the appropriate concentration of solution. Extractant Aliquat 336 had Cl^- which had to be removed so Aliquat 336 was equilibrated with HNO_3 (0.1M) in mechanical shaker for 15 min. After shaking solution was allowed to settle down

for 15 min and the two layers were separated. Treated organic layer containing Aliquat 336 was used further. Equal volume of Aliquate 336 and aqueous phase containing silver ion were equilibrated on mechanical shaker for 15 minutes and allowed to settle. The organic layer was then separated and $NaBH_4$ solution was added to reduce silver ions. The colour of the solution changed from pale yellow to slightly brown. The organic phase was evaporated on hot plate and the residue was heated in a furnace at 600 °C for 3hours. The sample was washed 2 times with ethanol and then with acetone. After the sample was dried in oven at 60-80° C for 8 hours.

2.4. Variations in the conditions for the preparation of silver nanoparticles.

The concentration of Cyanex 923, Cyanex 471X, Aliquat 336, $AgNO_3$ solution and HNO_3 were varied to study the effect of these variations on the size of nanoparticles. Variations employed are listed in the tables (5- 13).

Table 5. Change in concentration of Cyanex 923 , at constant Ag NO_3 and HNO_3.

S.No.	Cyanex 923 (M)	Ag (M)	HNO_3 (M)
1	0.01	0.01	0.1
2	0.02	0.01	0.1
3	0.05	0.01	0.1

Table 6. Change in concentration of Cyanex 923, at constant Ag NO_3 and HNO_3.

S.No.	Cyanex 923 (M)	Ag (M)	HNO_3 (M)
1	0.01	0.02	0.1
2	0.02	0.02	0.1
3	0.05	0.02	0.1

Table 7. Change in concentration of Cyanex 923, at constant Ag NO_3 and HNO_3.

S.No.	Cyanex 923 (M)	Ag (M)	HNO_3 (M)
1	0.01	0.01	0.5
2	0.02	0.01	0.5
3	0.05	0.01	0.5

Table 8. Change in concentration of Cyanex 923, at constant Ag NO_3 and HNO_3.

S.No.	Cyanex 923 (M)	Ag (M)	HNO_3 (M)
1	0.01	0.01	1
2	0.02	0.01	1
3	0.05	0.01	1

Table 9. Change in concentration of Cyanex 471X, at constant Ag NO_3 and HNO_3.

S.No.	Cyanex 471X (M)	Ag (M)	HNO_3 (M)
1	0.01	0.01	0.1
2	0.02	0.01	0.1
3	0.05	0.01	0.1

Table 10. Change in concentration of Cyanex 471X, at constant Ag NO_3 and HNO_3.

S.No.	Cyanex 471X (M)	Ag (M)	HNO_3 (M)
1	0.01	0.02	0.1
2	0.02	0.02	0.1
3	0.05	0.02	0.1

Table11. Change in concentration of Cyanex 471X, at constant Ag NO_3 and HNO_3

S.No.	Cyanex 471X (M)	Ag (M)	HNO_3(M)
1	0.01	0.01	0.5
2	0.02	0.01	0.5
3	0.05	0.01	0.5

Table12. Change in concentration of Cyanex 471X, at constant Ag NO_3 and HNO_3

S.No.	Cyanex 471X (M)	Ag (M)	HNO_3 (M)
1	0.01	0.01	1
2	0.02	0.01	1
3	0.05	0.01	1

Table 13. Change in concentration of Aliquat 336 , at constant Ag NO_3 and HNO_3

S.No.	Aliquat 336 (M)	Ag (M)	HNO_3 (M)
1	0.1	0.1	0.1
2	0.3	0.1	0.1

2.5 Characterization Techniques

The Following Techniques were used to characterize the nanoparticles

1. FE-SEM (Field Emission Scanning Electron Microscopy)

2. Atomic Force Microscopy (AFM)

3. X-ray diffraction

4. TEM (Tunneling Electron Microscopy)

5. FT IR

2.5.1 FE-SEM (Field Emission Scanning Electron Microscopy)

The **Scanning Electron Microscope** (**SEM**) is a type of electron microscope that images the sample surface by scanning it with a high-energy beam of electrons in a raster scan pattern. The electrons interact with the atoms that make up the sample producing signals that contain information about the sample surface topography, composition and other properties such as electrical conductivity.

The types of signal produced by an SEM include secondary electrons, back-scattered electrons (BSE), characteristic X-rays, light, specimen current and transmitted electrons. Secondary electron detectors are common in all SEMs, but it is rare that a single machine would have detectors for all possible signals. The signals result from interactions of the electron beam with atoms at or near the surface of the sample. In the most common or standard detection mode, secondary electron imaging or SEI, the SEM can produce very high-resolution images of a sample surface, revealing details about less than 1 to 5 nm in size. Due to the very narrow electron beam, SEM micrographs have a large depth of field yielding a characteristic three-dimensional appearance useful for understanding the surface structure of a sample. A wide range of magnifications is possible, from about 10 times (about equivalent to that of a powerful hand-lens)

to more than 500,000 times, about 250 times the magnification limit of the best light microscopes. Back-scattered electrons (BSE) are beam electrons that are reflected from the sample by elastic scattering. BSE are often used in analytical SEM along with the spectra made from the characteristic X-rays. Because the intensity of the BSE signal is strongly related to the atomic number (Z) of the specimen, BSE images can provide information about the distribution of different elements in the sample.. Characteristic X-rays are emitted when the electron beam removes an inner shell electron from the sample, causing a higher energy electron to fill the shell and release energy. These characteristic X-rays are used to identify the composition and measure the abundance of elements in the sample.

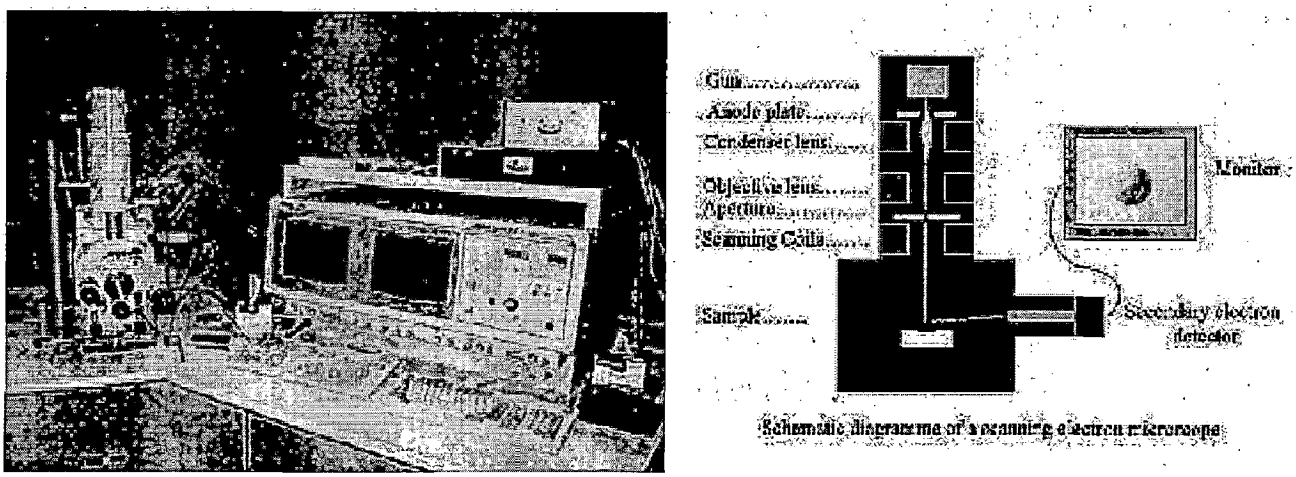

Figure 10: Field Emission Scanning Electron Microscope & Block Diagram

The FE-SEM micrographs and EDAX was taken using a FEI (make)-QUANTA 200F (model number) instrument the magnification of instrument is up to 1000KX, Resolution 2 nm and acceleration voltage 200V to 30 KV. During analysis magnification was up to 3000 and acceleration voltage was 20 KV.

2.5.2 AFM (Atomic Force Microscopy)

Atomic force microscopy (AFM) or scanning force microscopy (SFM) is a very high-resolution type of scanning probe microscopy, with demonstrated resolution of fractions of a nanometer, more than 1000 times better than the optical diffraction limit. The AFM is one of the foremost tools for imaging, measuring, and manipulating matter at the nanoscale. The information is

gathered by "feeling" the surface with a mechanical probe. Piezoelectric elements that facilitate tiny but accurate and precise movements on (electronic) command enable very precise scanning..

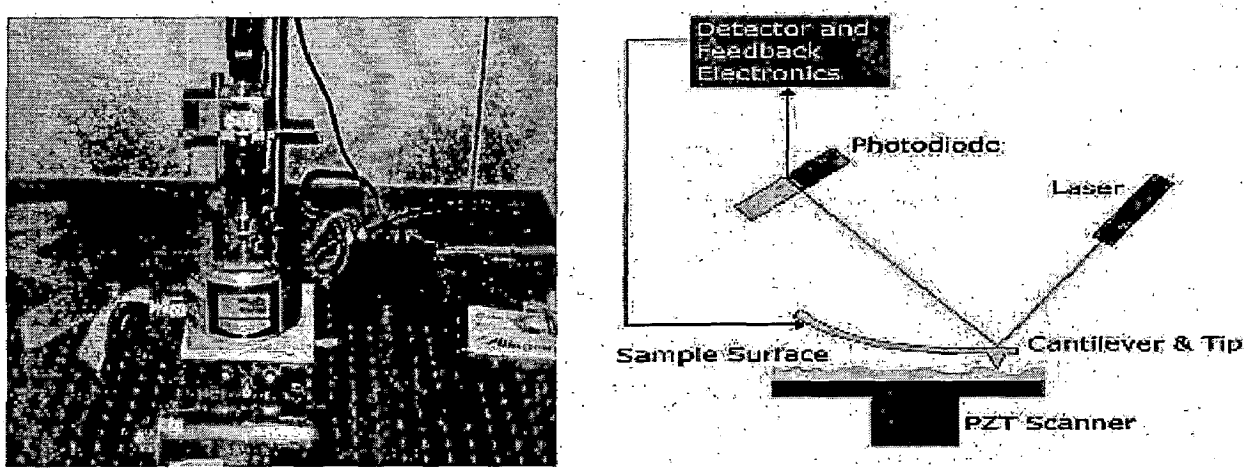

Figure 11: Atomic Force Microscope & Block Diagram of AFM

With the use of atomic force microscopy one can scan the surface and obtain three dimensional images of the sample. The tip of the AFM that is attached to the cantilever interacts with the surface of the sample. The force applied between the sample and the tip are recorded and analyzed in order to obtain the three dimensional images. The tip of the cantilever scans the surface in three different modes: contact, non-contact, or tapping-mode. In present studies the tapping mode was used where the cantilever oscillates in low frequency scanning the surface without coming in contact with the sample. The change in the intensity of laser measured by photodiode detector.

2.5.3 FT-IR (Fourier Transform Infra Red Spectroscopy)

Fourier transform infrared (FT-IR) spectroscopy is a measurement technique that allows one to record infrared spectra. Infrared light is guided through an interferometer and further across the sample (or vice versa). The recorded signal is an inter ferogram that includes two contributions. One from the instrument itself and another due to variation in "optical path difference" introduced by the sample. Performing a Fourier transform on these two sets of data (one with sample inserted, one without) results in spectra comparable to those obtained from a conventional

(dispersive) infrared spectrometer. The effect due to the sample can be isolated by calculating the ratio or the difference of the two spectra.

Determines the identities, surrounding environments or atomic arrangement, and concentrations of the chemical bond in the sample

2.5.4 X-ray Diffraction (XRD)

X-ray diffraction (XRD) is a non-destructive analytical technique for identification and quantitative determination of long-range order in various crystalline compounds. XRD uses the "fingerprint" of crystalline material to allow identification and quantification of unknown phases in a mixture. X-rays are electromagnetic radiations generated when an electron beam accelerated through a high voltage field hits a metal, which acts as an anode. The wavelength of x-ray is comparable to the size of atoms; therefore they can be effectively used to measure the structural arrangement of atoms in materials. When x-rays collide with electrons, some x-rays from the incident beam are deflected away from the incident direction. If the wavelengths of these scattered x-rays remain unchanged, the process is called an elastic scattering (Thompson Scattering) and in that case only momentum is transferred during collision. These are the x-rays that are measured in diffraction experiments. They carry information about the electron distribution in materials. On the other hand, during inelastic collision (Compton Scattering), x-rays transfer some of their energy to the electrons and so the scattered x-rays will have different wavelength than the incident x-rays.

X-rays diffracted from different atoms interfere with each other. If the atoms are arranged in a periodic fashion, as in the case of crystals, the peaks in the interference pattern will correspond to the distribution of atoms. The peaks in an x-ray diffraction pattern are directly related to the atomic distances by Bragg's law:

$$n\lambda = 2d \sin\theta$$

Where λ is the wavelength of x-ray, d is the inter-planar distance, 2θ is the scattering angle and n an integer representing the order of the diffraction peak.

A **shape factor** is used in **x-ray diffraction** and crystallography to correlate the size of sub-micrometer particles, or crystallites in a solid to the broadening of a peak in a diffraction pattern. In the Scherrer equation,

$$\tau = \frac{K\lambda}{\beta \cos\theta}$$

where K is the shape factor, λ is the x-ray wavelength, typically 1.54 Å, β is the line broadening at half the maximum intensity (FWHM) in radians, and θ is the Bragg angle, τ is the mean size of the ordered (crystalline) domains, which may be smaller or equal to the grain size. The dimensionless shape factor has a typical value of about 0.9, but varies with the actual shape of the crystallite. The Scherrer equation is limited to nano-scale particles. It is not applicable to grains larger than about 0.1 μm, which precludes those observed in most metallographic and ceramographic microstructure.

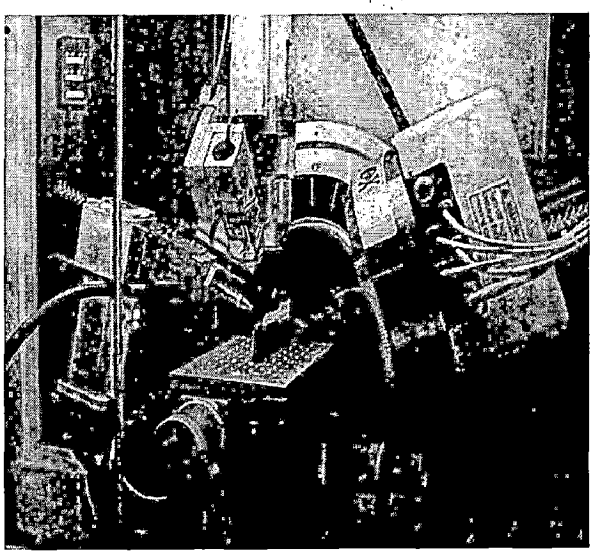

Figure 12: XRD Instrument

The X-ray Diffractometer patterns of the samples were obtained by Bruker AXS D8 Advance X-Ray Diffractometer with Cu-Kα radiation at 40kV between the scan ranges of 2θ from 5-80 degree by the scan rate of 2 degree/min. The system consists of a rotating anode generator with a Cu target. The generator was operated at 40 kV and 30 mA. All the experiments were performed

in the reflection mode. The d spacing was calculated by Bragg's formula where the λ was 0.154 nm.

2.5.5 Transmission Electron Microscopy (TEM)

Transmission electron microscopy (TEM) is a microscopy technique whereby a beam of electrons is transmitted through an ultra thin specimen, interacting with the specimen as it passes through. An image is formed from the interaction of the electrons transmitted through the specimen; the image is magnified and focused onto an imaging device, such as a fluorescent screen, on a layer of photographic film, or to be detected by a sensor such as a CCD camera.

TEMs are capable of imaging at a significantly higher resolution than light microscopes, owing to the small de Broglie wavelength of electrons. This enables to examine fine detail even as small as a single column of atoms, which is tens of thousands times smaller than the smallest resolvable object in a light microscope. TEM forms a major analysis method in a range of scientific fields, in both physical and biological sciences.

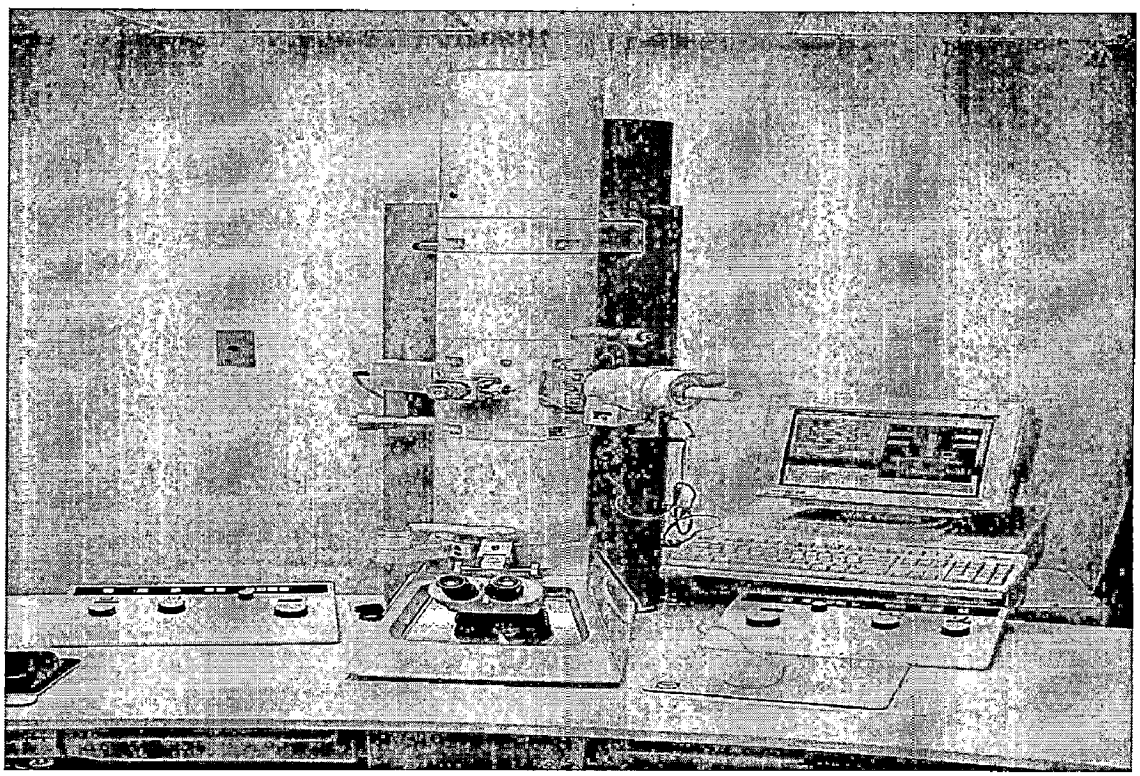

Figure 13. TEM Instrument

The first TEM was built by Max Knoll and Ernst Ruska in 1931, with this group developing the first TEM with resolving power greater than that of light in 1933 and the first commercial TEM in 1939.

At smaller magnifications TEM image contrast is due to absorption of electrons in the material, due to the thickness and composition of the material. At higher magnifications complex wave interactions modulate the intensity of the image, requiring expert analysis of observed images. Alternate modes of use allow for the TEM to observe modulations in chemical identity, crystal orientation, electronic structure and sample induced electron phase shift as well as the regular absorption based imaging.

We imaged the nanoparticles with a 200 kV high-resolution transmission electron microscope (Hitachi H-7500) with a magnification of about 3350000.

CHAPTER 3

Result and Discussion

3.1. AAS ANALYSIS

The AAS analysis was conducted to measure the amount of silver extracted from aqueous phase to organic phase. The concentration of silver in organic phase was calculated as follows-

$[Ag]_{Organic} = [Ag]_{Aqueous\ initial} - [Ag]_{Aqueous\ after\ extraction}$

The percent extraction was calculated using the following expression-

$$\%E = \frac{[Ag]organic}{[Ag]aqueous\ initial} \times 100$$

3.1.1. Extraction data for Silver in Cyanex 923/ Cyanex 471X / Aliquat 336

Table 14. AAS data for Silver in Cyanex 923 at 0.1M HNO_3.

S. No.	Cyanex 923 mol L^{-1}	$AgNO_3$ mol L^{-1}	Silver Extracted (%)
1	0.01	0.01	99.99
2	0.02	0.01	99.99
3	0.05	0.01	99.99
4	0.01	0.02	99.99
5	0.02	0.02	99.99
6	0.05	0.02	99.99

Table 15. AAS data for Silver in Cyanex 923 at 0.5M HNO_3.

S. No.	Cyanex 923 mol L^{-1}	$AgNO_3$ mol L^{-1}	Silver Extracted (%)
1	0.01	0.01	99.99
2	0.02	0.01	99.99
3	0.05	0.01	99.99

Table 16. AAS data for Silver in Cyanex 923 at 1M HNO_3.

S. No.	Cyanex 923 mol L^{-1}	$AgNO_3$ mol L^{-1}	Silver Extracted (%)
1	0.01	0.01	99.99
2	0.02	0.01	99.99
3	0.05	0.01	99.99

Table 17. AAS data for Silver in Cyanex 471 X at 0.1M HNO_3.

S. No.	Cyanex 471X mol L^{-1}	$AgNO_3$ mol L^{-1}	Silver Extracted (%)
1	0.01	0.01	99.99
2	0.02	0.01	99.99
3	0.05	0.01	99.99
4	0.01	0.02	99.99
5	0.02	0.02	99.99
6	0.05	0.02	99.99

Table 18. AAS data for Silver in Cyanex 471 X at 0.5M HNO_3.

S. No.	Cyanex 471 X mol L^{-1}	$AgNO_3$ mol L^{-1}	Silver Extracted (%)
1	0.01	0.01	99.99
2	0.02	0.01	99.99
3	0.05	0.01	99.99

Table 19. AAS data for Silver in Cyanex 471 X at 1M HNO_3.

S. No.	Cyanex 471 X mol L^{-1}	$AgNO_3$ mol L^{-1}	Silver Extracted (%)
1	0.01	0.01	99.99
2	0.02	0.01	99.99
3	0.05	0.01	99.99

Table 20. AAS data for Silver in Aliquat 336 at 0.1 M HNO_3.

S. No.	Aliquat 336 mol L^{-1}	$AgNO_3$ mol L^{-1}	Silver Extracted (%)
1	0.3 in 0.1 M HNO_3	0.01	69.13
2	0.3 in 0.5 M HNO_3	0.01	67.90

The AAS data show that the transfer of Silver ion from aqueous phase to organic phase was almost complete in Cyanex 923 and Cyanex 471X but in the case of Aliquat 336 the persentage extraction was less (68 %). The extraction data further indicates that variation in the molarity of nitric acid, Cyanex 923, Cyanex 471X and Aliquat does not affect the extraction of silver significantly.

3.2. FTIR Spectra (FTIR)

The Silver nanoparticles synthesized using different schemes were analyzed by FTIR to study the interaction between Ag nanoparticle and Cyanex/ Aliquat. The different FTIR spectra are shown in figures (14-26).

3.2.1 FTIR analysis of Silver -Cyanex 923 sample.

The FTIR spectrum of pure Cyanex 923 provides information about different groups present in the system. The peak at 3400- 3500 cm^{-1} in the spectrum of pure Cyanex is attributed to –OH stretching due to some moisture present in the system and –OH bending frequency observed at about 1630 – 1645 cm^{-1} attributed to bending vibration. The peak at 2850-2950 cm^{-1} is attributed to $(-CH_2)_n$ stretching vibrations and the bending vibration of $(-CH_2)_n$ are present at 1440 to 1470 cm^{-1}, this is also assigned to asymmetric deformation of $-CH_3$ group. The peak at 810-830 cm^{-1} is assigned to the -(C-H) out of plane bending vibration. The peak at 710-740 cm^{-1} is attributed to –CH bending vibration but it appears as weak vibration. The peak at 1370- 1390 cm^{-1} is due to (P=O) stretching vibration and peak at 1130- 1160 cm^{-1} is due to $(R\text{-}P^{+}\text{-}O^{-})$.

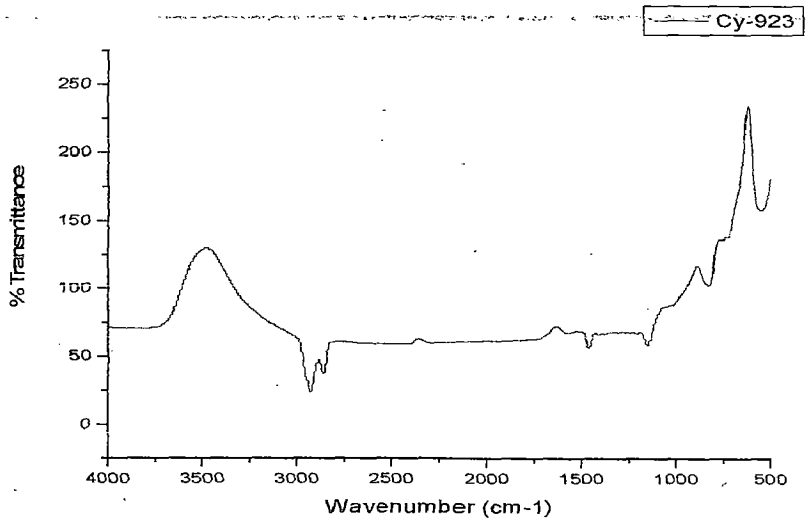

Figure 14. FTIR spectra of Cyanex 923

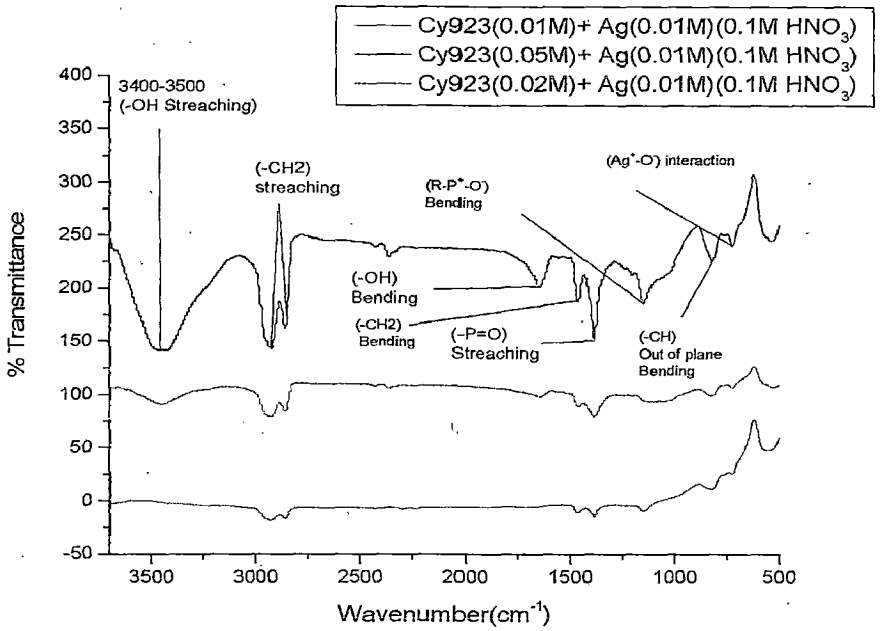

Figure 15. FTIR spectra of Silver- Cyanex 923 Sample

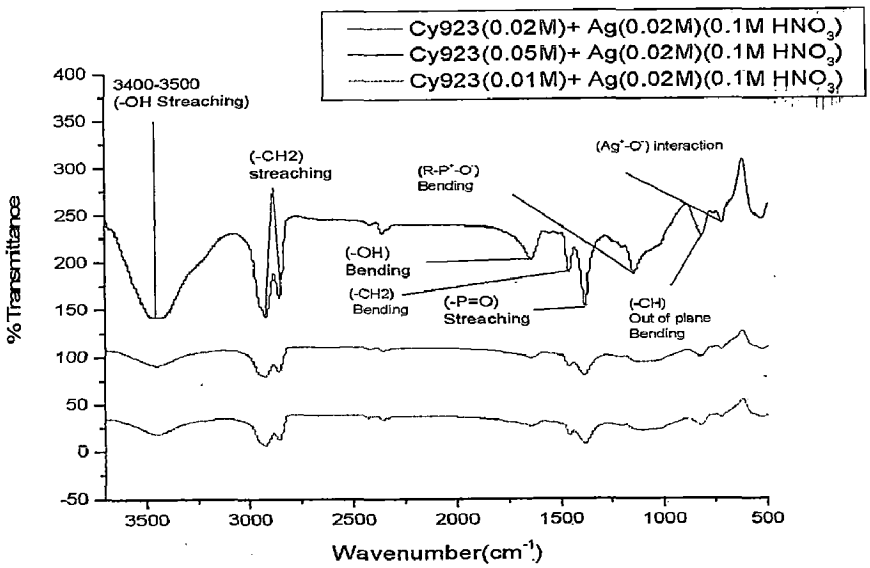

Figure 16 : FTIR spectra of Silver- Cyanex 923 Sample

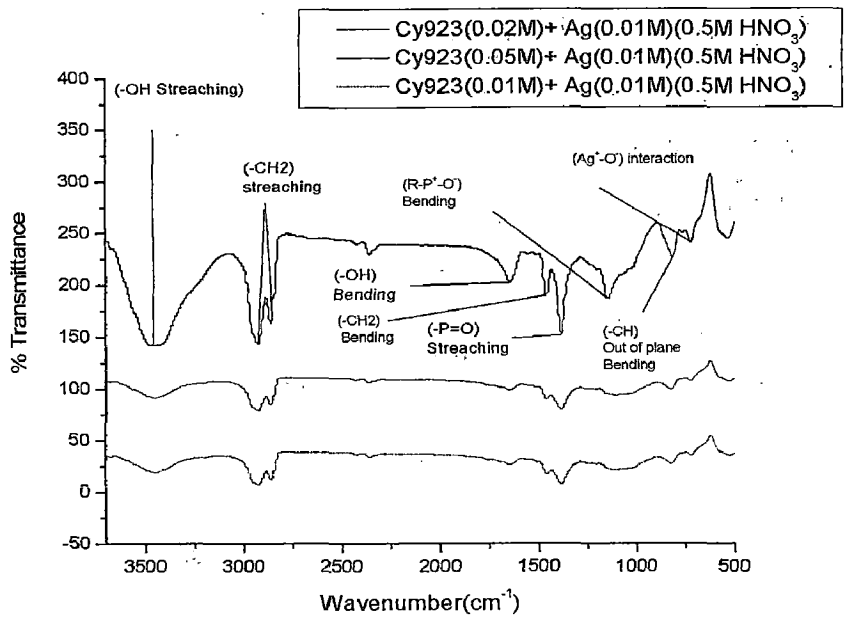

Figure 17. FTIR spectra of Silver- Cyanex 923 Sample

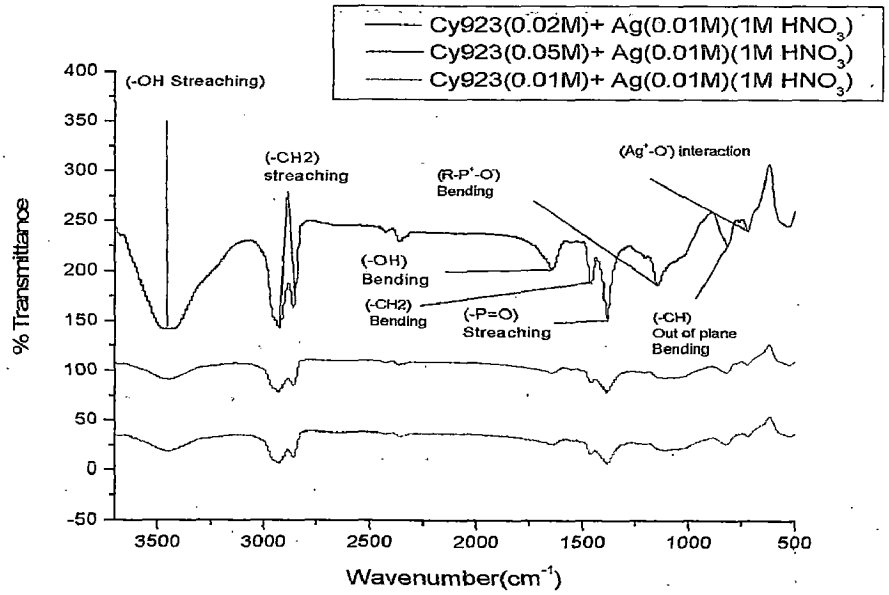

Figure 18. FTIR spectra of Silver - Cyanex 923 Sample

The FR-IR spectra of silver nanoparticles with different Cyanex 923 concentrations show similar peaks as the pure Cyanex 923 sample but some differences were observed.. The peak at 3400 - 3500 cm^{-1} due to (-OH) stretching vibration is more intense in comparison to pure Cyanex 923 as the moisture is more in the system due to mixing of aqueous and organic layer. The $(-CH_2)_n$ stretching vibration frequencies are found almost in the same region as in pure Cyanex 923, the peaks appears at 2850 - 2950 cm^{-1}. The peak of (-OH) bending vibration appears in the same region as in pure Cyanex 923 (1630 - 1650 cm^{-1}). The peaks at 1450 - 1465 cm^{-1} , 810 - 850 cm^{-1}, 710 – 740 cm^{-1} , 1360 - 1390 cm^{-1} , 1140 – 1170 cm^{-1} are same as in pure Cyanex 923. A new intense peak appears at 634cm^{-1} due to interaction of Ag and Cyanex 923. Further it is observed that as the concentration of Cyanex 923 increases the peaks in the region of 630 -650 cm^{-1} become more intense.

3.2.2 FTIR analysis of Silver - Cyanex 471X Sample.

The FTIR spectrum of pure Cyanex 471X shows following peaks

The peak at 3400-3600 cm^{-1} observed in the spectrum of pure Cyanex 923 is absent in Cyanex 471X due to absence of Hydrogen Bonding in -(S-H), and the –OH bending vibration is also absent in the system. The peak at 2850-2950 cm^{-1} is attributed to $(-CH_2)_n$ stretching vibrations and the bending vibration of $(-CH_2)_n$ are present at 1440-1470 cm^{-1}. The peak at 810-830 cm^{-1} is assigned to the -(C-H) out of plane bending vibration. The peak at 710-740 cm^{-1} is attributed to –CH bending vibration. The peak at 1350 -1380 cm^{-1} is due to (P=S) stretching vibration and peak at 1150 – 1180 cm^{-1} is due to $(R\text{-}P^{+}\text{-}S^{-})$.

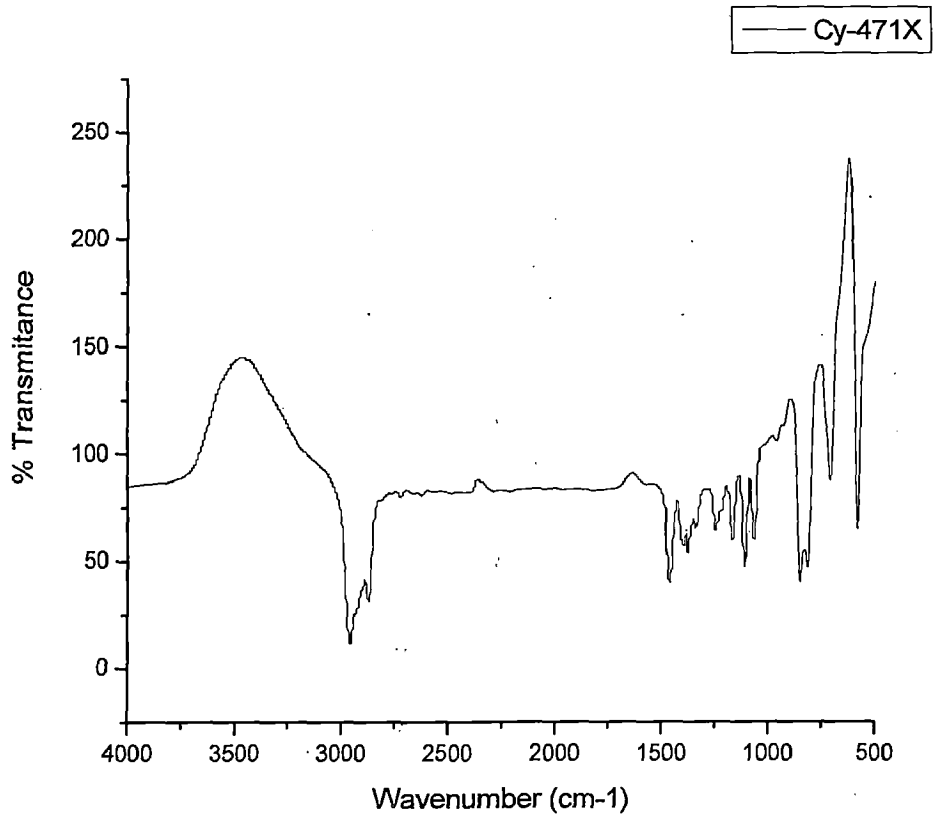

Figure 19. FTIR spectra of Cyanex 471X

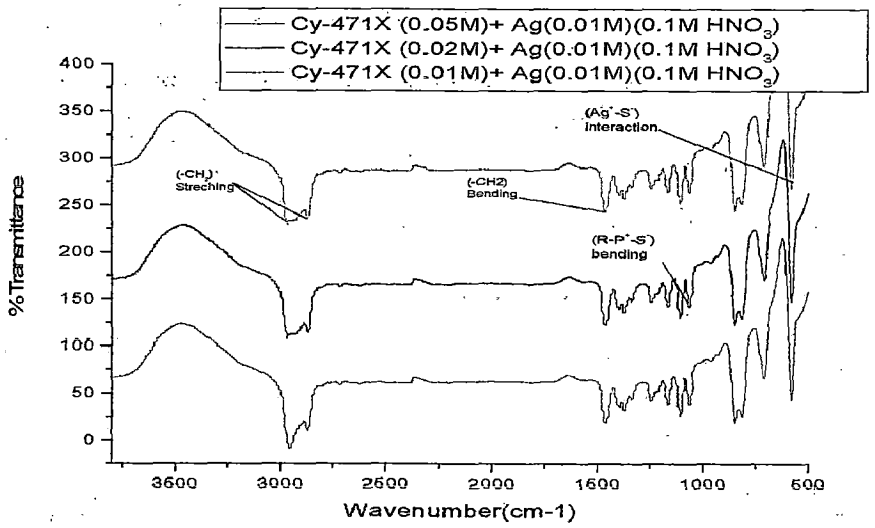

Figure 20. FTIR spectra of Silver - Cyanex 471X Sample

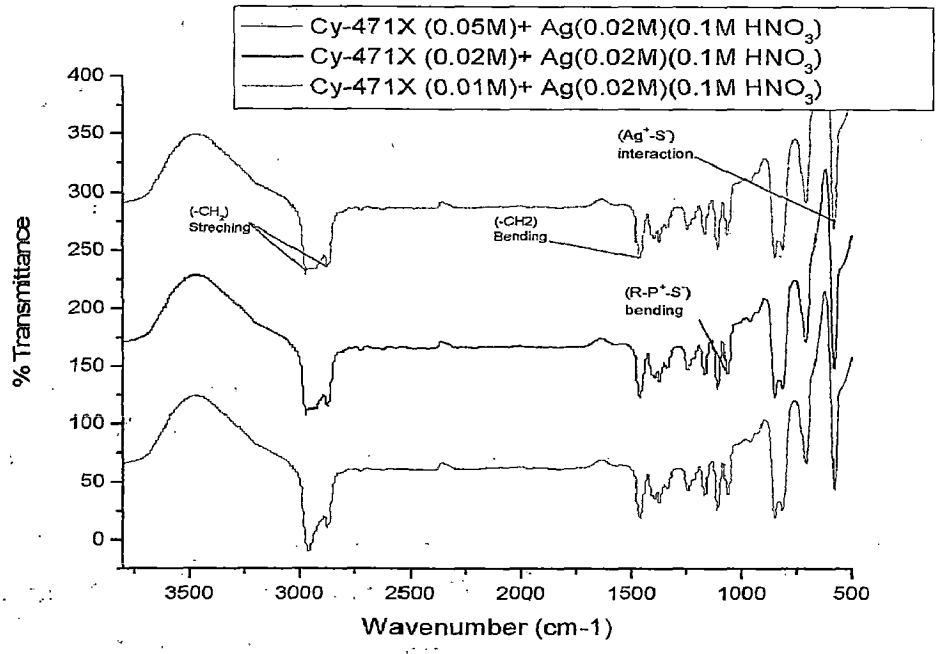

Figure 21. FTIR spectra of Silver - Cyanex 471X Sample

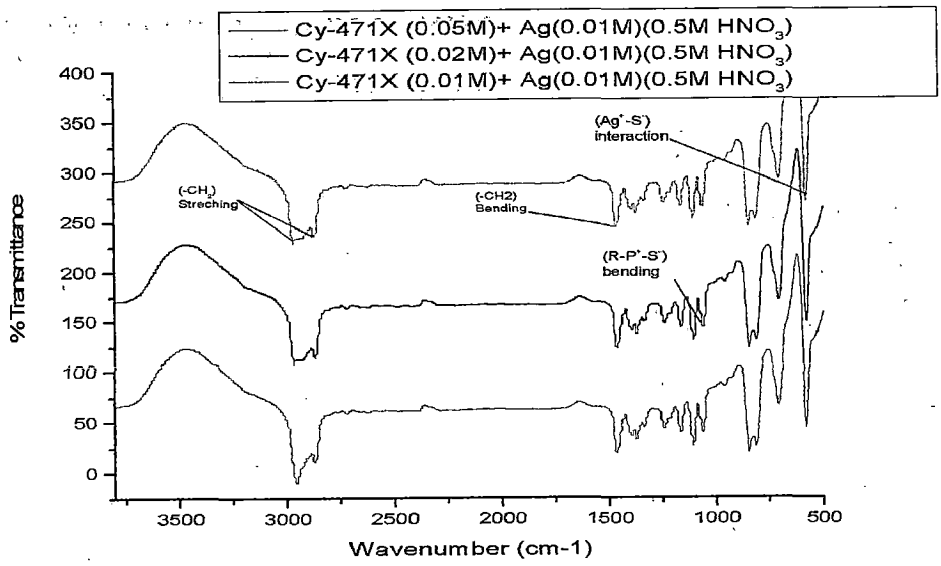

Figure 22. FTIR spectra of Silver - Cyanex 471X Sample

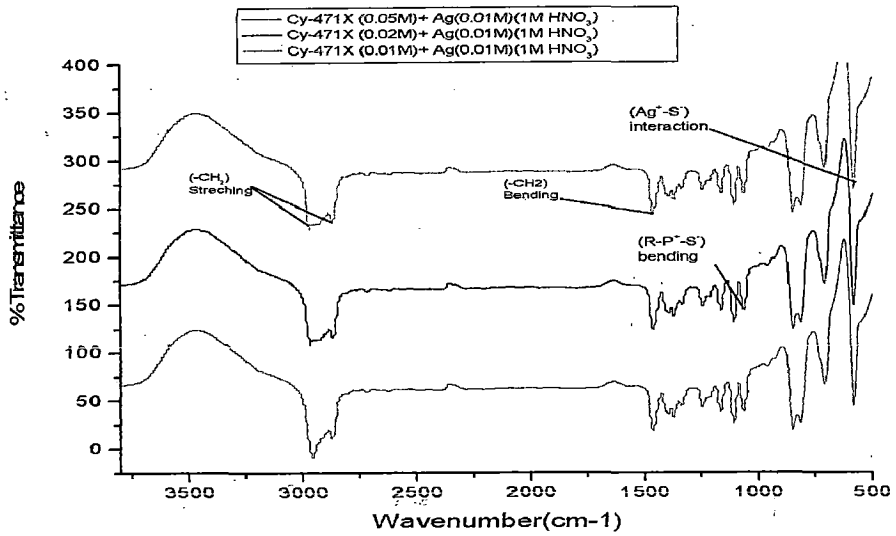

Figure 23. FTIR spectra of Silver - Cyanex 471X Sample

The FR-IR spectra of silver nanoparticles with different Cyanex 471 X concentrations reveal a new intense peak at 580 - 570 cm^{-1} due to interaction of Ag and Cyanex 471X. As the concentration of Cyanex 471 X increases the interaction between Ag and Cyanex is more and is reflected in the region 580 to 570 cm^{-1}.

3.2.3 FTIR analysis of Silver - Aliquat 336 sample.

The FTIR spectrum of pure Aliquat 336 provides following information. The peak at 2850-2950 cm^{-1} is attributed to $(-CH_2)_n$ stretching vibration the bending vibration of $(-CH_2)_n$ are present at 1440-1470 cm^{-1}. The peak at 810-830 cm^{-1} is assigned to the -(C-H) out of plane bending vibration. The peak at 710-740 cm^{-1} is attributed to –CH bending vibration but it appears as weak vibration. The peak at 2310 cm-1 is due to -(C-N) stretching vibration and peak at 1630- 1660 cm^{-1} is due to- (C-N) bending vibrations.

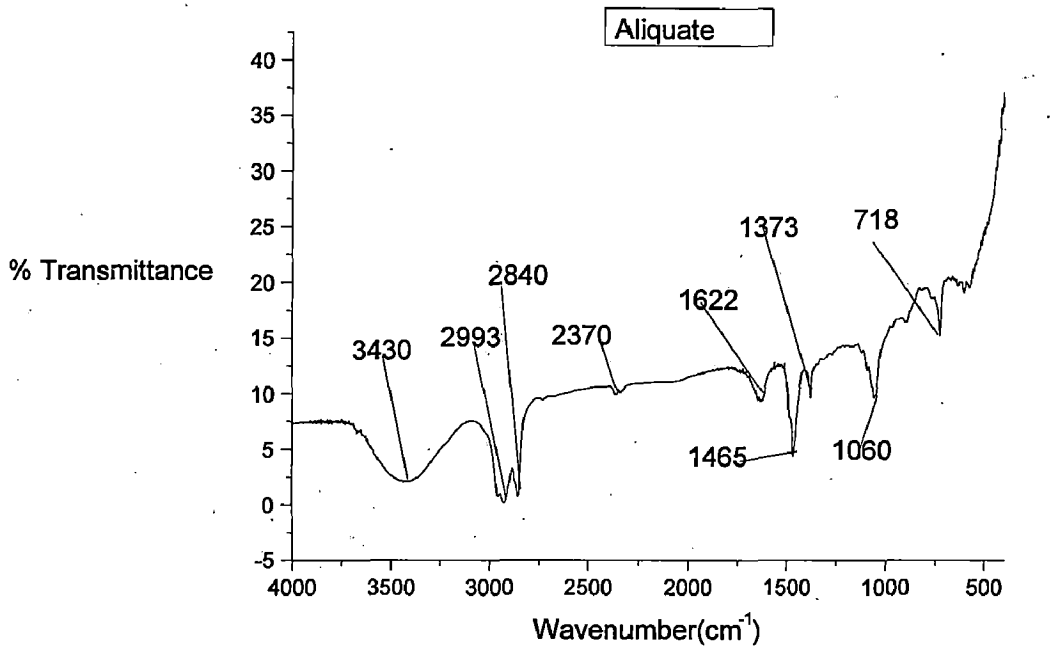

Figure 24. FTIR spectrum of Pure Aliquat 336 .

The FR-IR spectra of silver nanoparticles with different Aliquat 336 concentrations show similar peaks as the pure Aliquat 336 spectrum. A new broad peak appeares at 625 cm^{-1}due to interaction of Ag and Aliquat 336.

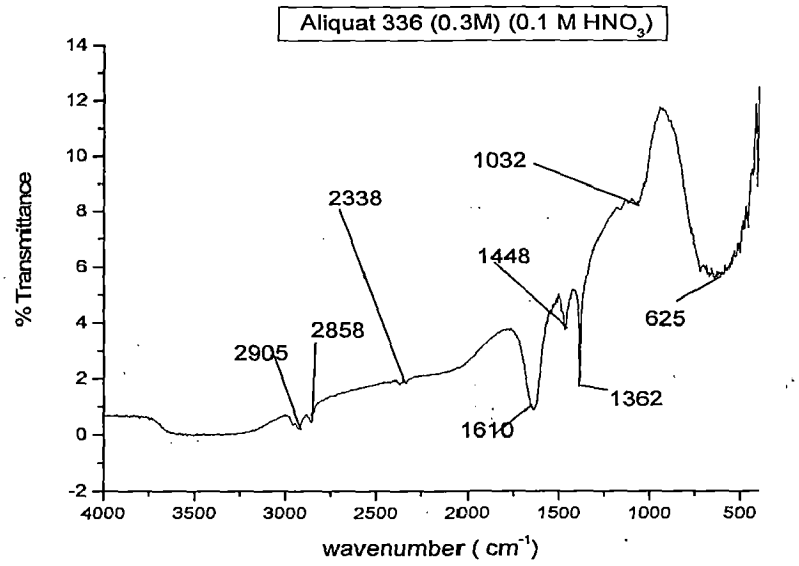

Figure 25. FTIR of Spectrum of Silver - Aliquat 336 sample

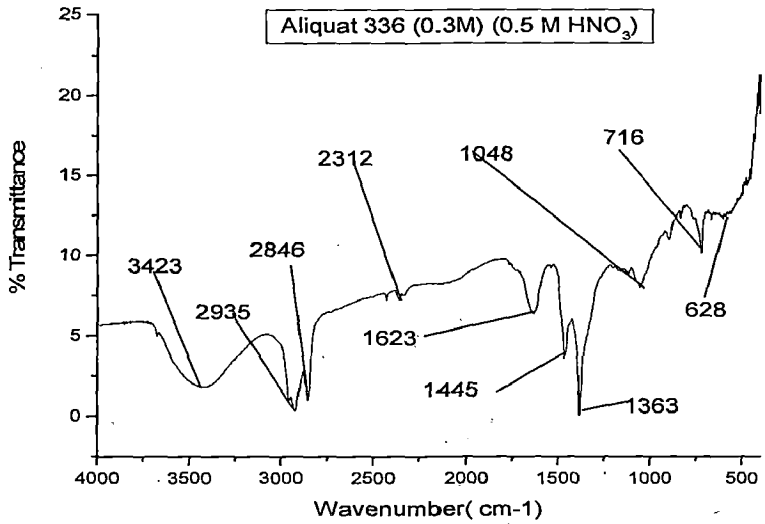

Figure 26. FTIR of Spectrum of Silver -Aliquat 336 sample

As the concentration of Cyanex increase the interaction between Ag and Aliquat 336 is more and it is shown in region of 680 to 570 cm^{-1}.

3.3. Atomic Force Microscopy (AFM) Studies

AFM is used to study the particle size, grain and roughness of nanoparticles. Silver nanoparticles synthesized following different schemes were examined by AFM. Various parameter were determined by software itself. AFM images of silver nanoparticles placed on glass plate revealed that the particles are spherical in nature with diameter ranging from 10 to 70 nm. The results of AFM analysis are shown in figure (27-42).

3.3.1 AFM analysis of Silver - Cyanex 923 Sample

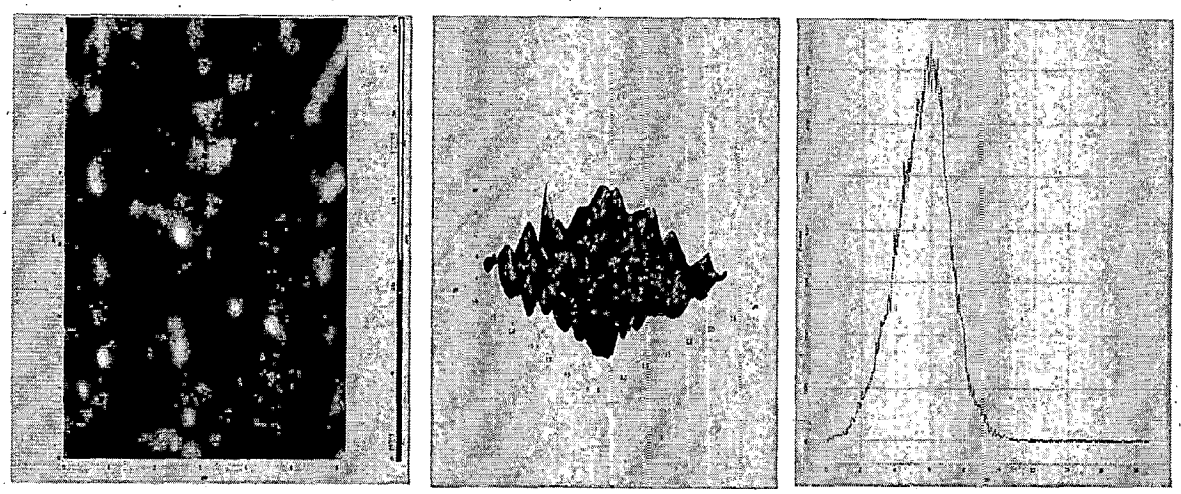

Scheme	Roughness (nm)	Particle Size (nm)	Grain
Cyanex 923 (0.01 M) , Ag (0.01 M), HNO_3(0.1M)	2 nm	9 nm	12

Figure 27. AFM image and Histogram of Silver - Cyanex 923 sample.

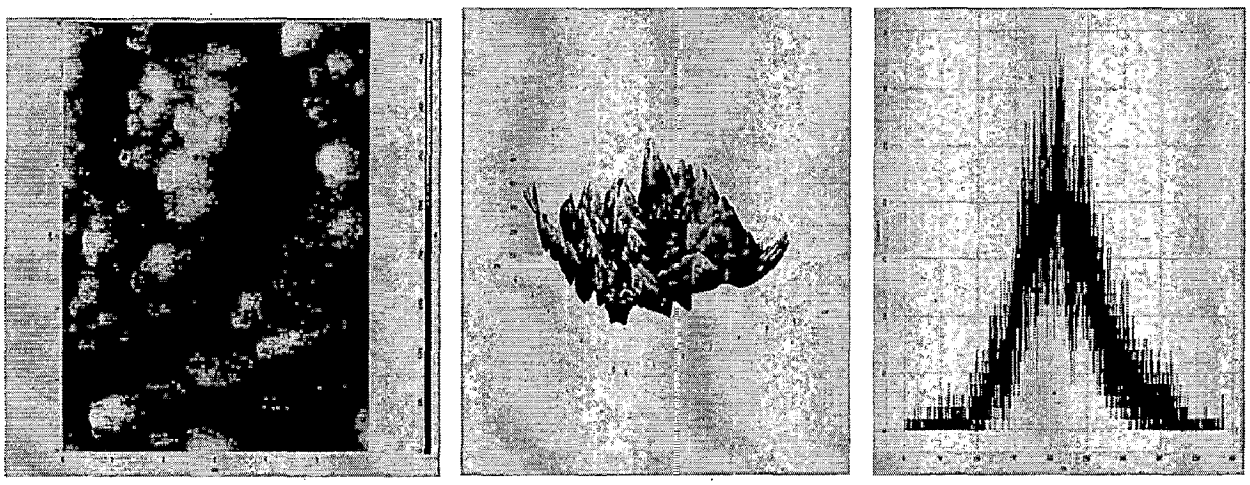

Scheme	Roughness (nm)	Particle Size (nm)	Grain
Cyanex 923 (0.02M), Ag (0.01 M), HNO_3 (0.1M)	28 nm	53nm	42

Figure 28. AFM image and Histogram of Silver - Cyanex 923 sample.

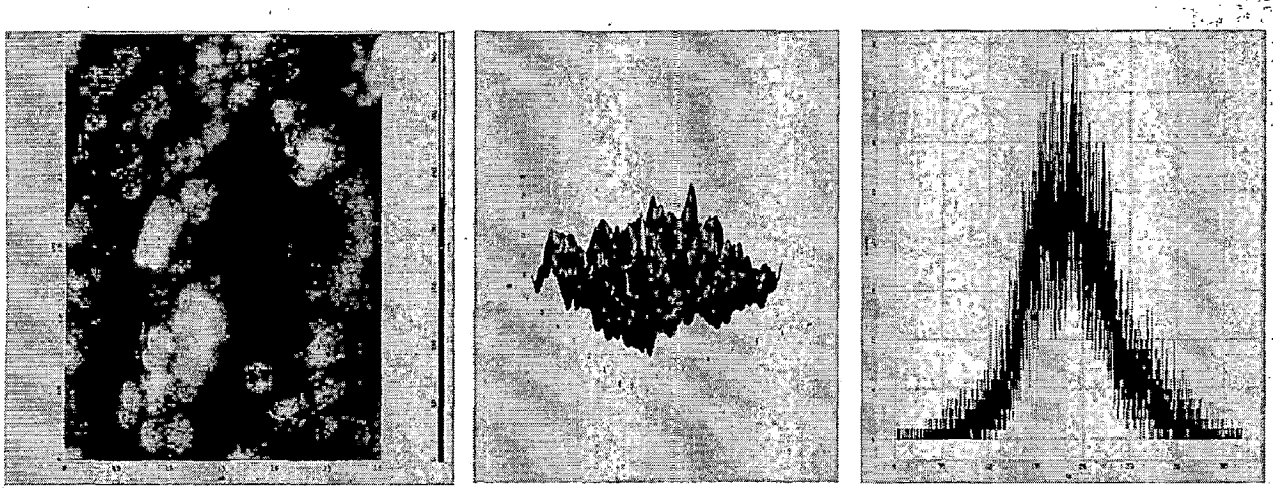

Scheme	Roughness (nm)	Particle Size (nm)	Grain
Cyanex 923 (0.05M) , Ag (0.01 M) , HNO_3 (0.1 M)	48 nm	63nm	59

Figure 29. AFM image and Histogram of Silver - Cyanex 923 sample.

Scheme	Roughness (nm)	Particle Size (nm)	Grain
Cyanex 923 (0.01M) , Ag (0.02 M) , HNO_3 (0.1 M)	37 nm	51nm	65

Figure 30 . AFM image and Histogram of Silver - Cyanex 923 sample.

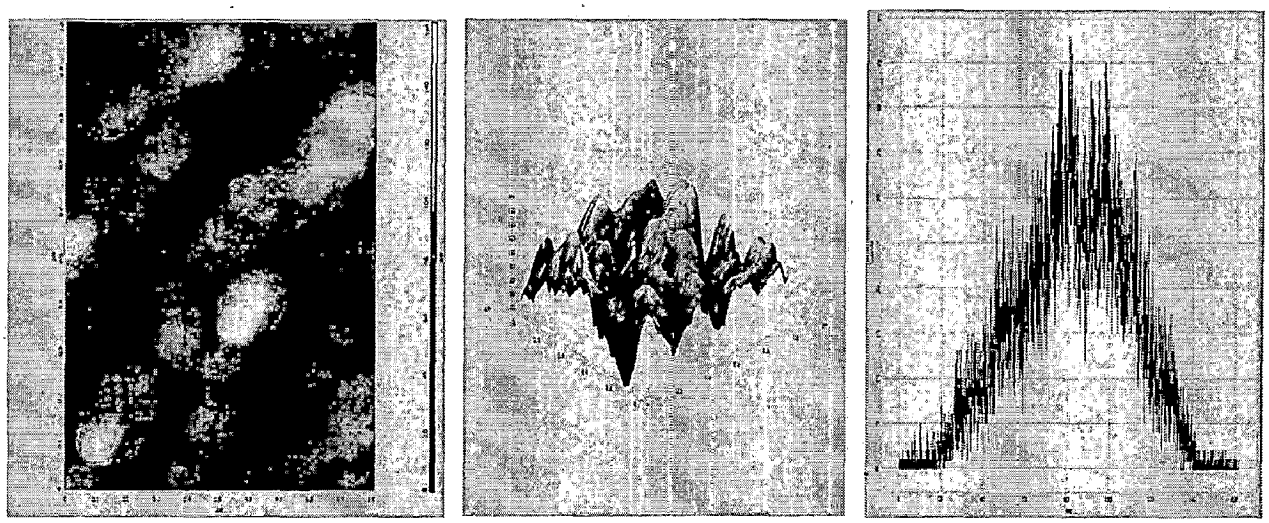

Scheme	Roughness (nm)	Particle Size (nm)	Grain
Cyanex 923 (0.02M) , Ag (0.02 M) , HNO_3 (0.1 M)	26 nm	61nm	45

Figure 31. AFM image and Histogram of Silver - Cyanex 923 sample.

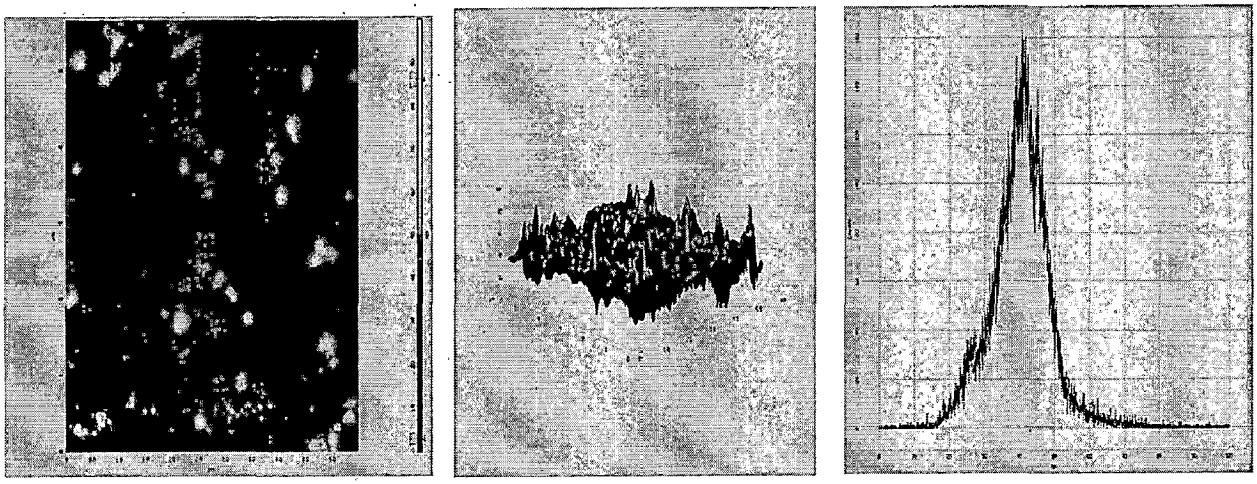

Scheme	Roughness (nm)	Particle Size (nm)	Grain
Cyanex 923 (0.05M) , Ag (0.02 M) , HNO_3 (0.1 M)	19 nm	50nm	79

Figure 32. AFM image and Histogram of Silver - Cyanex 923 sample.

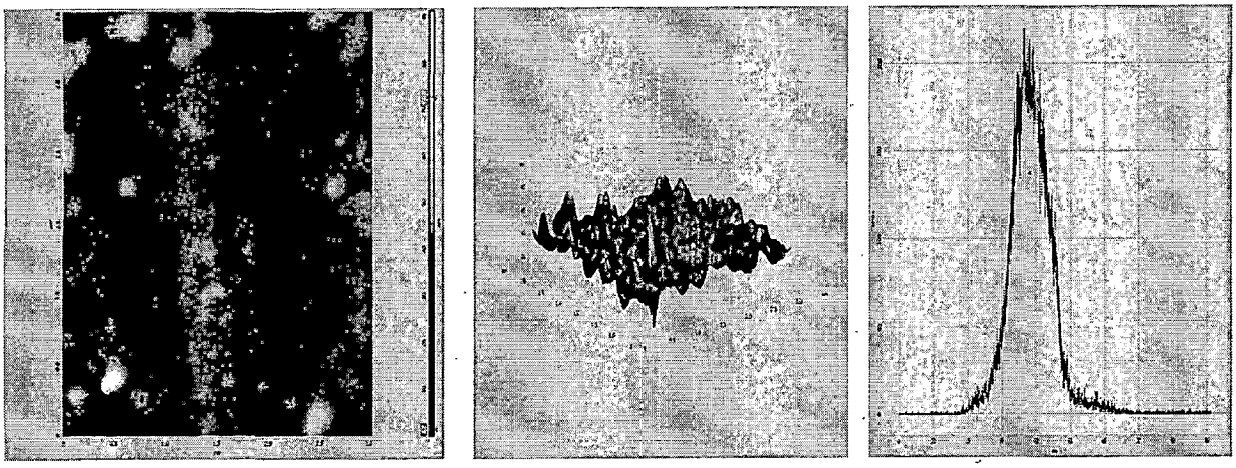

Scheme	Roughness (nm)	Particle Size (nm)	Grain
Cyanex 923 (0.01M) , Ag (0.01 M) HNO_3, (0.5 M)	6 nm	45nm	40

Figure 33. AFM image and Histogram of Silver - Cyanex 923 sample.

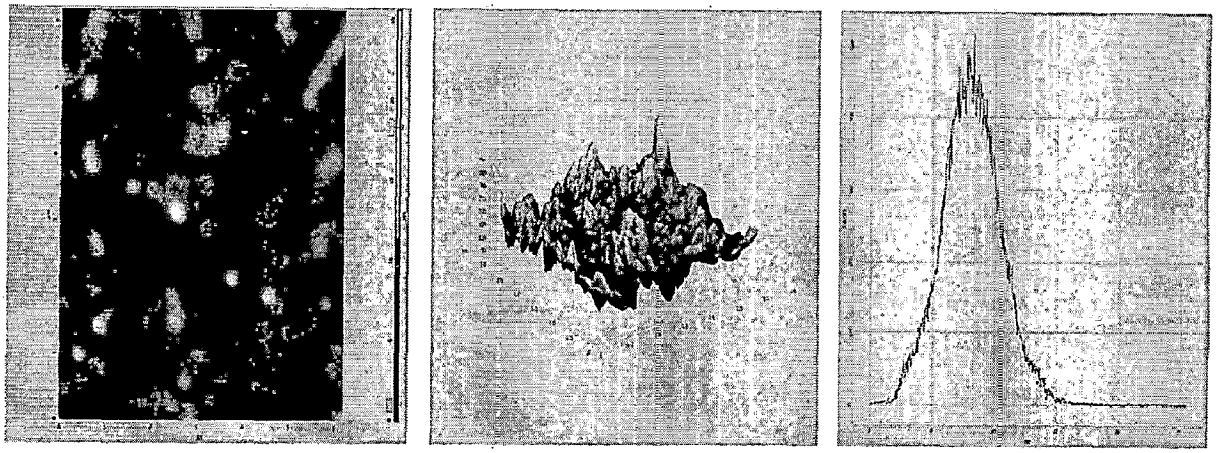

Scheme	Roughness (nm)	Particle Size (nm)	Grain
Cyanex 923 (0.02M) , Ag (0.01 M), HNO_3 (0.5 M)	8 nm	14nm	30

Figure 34. AFM image and Histogram of Silver - Cyanex 923 sample.

3.3.2 AFM analysis of Silver - Cyanex 471X Sample.

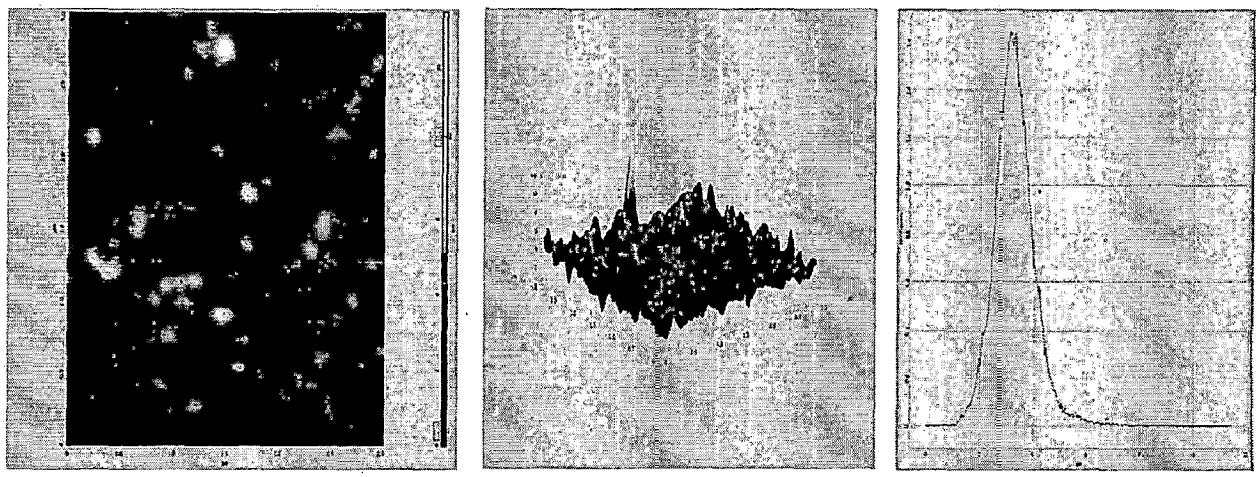

Scheme	Roughness (nm)	Particle Size (nm)	Grain
Cyanex 471X (0.01 M) , Ag (0.01 M), HNO_3 (0.1 M)	1	6	19

Figure 35. AFM image and Histogram of Cyanex 471X - Silver nanoparticles.

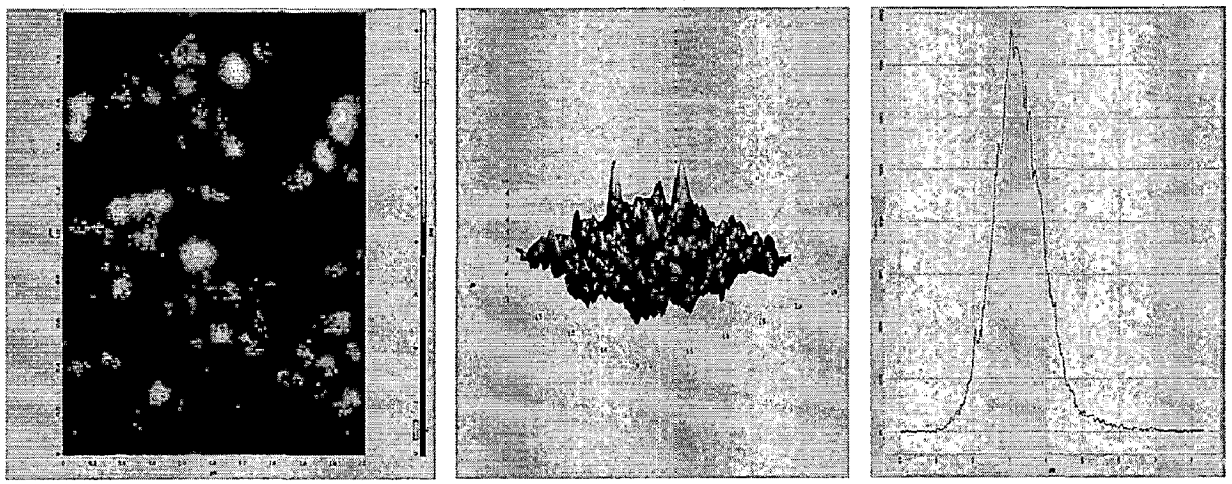

Scheme	Roughness (nm)	Particle Size (nm)	Grain
Cyanex 471X (0.02 M) , Ag (0.01 M) , HNO_3 (0.1 M)	1	4	51

Figure 36. AFM image and Histogram of Silver - Cyanex 471X sample.

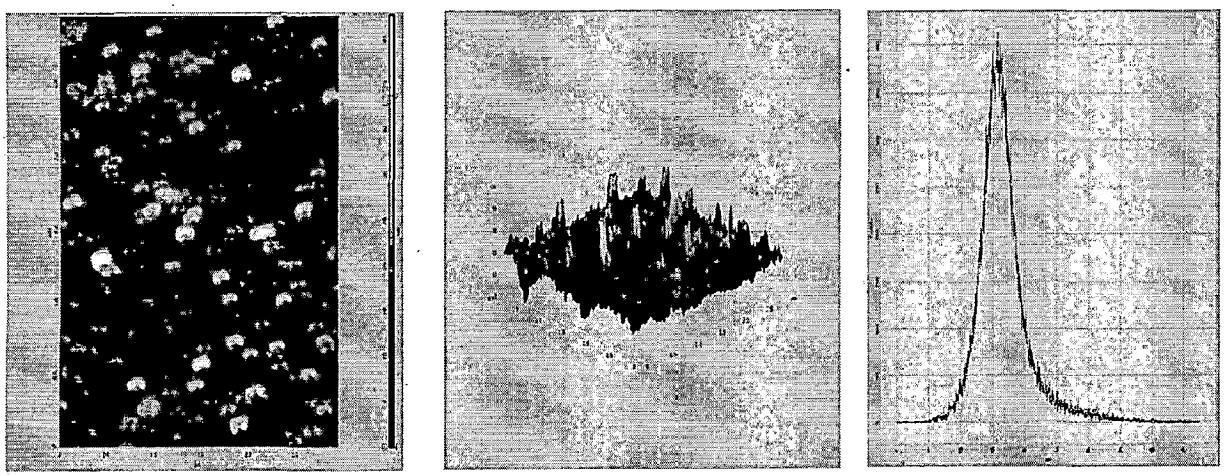

Scheme	Roughness (nm)	Particle Size (nm)	Grain
Cyanex 471X (0.05 M) , Ag (0.01 M), HNO_3 (0.1 M)	4	23	92

Figure 37. AFM image and Histogram of Silver - Cyanex 471X sample.

G 21216

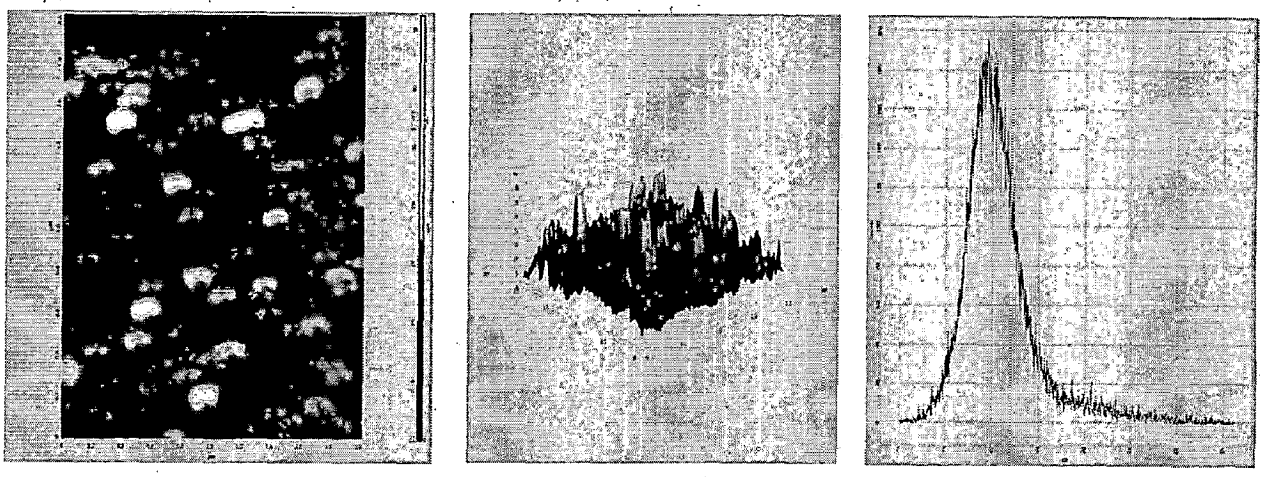

Scheme	Roughness (nm)	Particle Size (nm)	Grain
Cyanex 471X (0.01 M) , Ag (0.02 M), HNO_3 (0.1 M)	2	18	41

Figure 38. AFM image and Histogram of Silver - Cyanex 471X sample.

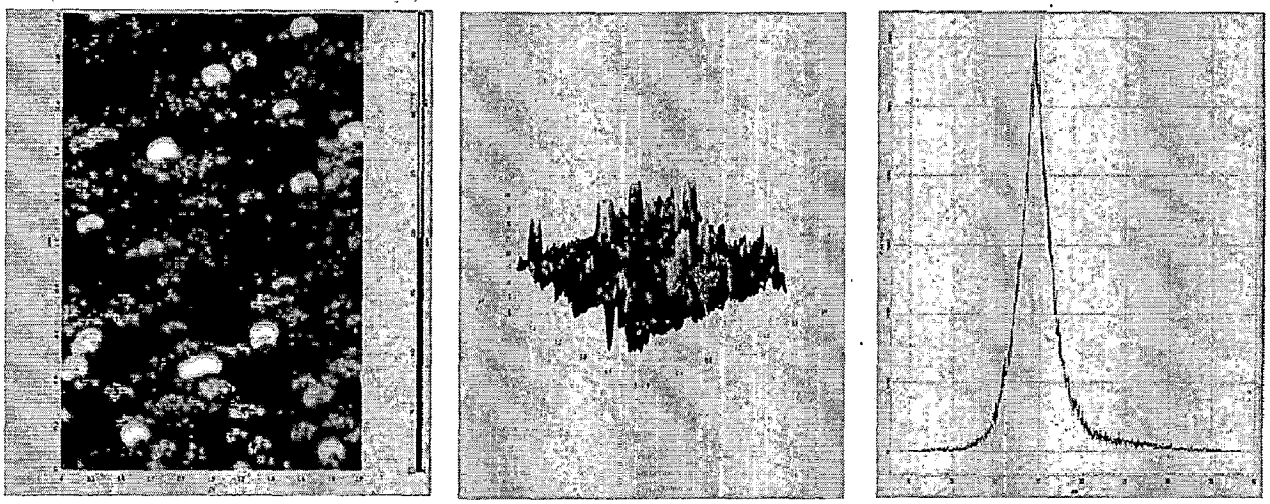

Scheme	Roughness (nm)	Particle Size (nm)	Grain
Cyanex 471X (0.02 M) , Ag (0.02 M), HNO_3 (0.1 M)	4	19	113

Figure 39. AFM image and Histogram of Silver - Cyanex 471X sample.

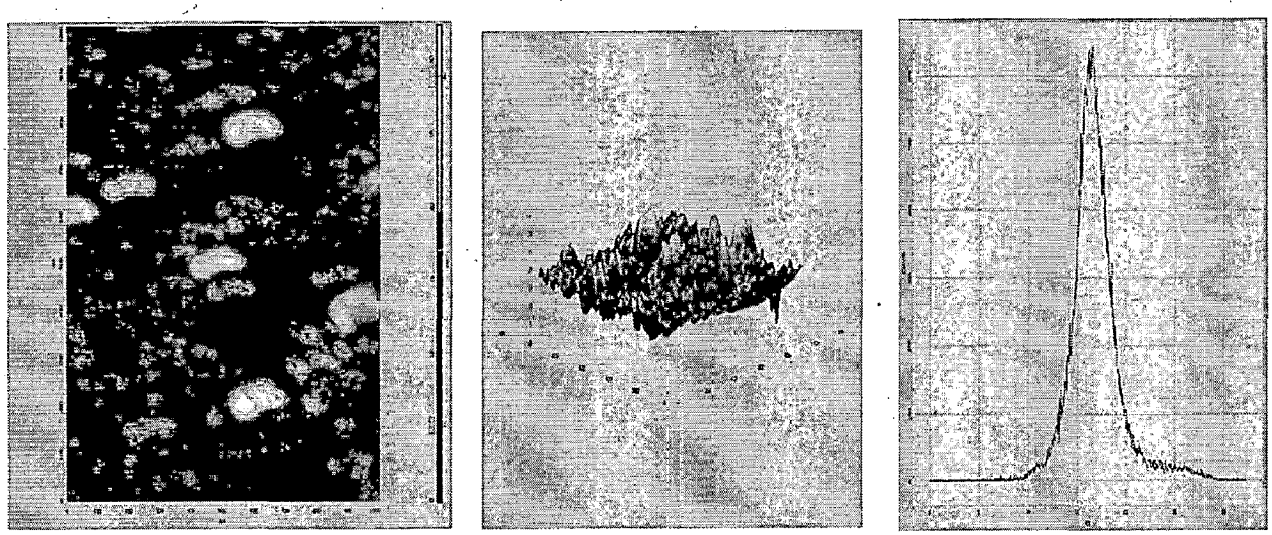

Scheme	Roughness (nm)	Particle Size (nm)	Grain
Cyanex 471X (0.05 M) ,Ag (0.02 M) , HNO_3 (0.1 M)	3	16	104

Figure 40. AFM image and Histogram of Silver - Cyanex 471X sample.

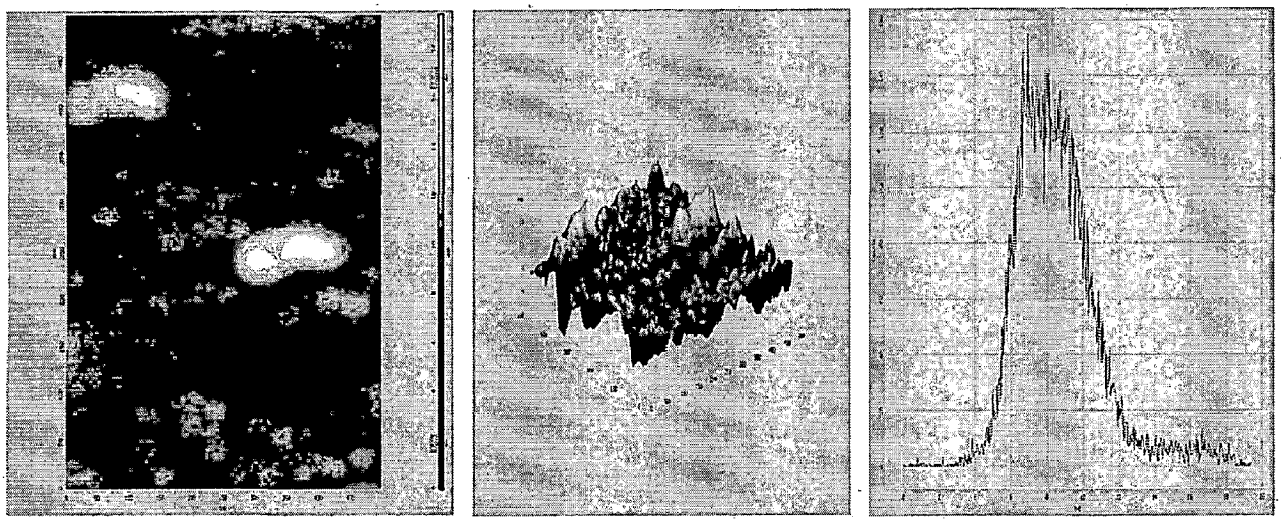

Scheme	Roughness (nm)	Particle Size (nm)	Grain
Cyanex 471X (0.01M) , Ag (0.01 M) , HNO_3 (0.5 M)	2	10	55

Figure 41. AFM image and Histogram of Silver - Cyanex 471X sample.

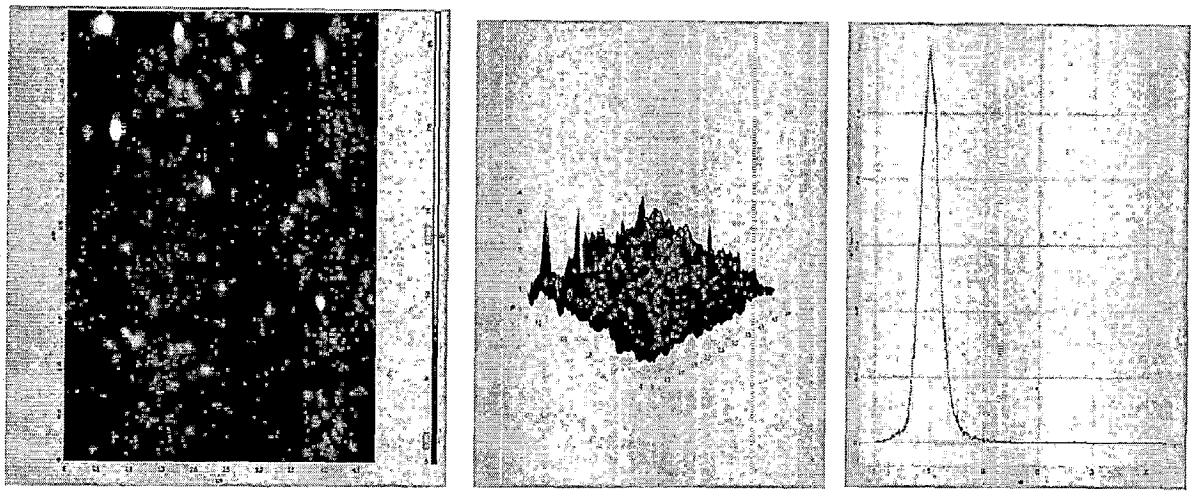

Scheme	Roughness (nm)	Particle Size (nm)	Grain
Cyanex 471X (0.02M) , Ag (0.01 M), HNO_3 (0.5 M)	1	13	16

Figure 42. AFM image and Histogram of Silver - Cyanex 471X sample.

AFM analysis of silver – Cyanex nanoparticles revealed that the particles were spherical in shape and the particle size in Silver – Cyanex 923 samples vary from 9 to 63 nm whereas in case of Silver – Cyanex 471X samples it varies from was 4 to 23 nm. Thus AFM analysis revealed that with Cyanex 471 X small size nanoparticles are obtained as compared to Cyanex 923.

3.4. XRD Analysis

The evidence of formation of silver nanoparticles is analyzed by XRD. The X-ray 2θ range was 10° to 90 °. Figures (43-54) show the XRD pattern of modified silver nanoparticles by Cyanex 923/ Cyanex 471X / Aliquate 336. The peaks were well matched with the cubic standard positions (JSPDS Data sheet no 41-1402). The particle size calculation was done by scherrer formula.

The scherrer formula is $\mathbf{t = 0.9\ \lambda / \beta \cos\theta}$

Where λ= 1.54 Å,

β = FWHM of the peak,

$\cos\theta$ = angle of rotation.

3.4.1 XRD Analysis of Silver - Cyanex 923 Sample.

XRD pattern (Figures 43- 46) shows different peaks which were indexed as (111) , (200), (220), and (311). The indexing pattern shows that the Ag nanoparticles have Face centered cubic crystal structure. There is no impurity peak in the spectra. The data is correlated with JSPDS Data sheet no (41-1402).

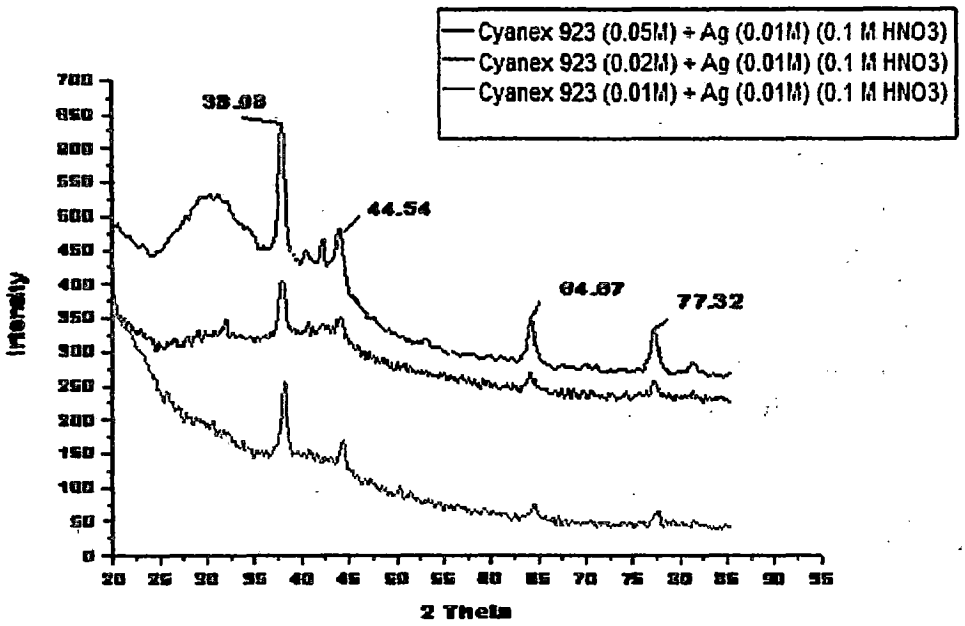

Figure 43. XRD Pattern of Silver - Cyanex 923 Sample.

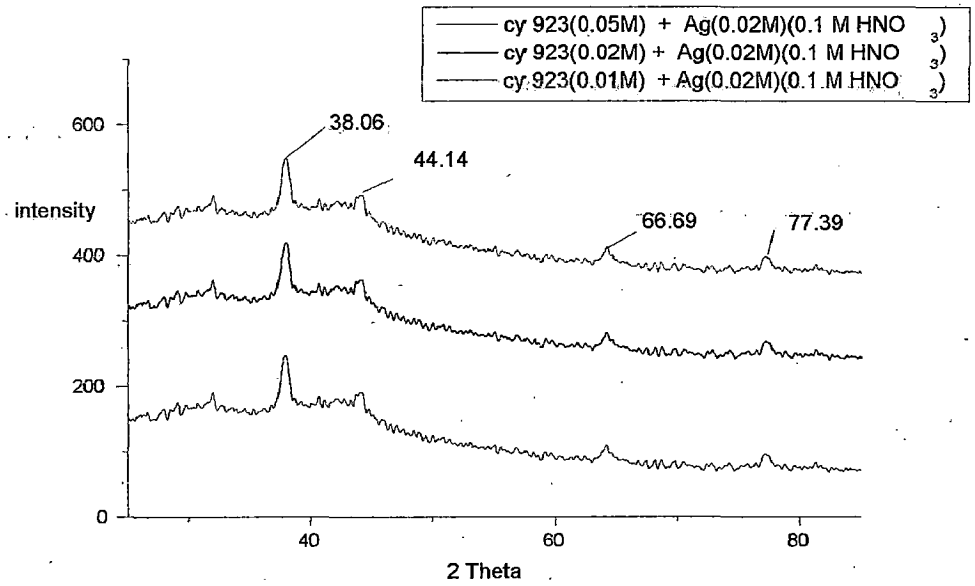

Figure 44. XRD Pattern of Silver - Cyanex 923 sample.

Table 21. Particle Size Calculation For Silver - Cyanex 923 nanoparticles by Scherrer Formula

S.No.	Matrix	β Value in radian	2θ (Degree)	Partical Size (nm)
1	Cyanex923(0.01M) + Ag(0.01M) (O.1M HNO_3)	0.01256	38.16	7.45 nm
2	Cyanex923(0.02M) + Ag(0.01M) (O.1M HNO_3)	0.01344	38.36	10.9 nm
3	Cyanex923(0.05M) + Ag(0.01M) (O.1M HNO_3)	0.01512	37.39	9.69 nm
4	Cyanex923(0.01M) + Ag(0.02M) (O.1M HNO_3)	0.01639	38.12	8.94 nm
5	Cyanex923(0.02M) + Ag(0.02M) (O.1M HNO_3)	0.01467	38.13	9.99 nm
6	Cyanex923(0.05M) + Ag(0.02M) (O.1M HNO_3)	0.1569	38.07	9.34 nm

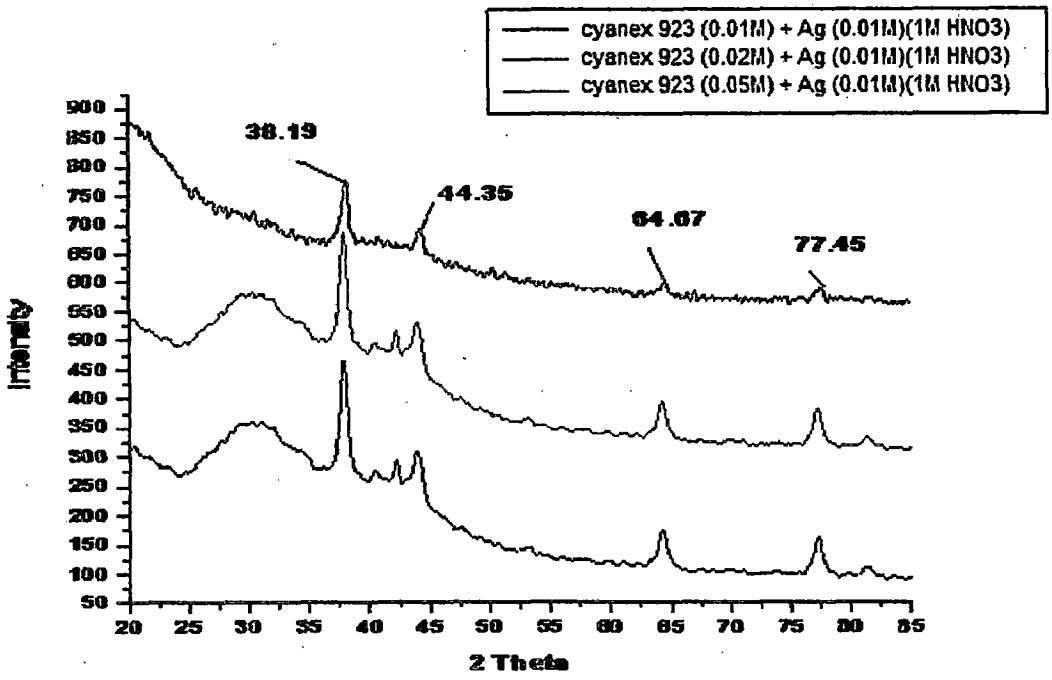

Figure 45. XRD Pattern of Silver - Cyanex 923 sample.

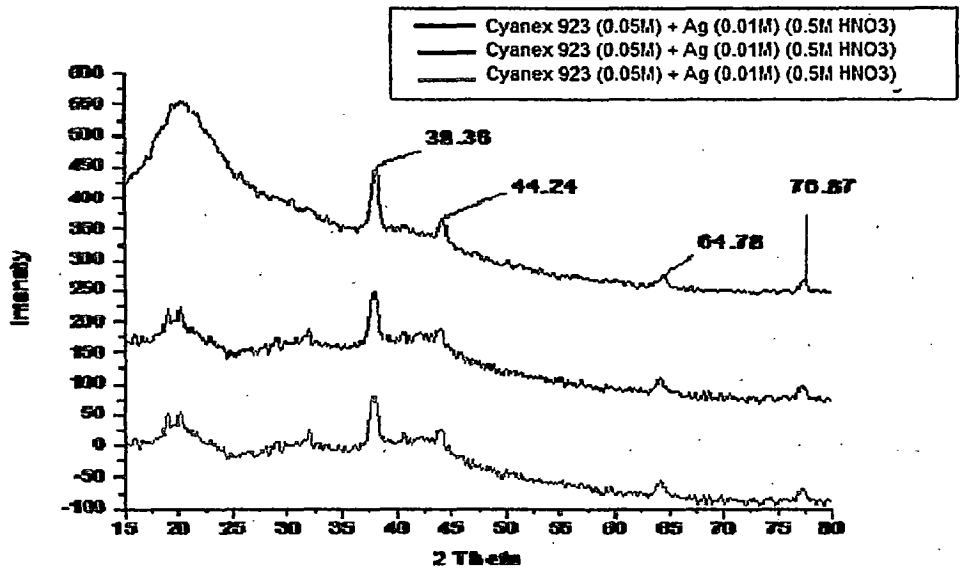

Figure 46. XRD Pattern of Silver - Cyanex 923 sample.

Table 22. Particle Size Calculation For Silver - Cyanex 923 nanoparticles by Scherrer Formula

S.No.	Matrix	β Value in radian	2θ (Degree)	Partical Size (nm)
1	Cyanex923(0.01M), Ag(0.01M) (1M HNO_3)	0.01694	38.19	8.66 nm
2	Cyanex923(0.02M), Ag(0.01M) (1M HNO_3)	0.01399	38.13	10.48 nm
3	Cyanex923(0.05M), Ag(0.01M) (1M HNO_3)	0.01236	38.16	11.21 nm
4	Cyanex923(0.01M), Ag(0.01M) (O.5M HNO_3)	0.01121	38.28	13.08 nm
5	Cyanex923(0.02M), Ag(0.01M) (O.5M HNO_3)	0.01094	38.24	13.40 nm
6	Cyanex923(0.05M), Ag(0.01M) (O.5M HNO_3)	0.01138	38.36	12.84 nm

3.4.2 XRD analysis of Silver - Cyanex 471X Sample.

XRD patterns (figure 47-50) show different peaks which were indexed as (111) , (200), (220), and (311). The indexing pattern shows that the Ag nanoparticles have Face cantered cubic crystal structure. The impurity peaks were also observed in the spectrum between 25° to 37°. The data is correlated with JSPDS Data sheet (41-1402). The main peak which should be observed at 38.26° is slightly merged with nearby peaks but the other peaks are relatively well defined and clear.

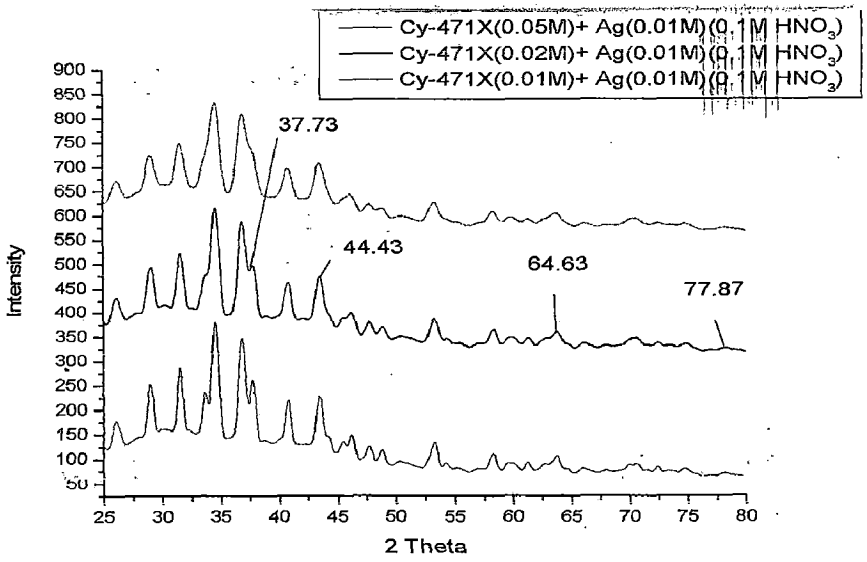

Figure 47. XRD Pattern of Silver - Cyanex 471X sample.

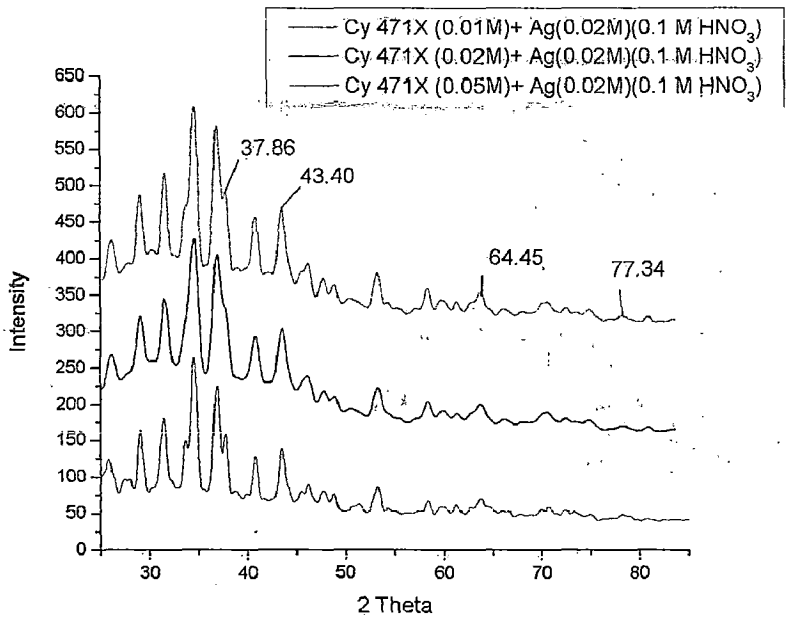

Figure 48. XRD Pattern of Silver - Cyanex 471X sample.

Table23. Particle Size Calculation For Silver - Cyanex 471X nanoparticles by Scherrer Formula.

S.No.	Matrix	β Value in radian	2θ (Degree)	Partical Size (nm)
1	Cyanex 471 X (0.01M) , Ag(0.01M) (O.1M HNO_3)	0.01256	43.41	11.88
2	Cyanex 471 X (0.02M) , Ag(0.01M) (O.1M HNO_3)	0.01385	43.43	10.77
3	Cyanex 471 X (0.05M) , Ag(0.01M) (O.1M HNO_3)	0.00831	43.42	16.66
4	Cyanex 471 X (0.01M) , Ag(0.02M) (O.1M HNO_3)	0.01255	43.41	11.88
5	Cyanex 471 X (0.02M) , Ag(0.02M) (O.1M HNO_3)	0.01394	43.45	10.71
6	Cyanex 471 X (0.05M) , Ag(0.02M) (O.1M HNO_3)	0.01046	43.45	14.25

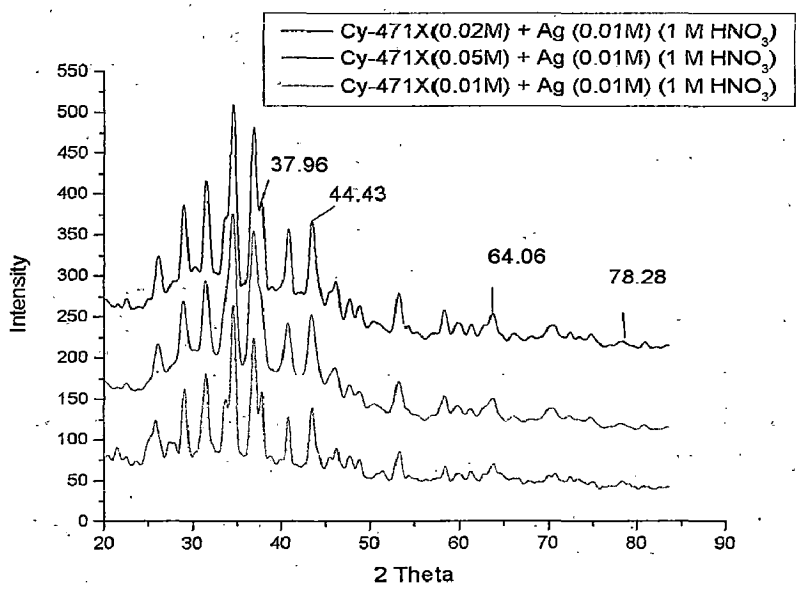

Figure 49. XRD Pattern of Silver - Cyanex 471X sample

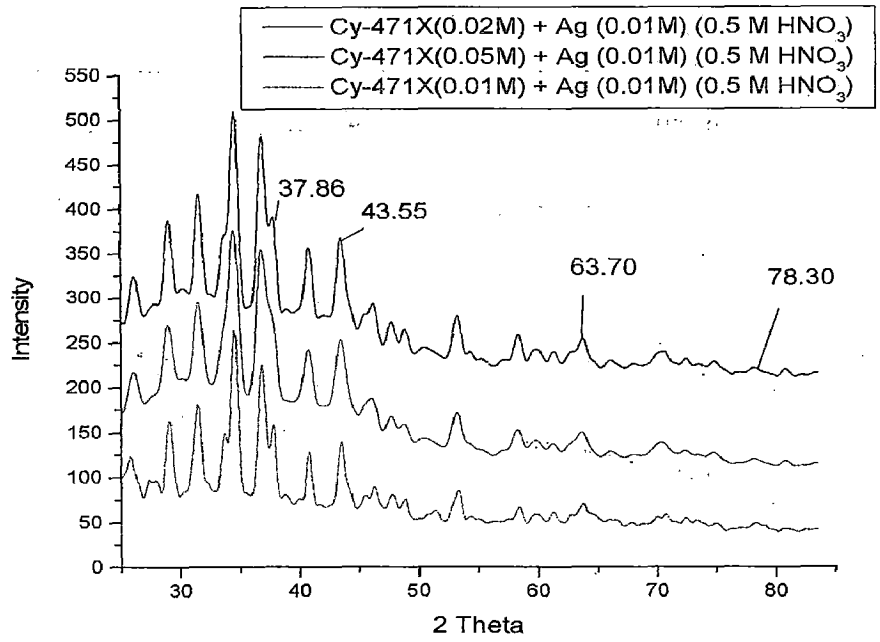

Figure 50. XRD Pattern of Silver - Cyanex 471X sample.

Table 24 Particle Size Calculation For Silver - Cyanex 471X nanoparticles by Scherrer Formula.

S.No.	Matrix	β Value in radian	2θ (Degree)	Partical Size (nm)
1	Cyanex 471 X (0.01M) , Ag(0.01M) (1M HNO_3)	0.01395	43.44	10.69
2	Cyanex 471 X (0.02M) , Ag(0.01M) (1M HNO_3)	0.01463	43.44	10.19
3	Cyanex 471 X (0.05M) , Ag(0.01M) (1M HNO_3)	0.01133	43.44	12.23
4	Cyanex 471 X (0.01M) , Ag(0.01M) (O.5M HNO_3)	0.01208	43.45	12.34
5	Cyanex 471 X (0.02M) , Ag(0.01M) (O.5M HNO_3)	0.01511	43.45	9.87
6	Cyanex 471 X (0.05M) , Ag(0.01M) (O.5M HNO_3)	0.01231	43.41	11.25

Few samples of Cyanex 923 and Cyanex 471 X were heated in muffle furnace at 600 °C to check the change in particle size and morphology.

The samples chosen were Ag (0.01M) at (0.1M HNO_3) in Cyanex 923 (0.01M) and Ag (0.01M) at(0.1M HNO_3) in Cyanex 471X (0.01M).

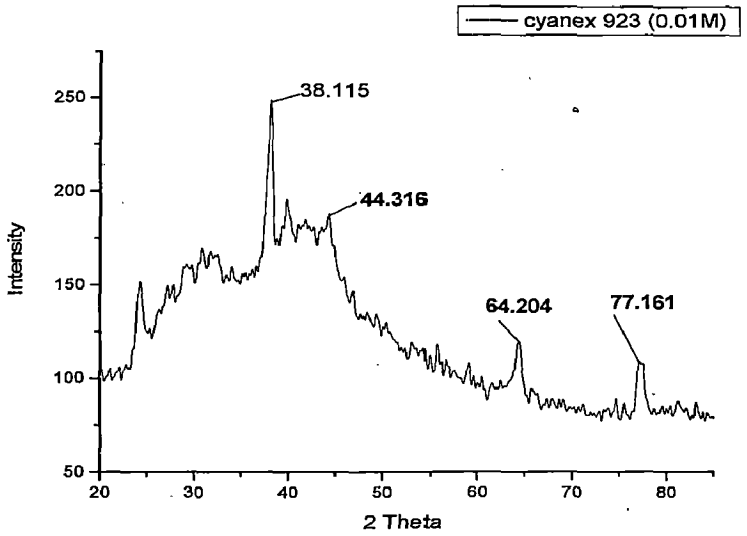

Figure 51. XRD pattern of Silver - Cyanex 923 heated at 600 °C

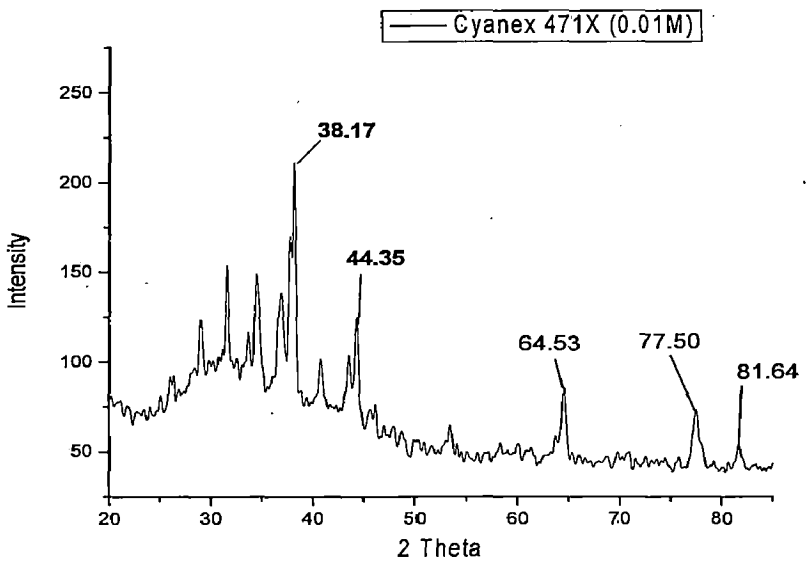

Figure 52. XRD pattern of Silver Cyanex 471X heated at 600 °C

XRD data of heated samples does not show appreciable change in pattern and the particle size calculated by scherrer formula was about 12.6 and 13.2 nanometer for Cyanex 923 and Cyanex 471X respectively.

3.4.3 XRD analysis of Silver - Aliquat 336 sample.

XRD pattern (figure 53-54) show different peaks which were indexed as (111) , (200), (220), (311) and (312). The indexing pattern shows that the Ag nanoparticles have Face centered cubic crystal structure. Few impurity peaks were observed in the spectrum.

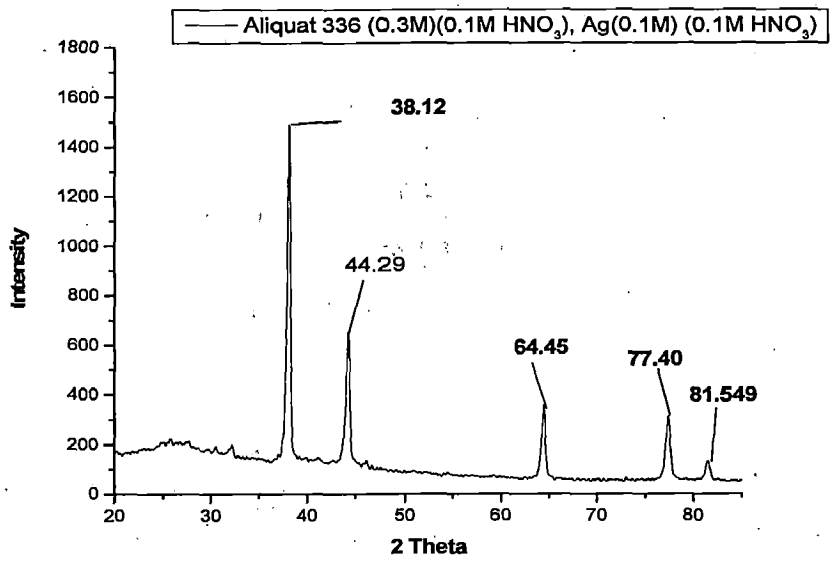

Figure 53 . XRD pattern of Silver - Aliquat 336 Sample.

Table 25 . Particle Size Calculation for Silver - Aliquat 336 nanoparticles by Scherrer Formula.

S.No.	Matrix	β Value in radian	2θ (Degree)	Partical Size (nm)
1	Aliquat 336 (0.3 M) (0.1 M HNO_3) , Ag (0.1M) (O.1M HNO_3)	0.009287	38.12	14.9 nm
2	Aliquat 336 (0.3 M) (0.5 M HNO_3) , Ag (0.1M) (O.1M HNO_3)	0.00999	38.25	13.8 nm

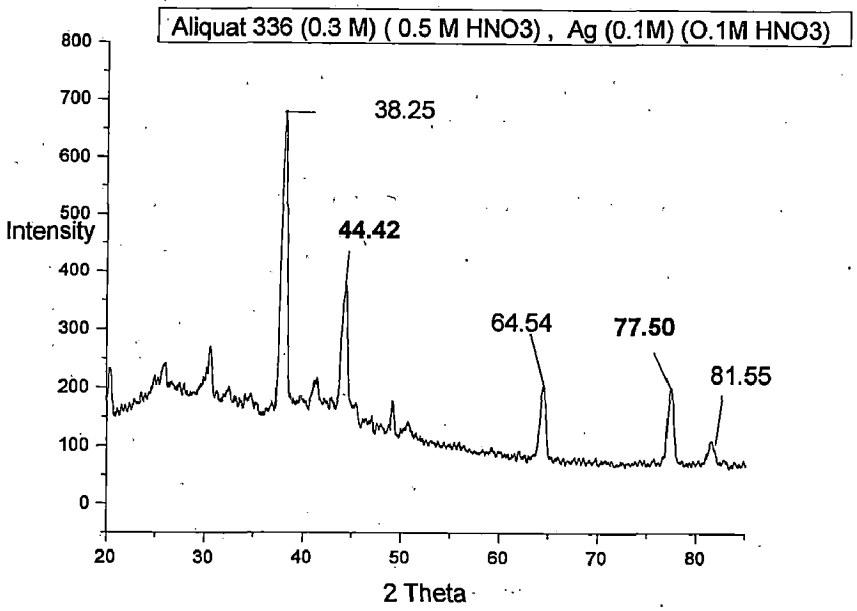

Figure 54. XRD pattern of Silver - Aliquat 336 sample.

XRD patterns of Silver nanoparticle modified under different conditions are almost same. The particle size calculated by scherrer formula also indicates that the variation in the molarity of Cyanex / Aliquat 336, $AgNO_3$ and HNO_3 has no significant effect on the position of peaks and size of the silver nanoparticles.

3.5. Field Emission Scanning Electron Microscopy Analysis (FE-SEM)

The morphology of silver nanoparticle extracted from Cyanex / aliquat 336 is characterized by FE-SEM as shown in figures (55-82). FE-SEM images of the samples show the presence of spherical nanoparticles. Analysis of an individual particle depicts an average diameter of the order of about 100 nm with a size distribution of 100 ± 30 nm. FE-SEM images show high agglomeration in the system but these agglomerates are formed by small nanoparticles of size 10 to 30 nm.

The FE-SEM analysis suggested that variation in concentration of Cyanex, aliquat, Silver nitrate and nitric acid does not change the particle size significantly.

EDAX analysis was carried out at selected locations and at selected points which sohwed the presence of characteristic X-rays of Ag, C,O, P and S.

3.5.1 FE-SEM Analysis of Silver - Cyanex 923 sample.

From the SEM Images the particle size is not determined properly because of high agglomeration in the sample. Particles were found to be spherical in nature with size varying from 50 to 100 nm.

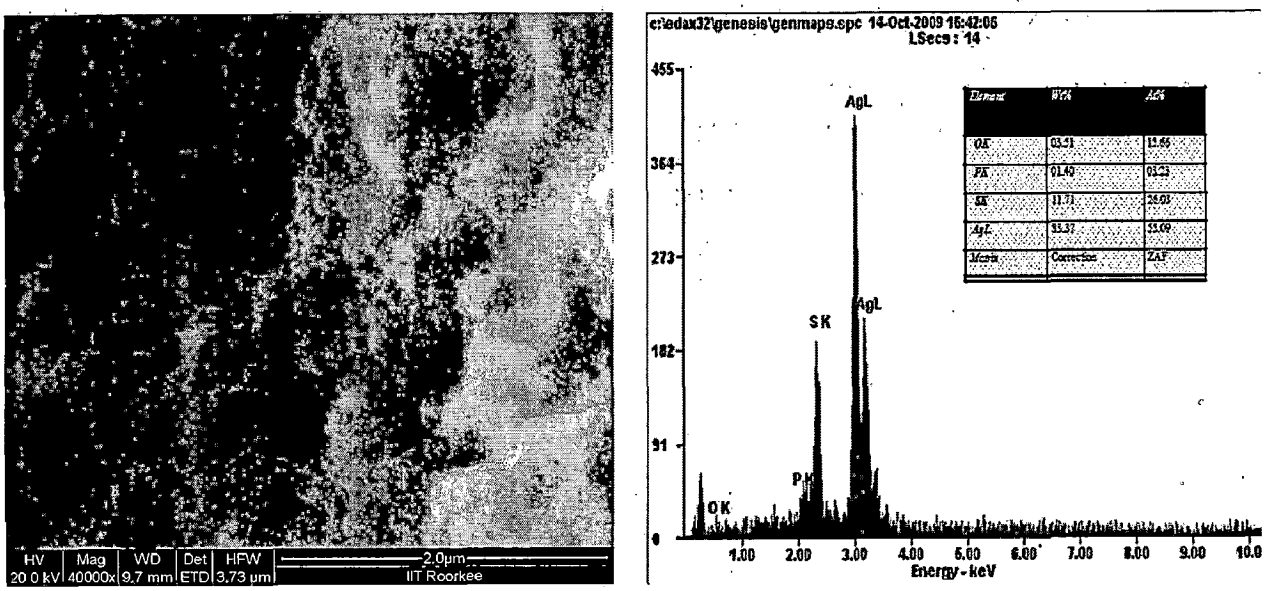

Figure 55. FE-SEM image of silver nanoparticles and Corresponding EDAX

{Cyanex 923 (0.01M) , Ag (0.01M), HNO_3 (O.1M HNO_3)}

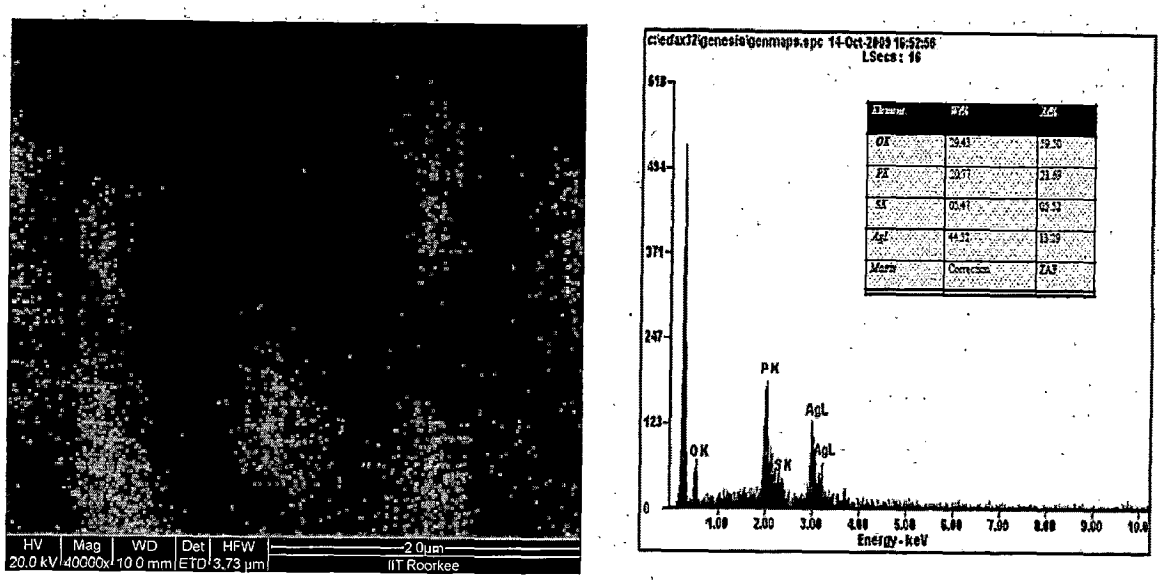

Figure 56. FE-SEM image of silver nanoparticles and Corresponding EDAX

{Cyanex 923 (0.02M) , Ag (0.01M) (O.1M HNO_3)}

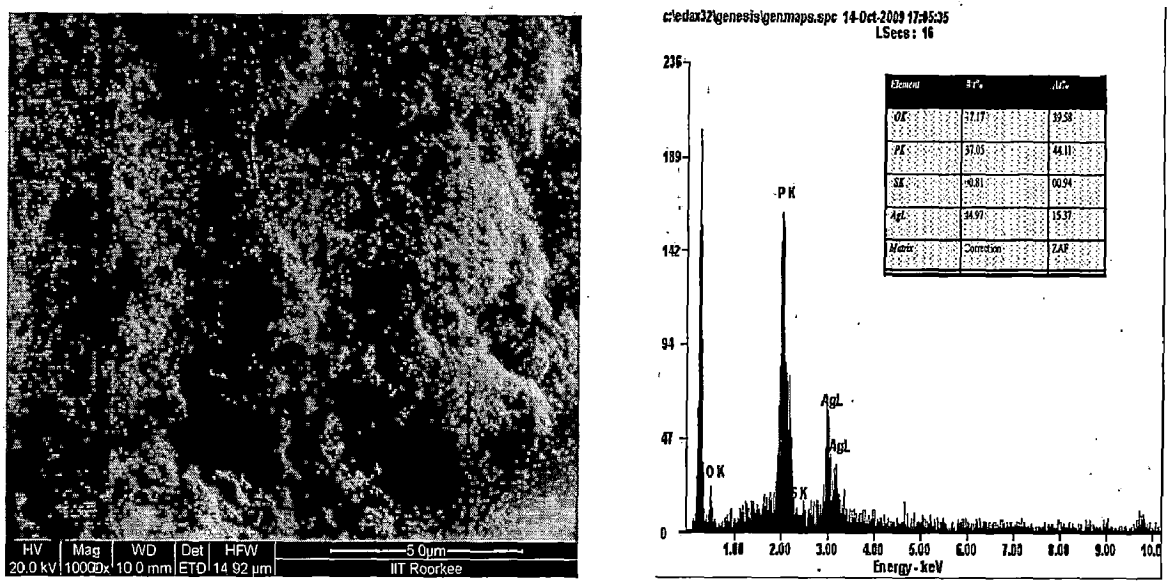

Figure 57. FE- SEM image of silver nanoparticles and Corresponding EDAX

{Cyanex 923 (0.05M) , Ag (0.01M) (O.1M HNO_3)}

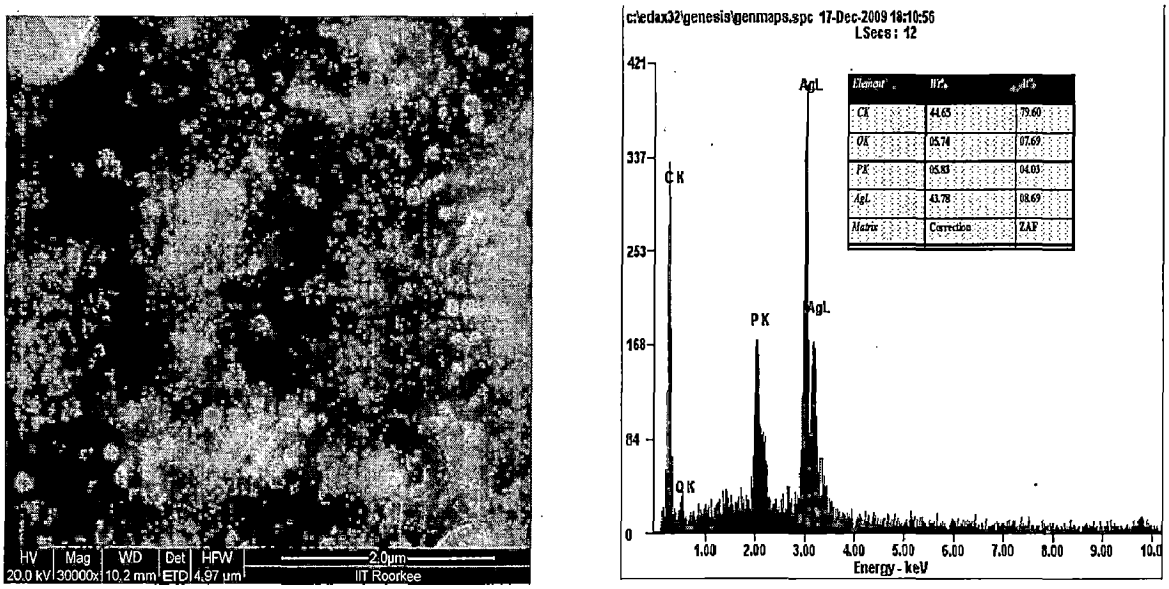

Figure 58. FE-SEM image of silver nanoparticles and Corresponding EDAX

{Cyanex 923 (0.01M) , Ag (0.02M) (O.1M HNO_3)}

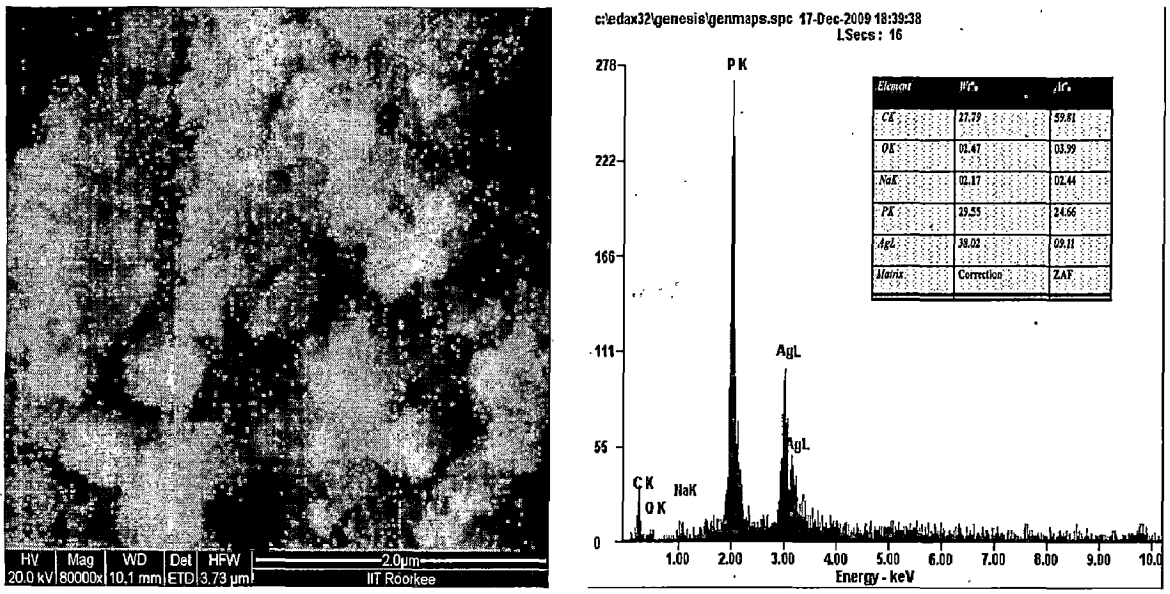

Figure 59. FE-SEM image of silver nanoparticles and Corresponding EDAX

{Cyanex 923 (0.02M) , Ag (0.02M) (O.1M HNO_3)}

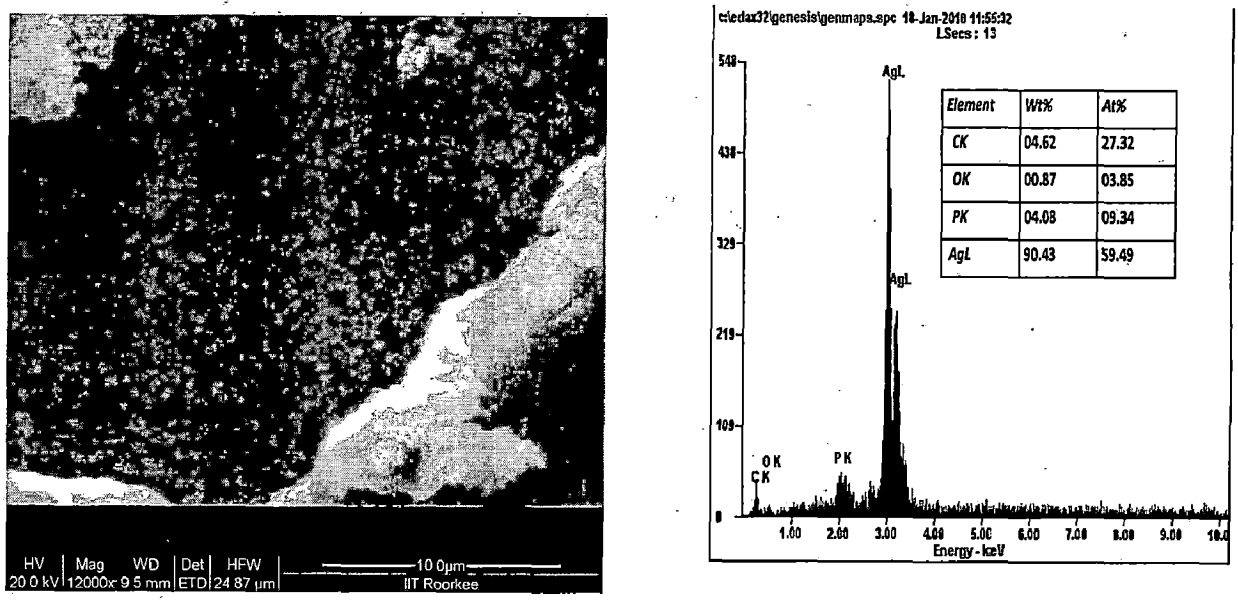

Figure 60. FE- SEM image of silver nanoparticles and Corresponding EDAX

{Cyanex 923 (0.05M) , Ag(0.02M) (O.1M HNO_3)}

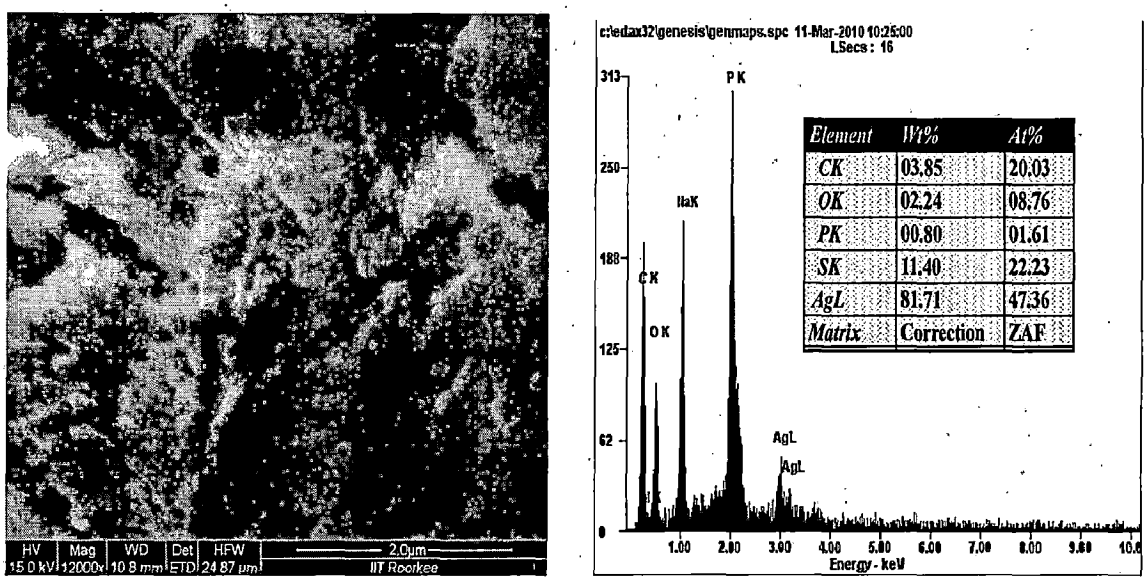

Figure 61. FE-SEM image of silver nanoparticles and Corresponding EDAX

{Cyanex923(0.01M) , Ag(0.01M) (O.5M HNO_3)}

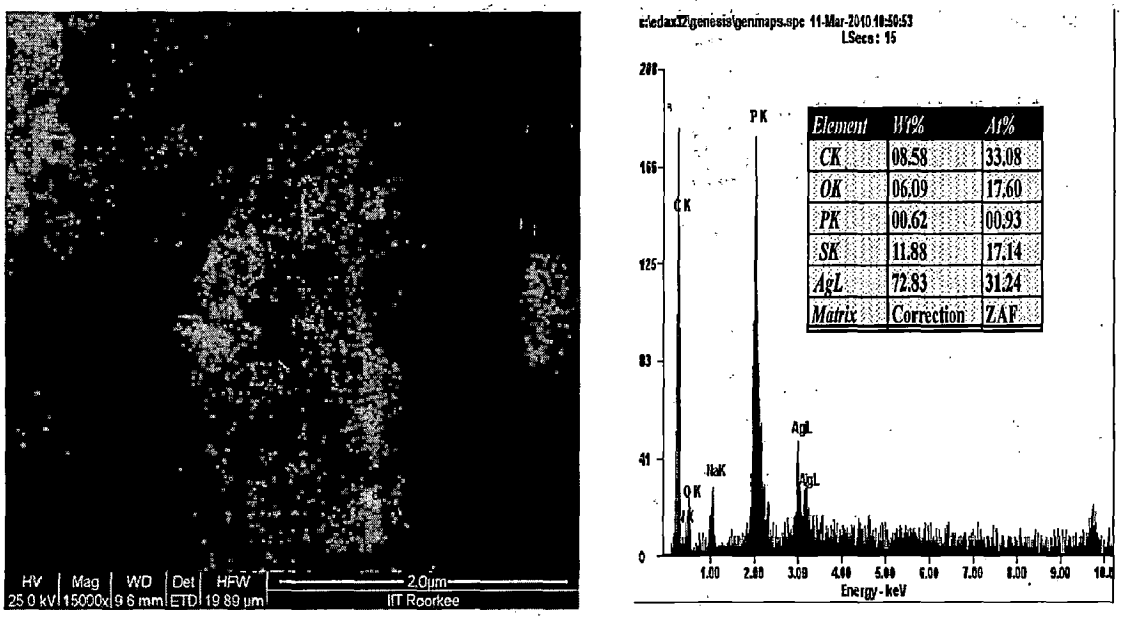

Figure 62 . FE-SEM image of silver nanoparticles and Corresponding EDAX

{Cyanex 923 (0.02M) , Ag (0.01M) (O.5M HNO_3)}.

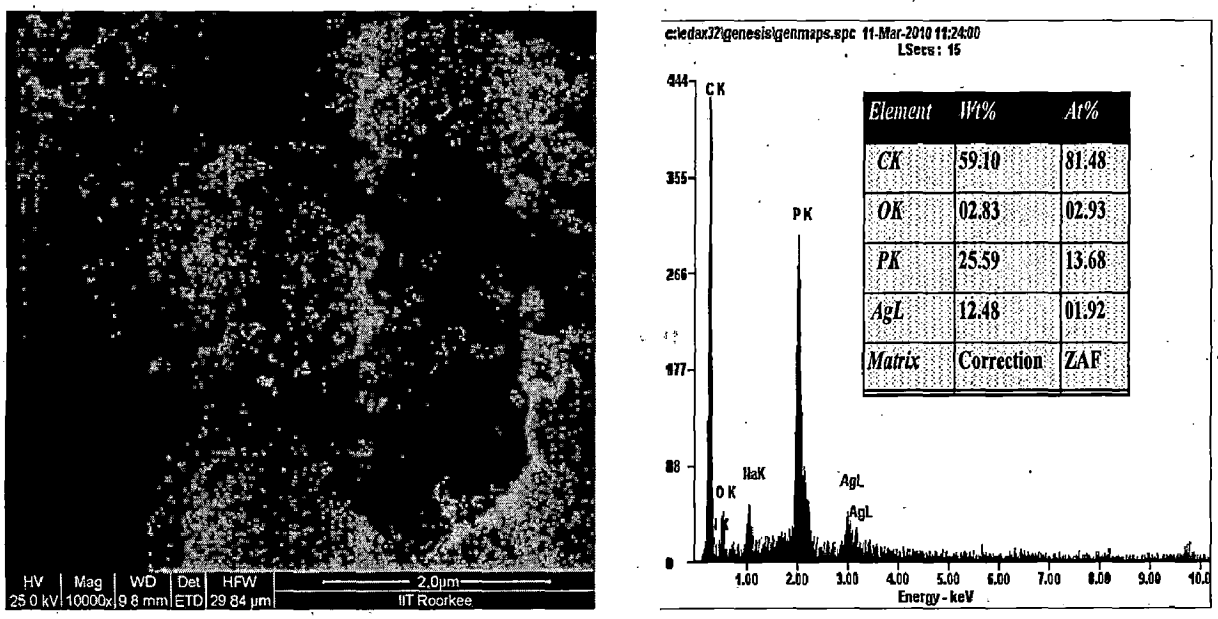

Figure 63. FE-SEM image of silver nanoparticles and Corresponding EDAX

{Cyanex 923 (0.05M) , Ag (0.01M) (O.5M HNO_3)}

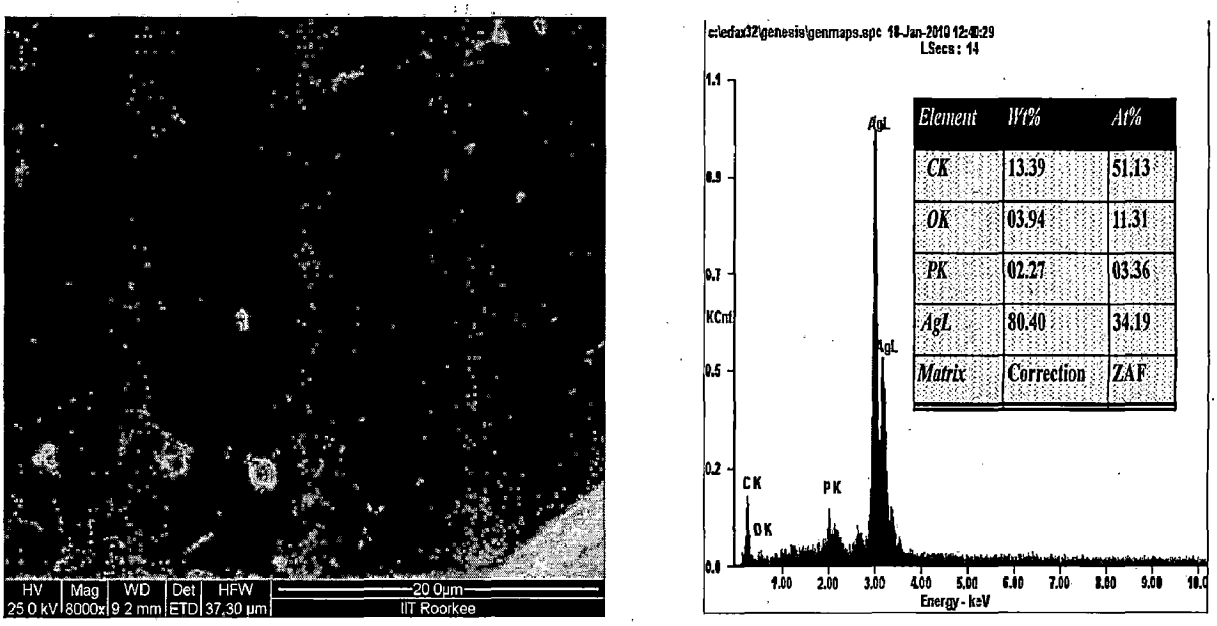

Figure 64. FE-SEM image of silver nanoparticles and Corresponding EDAX

{Cyanex 923 (0.01M) , Ag (0.01M) (1M HNO_3)}

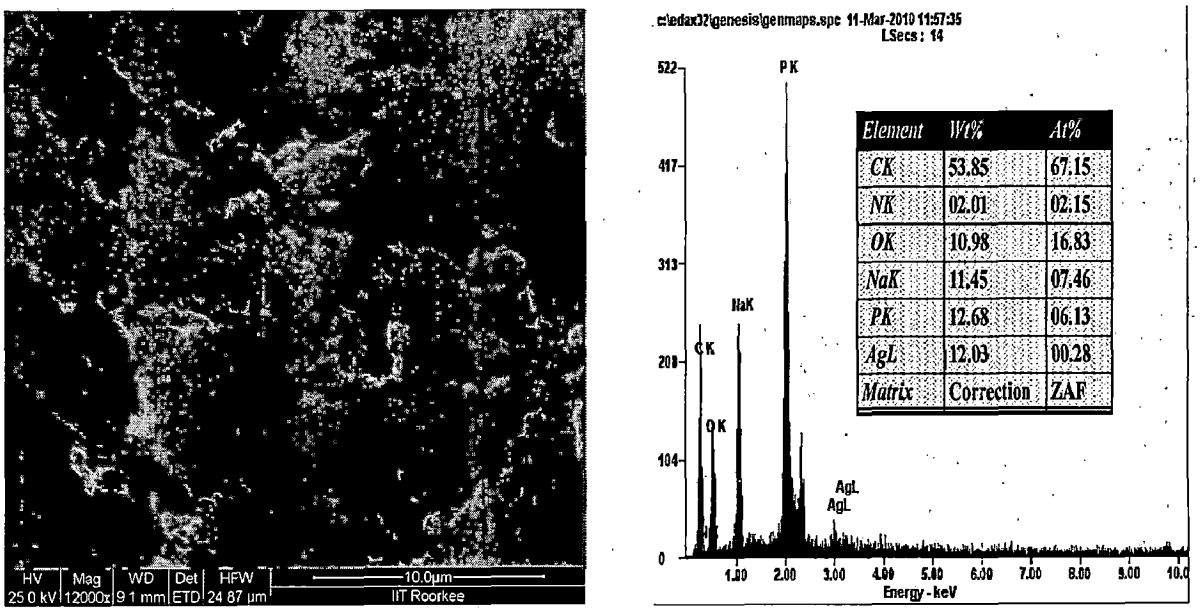

Figure 65. FE-SEM image of silver nanoparticles and Corresponding EDAX

{Cyanex923 (0.02M) , Ag (0.01M) (1M HNO_3)}

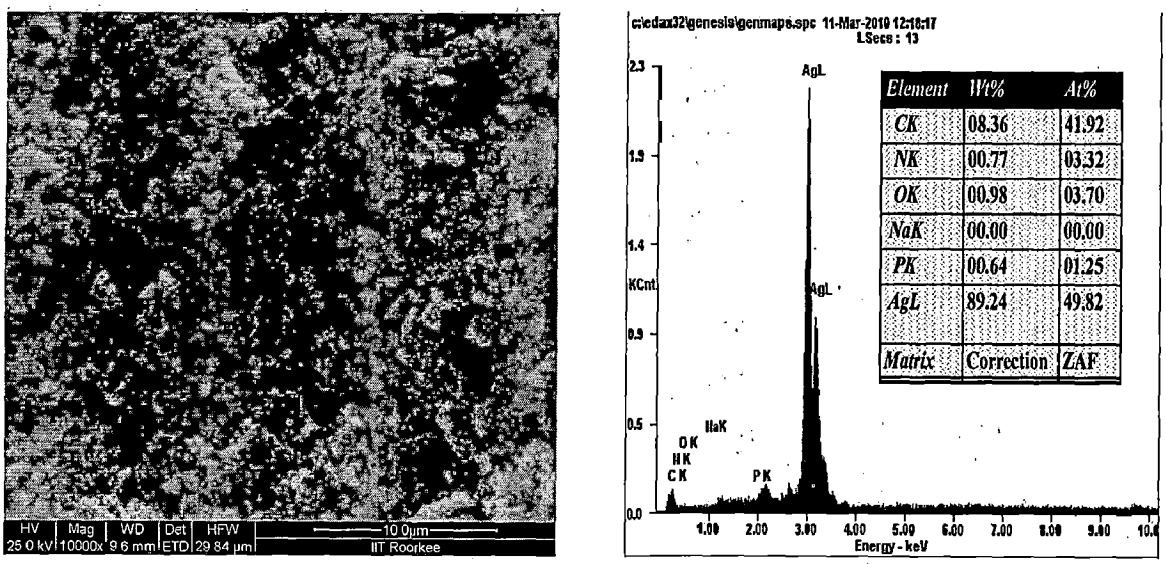

Figure 66. FE-SEM image of silver nanoparticles and Corresponding EDAX

{Cyanex 923 (0.05M) , Ag (0.01M) (1M HNO_3)}

3.5.2 FE-SEM of Silver - Cyanex 471X Sample.

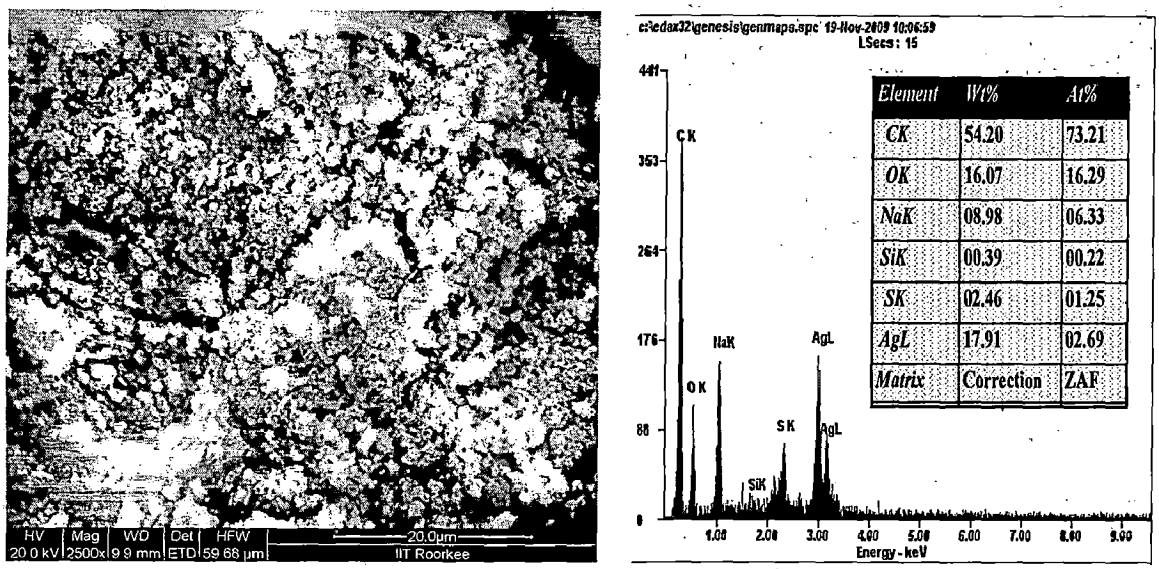

Figure67. FE-SEM image of silver nanoparticles and Corresponding EDAX

{Cyanex 471X (0.01M) , Ag(0.01M) (O.1M HNO_3)}

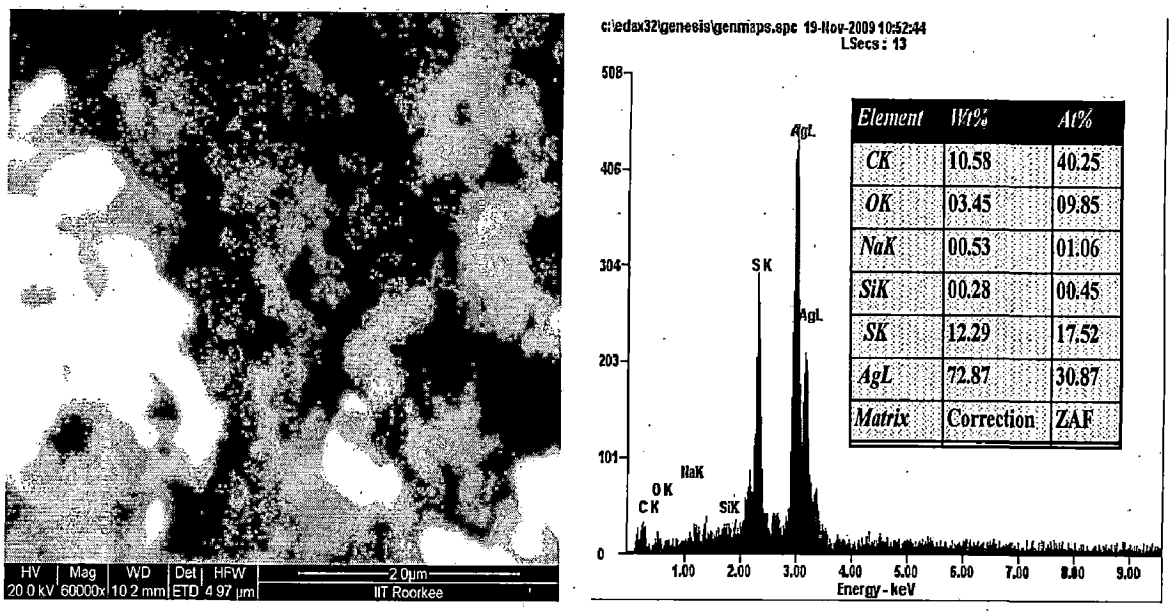

Figure 68. FE-SEM image of silver nanoparticles and Corresponding EDAX

{Cyanex 471X (0.02M), Ag (0.01M) (O.1M HNO_3)}

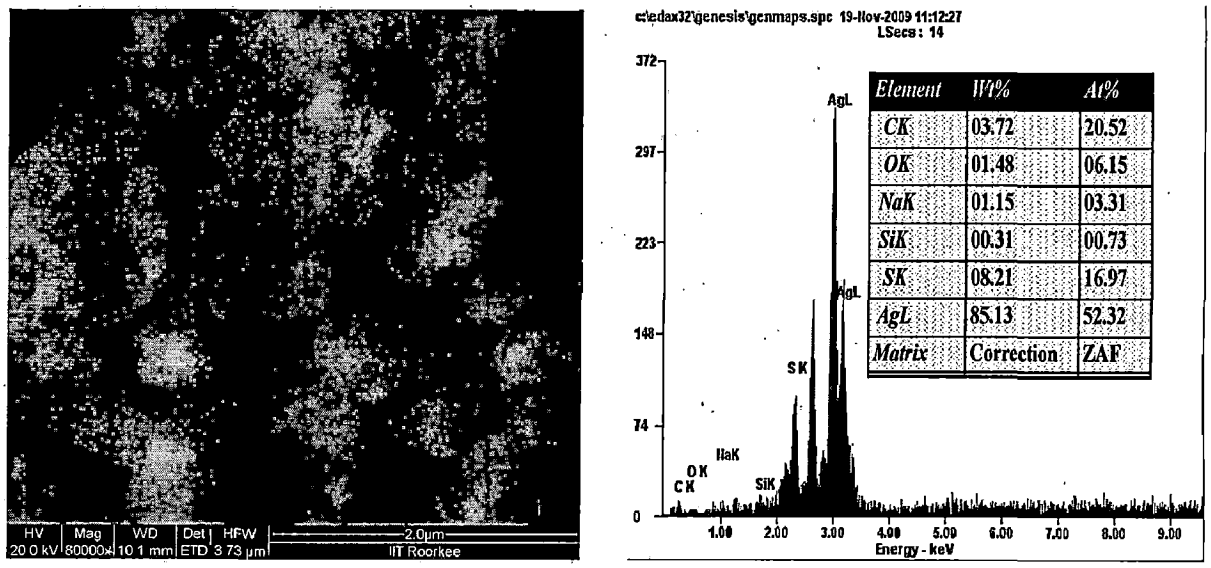

Figure 69. FE-SEM image of silver nanoparticles and Corresponding EDAX

{Cyanex 471X (0.05M) , Ag (0.01M) (O.1M HNO_3)}

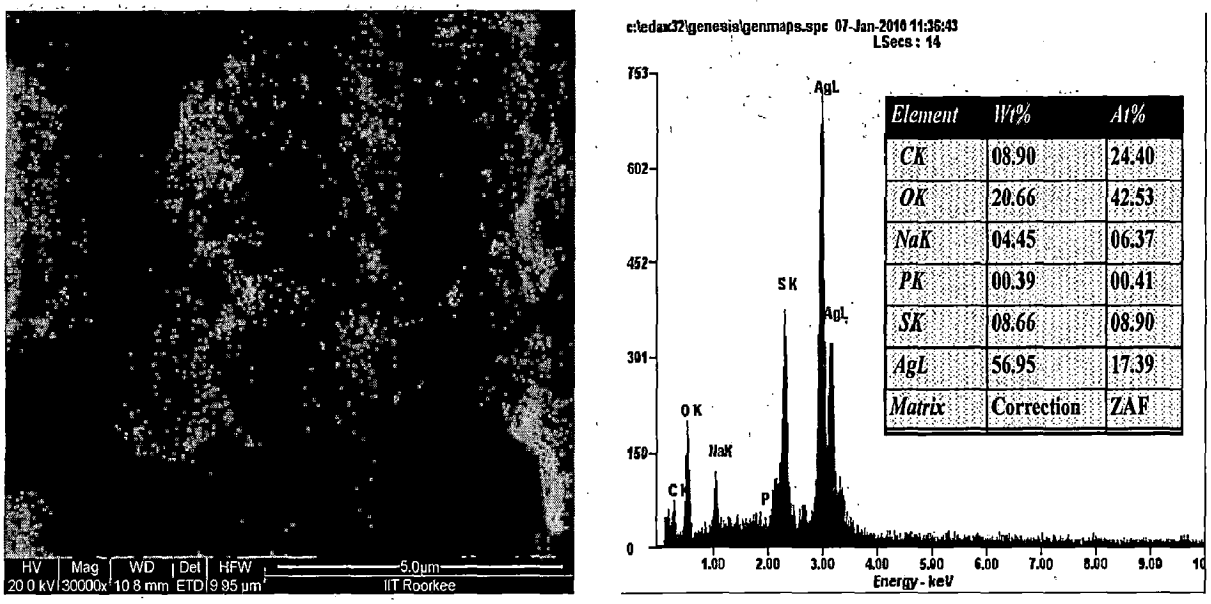

Figure 70. FE-SEM image of silver nanoparticles and Corresponding EDAX

{Cyanex 471X (0.01M), Ag (0.02M) (O.1M HNO_3)}

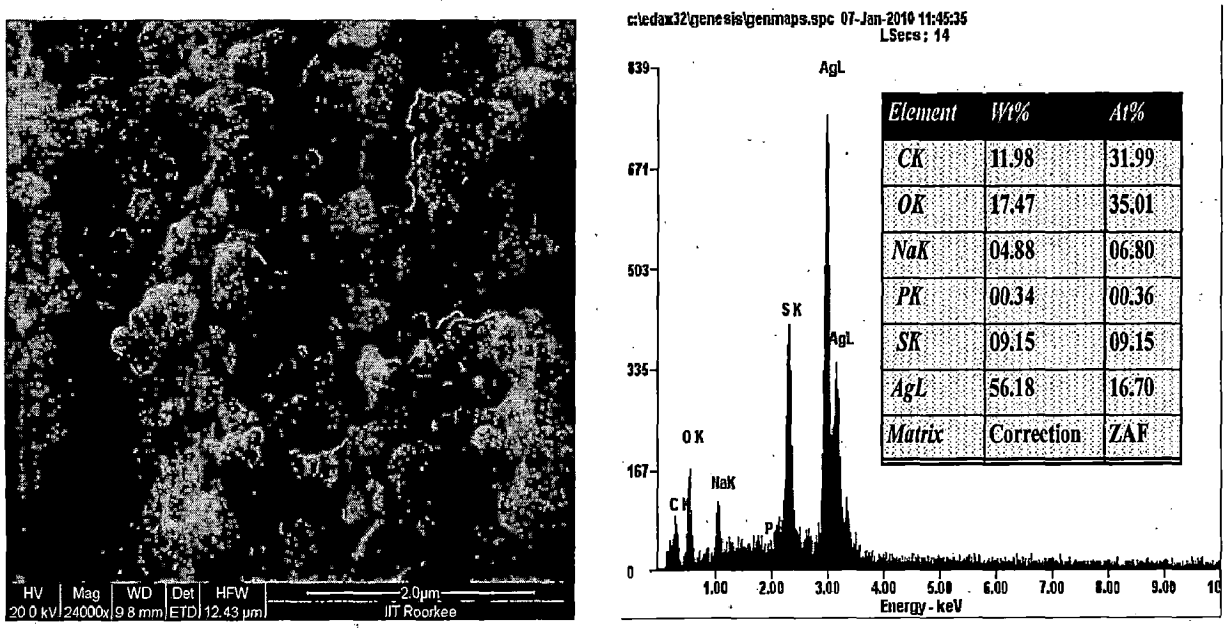

Figure 71. FE-SEM image of silver nanoparticles and Corresponding EDAX

{Cyanex 471X (0.02M), Ag (0.02M) (O.1M HNO_3)}.

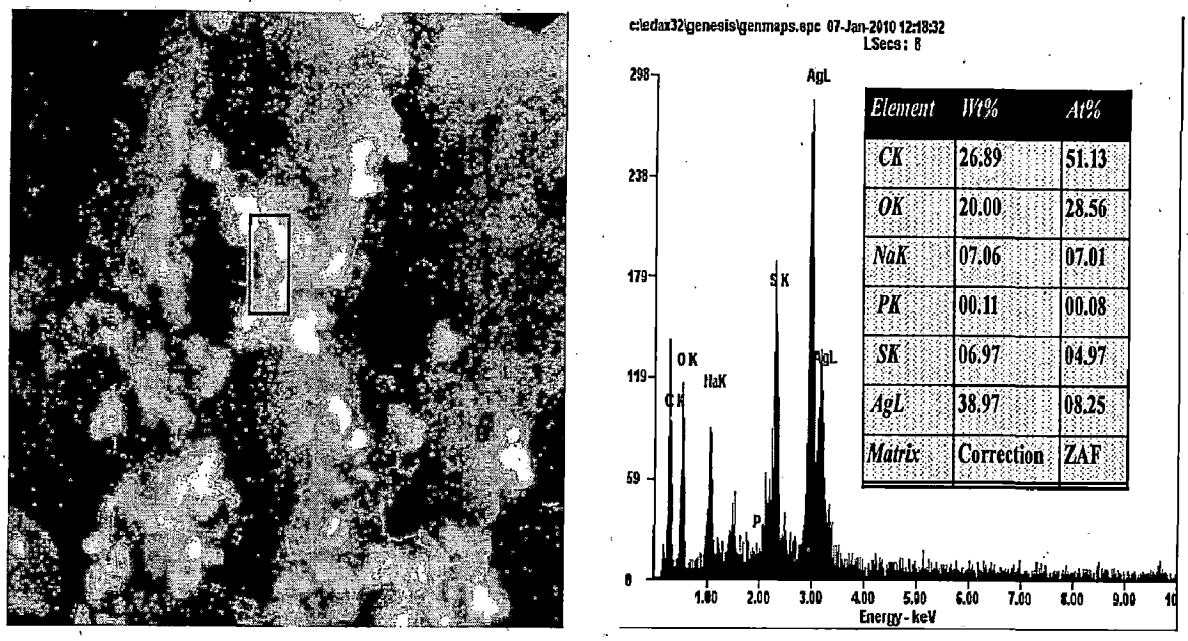

Figure 72. FE-SEM image of silver nanoparticles and Corresponding EDAX

{Cyanex 471X (0.05M), Ag (0.02M) (O.1M HNO_3)}

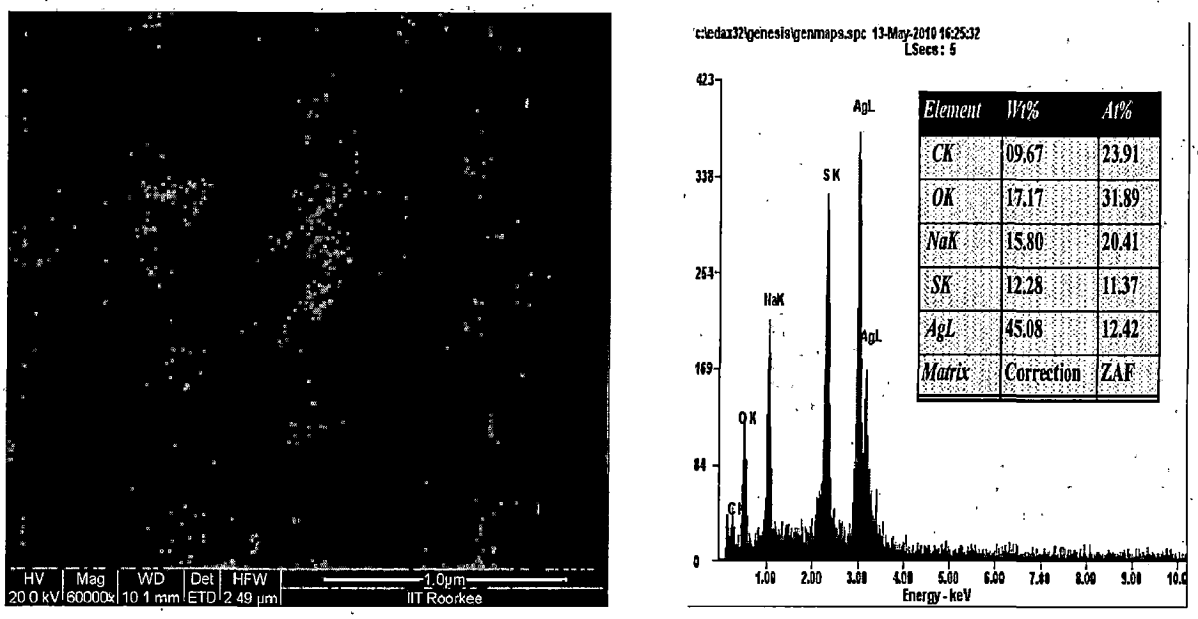

Figure 73. FE-SEM image of silver nanoparticles and Corresponding EDAX

{Cyanex 471X (0.01M), Ag (0.01M) (O.5M HNO_3)}

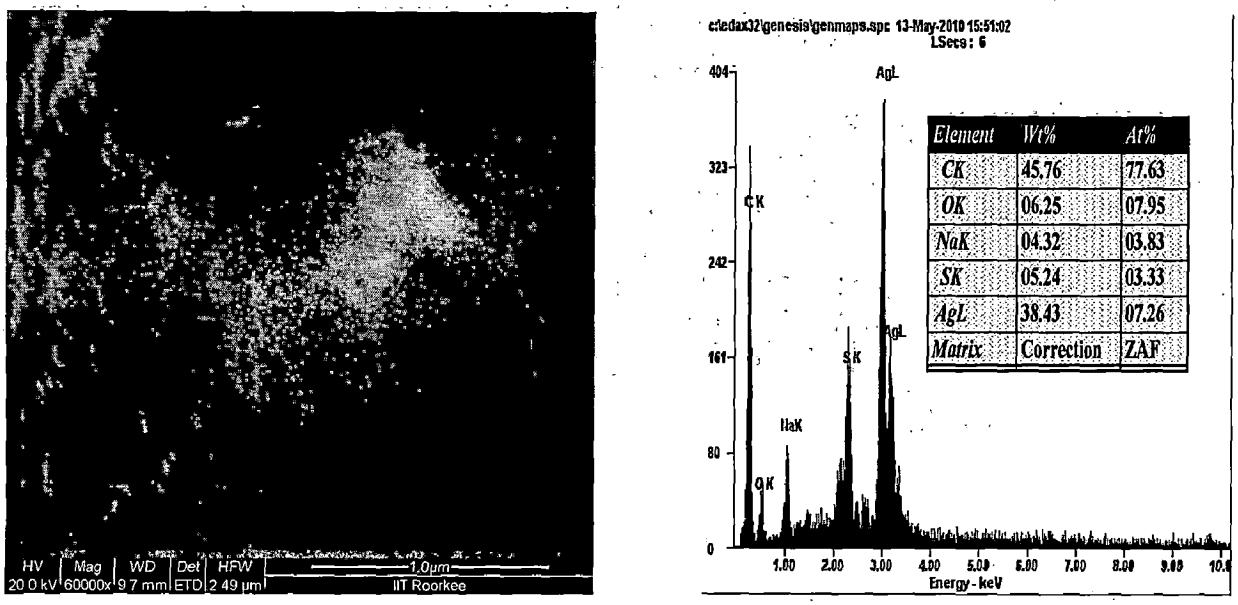

Figure 74. FE-SEM image of silver nanoparticles and Corresponding EDAX

{Cyanex 471X (0.02M), Ag (0.01M) ($O.5M\ HNO_3$)}

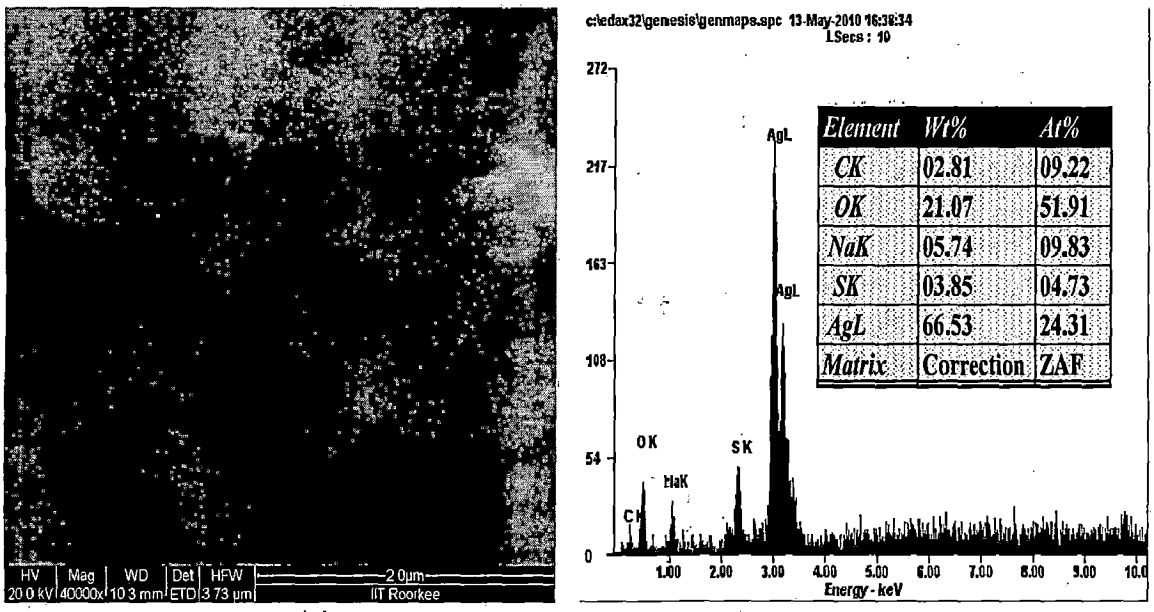

Figure 75. FE-SEM image of silver nanoparticles and Corresponding EDAX

{Cyanex 471X (0.05M) , Ag(0.01M) ($O.5M\ HNO_3$)}

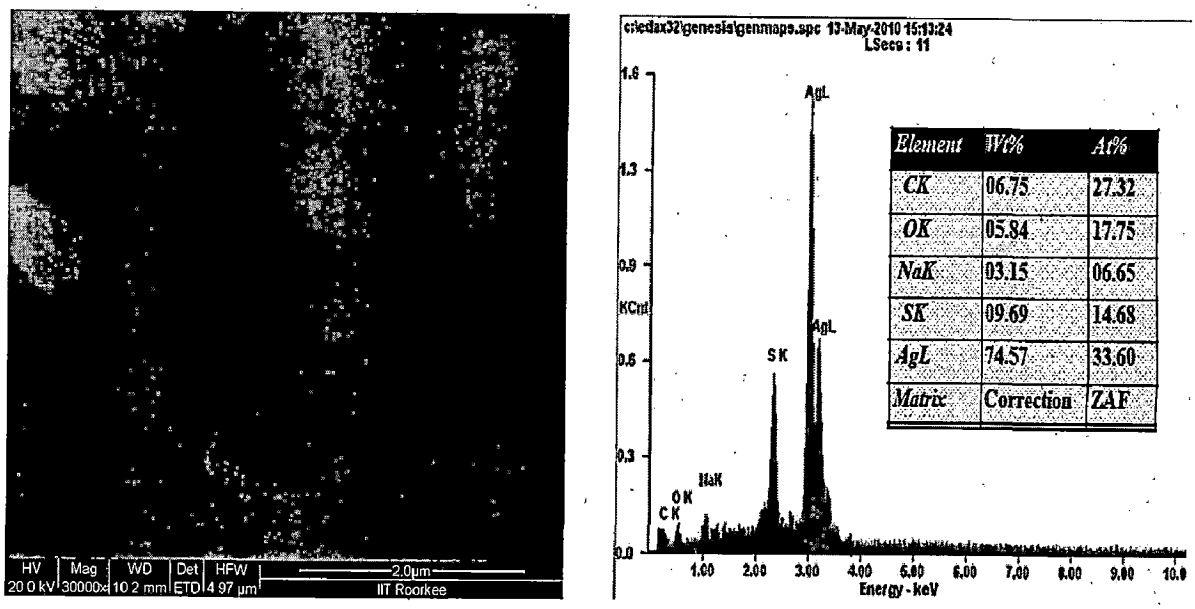

Figure 76. FE-SEM image of silver nanoparticles and Corresponding EDAX

{Cyanex 471X (0.01M), Ag (0.01M) (1 M HNO_3)}

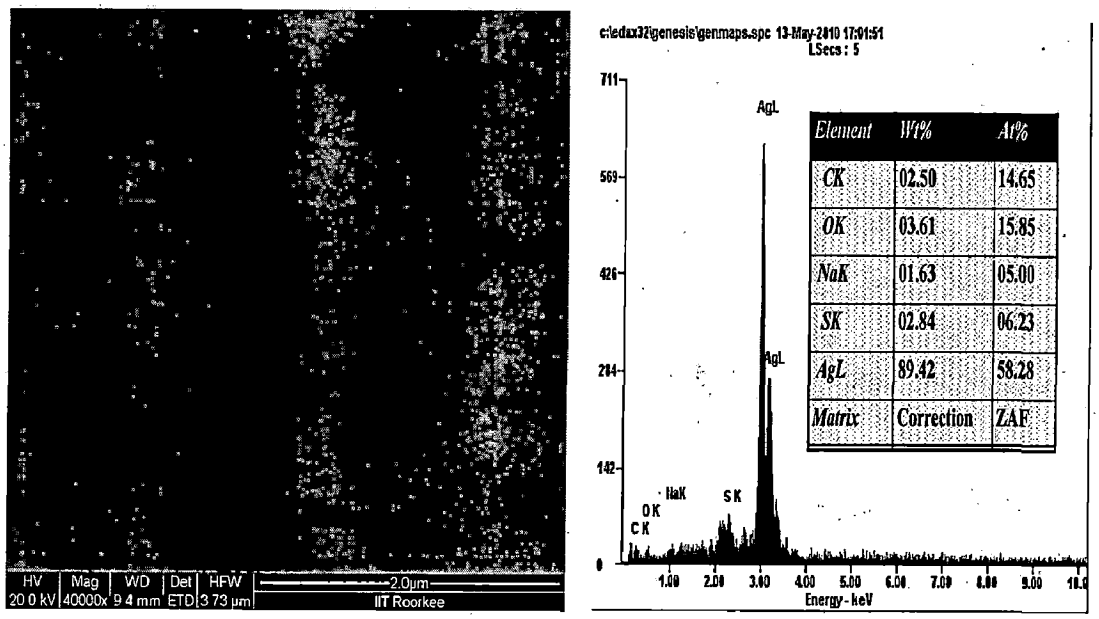

Figure 77. FE-SEM image of silver nanoparticles and Corresponding EDAX

{Cyanex 471X (0.02M) , Ag(0.01M) (1 M HNO_3)}

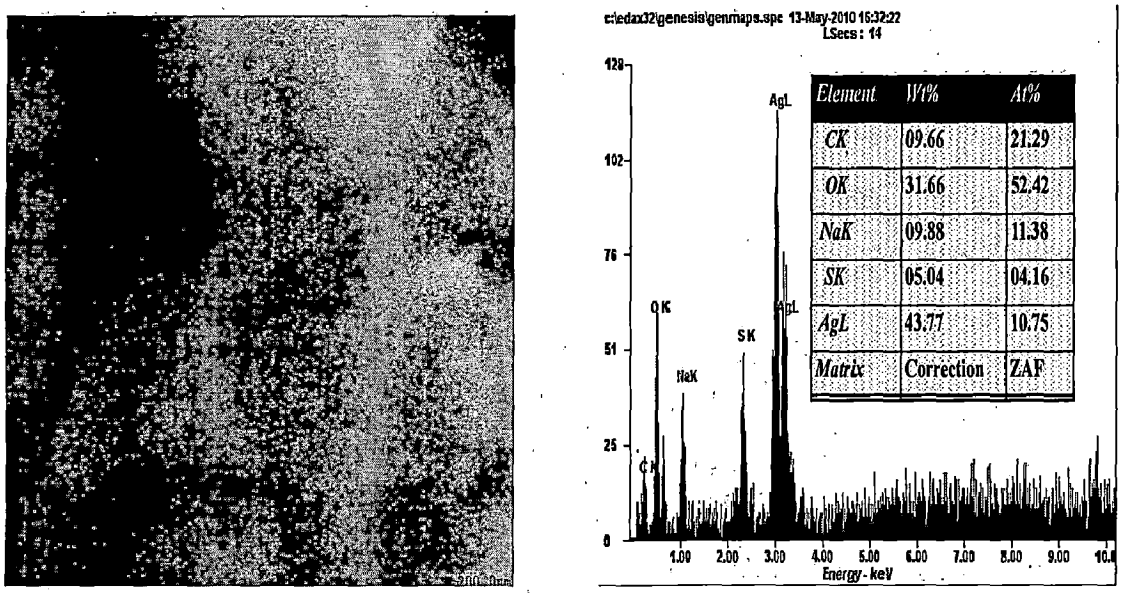

Figure 78. FE-SEM image of silver nanoparticles and Corresponding EDAX of

{Cyanex 471X (0.05M), Ag(0.01M) (1 M HNO_3)}

3.5.3. FE- SEM of Heated samples of Silver- Cyanex 923 / Cyanex 471X

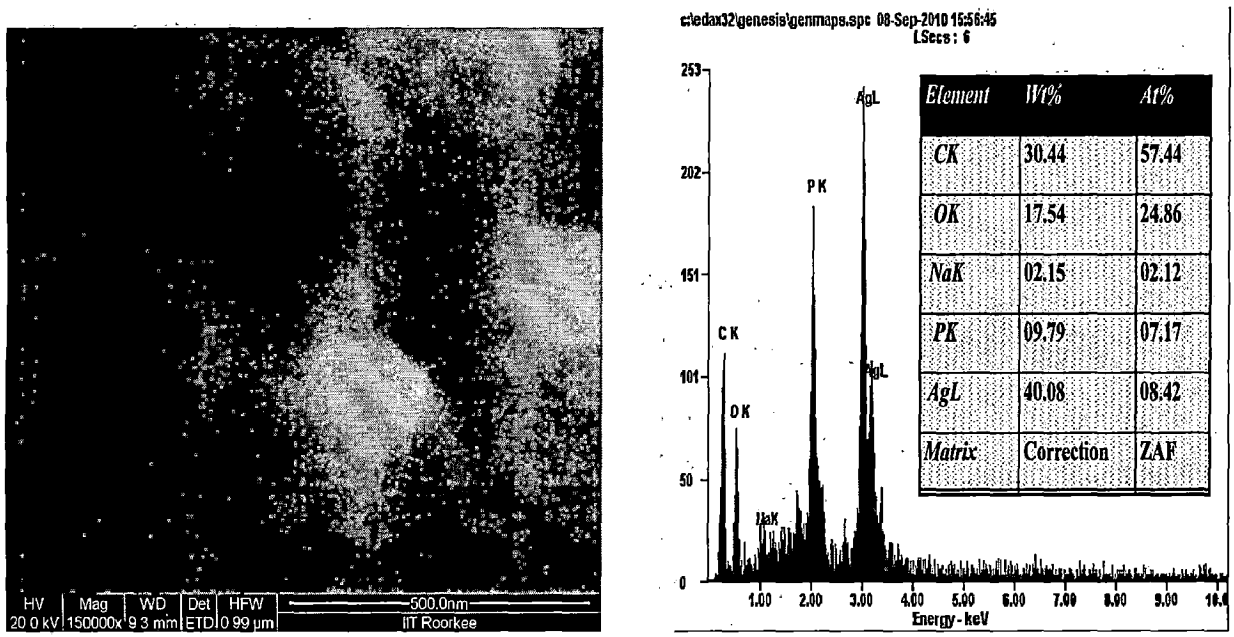

Figure 79. FE-SEM image of silver nanoparticles and Corresponding EDAX

{Cyanex 923 (0.01M) , Ag(0.01M) (0.1 M HNO_3) heated at 600 °C}

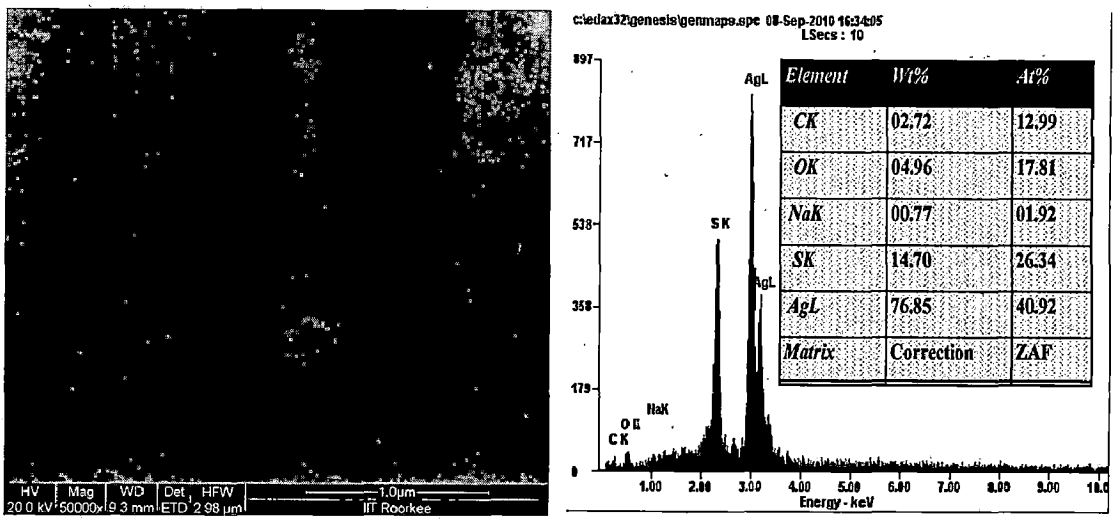

Element	Wt%	At%
CK	02.72	12.99
OK	04.96	17.81
NaK	00.77	01.92
SK	14.70	26.34
AgL	76.85	40.92
Matrix	Correction	ZAF

Figure 80. FE-SEM image of silver nanoparticles and Corresponding EDAX

{Cyanex 471X (0.01M) , Ag(0.01M) (0.1 M HNO_3) heated at 600 °C}

The FE-SEM images of heated samples show that the particle are less agglomerated and have smaller particle size in comparison to non heated samples.

3.5.4. FE-SEM of Silver - Aliquat 336 sample.

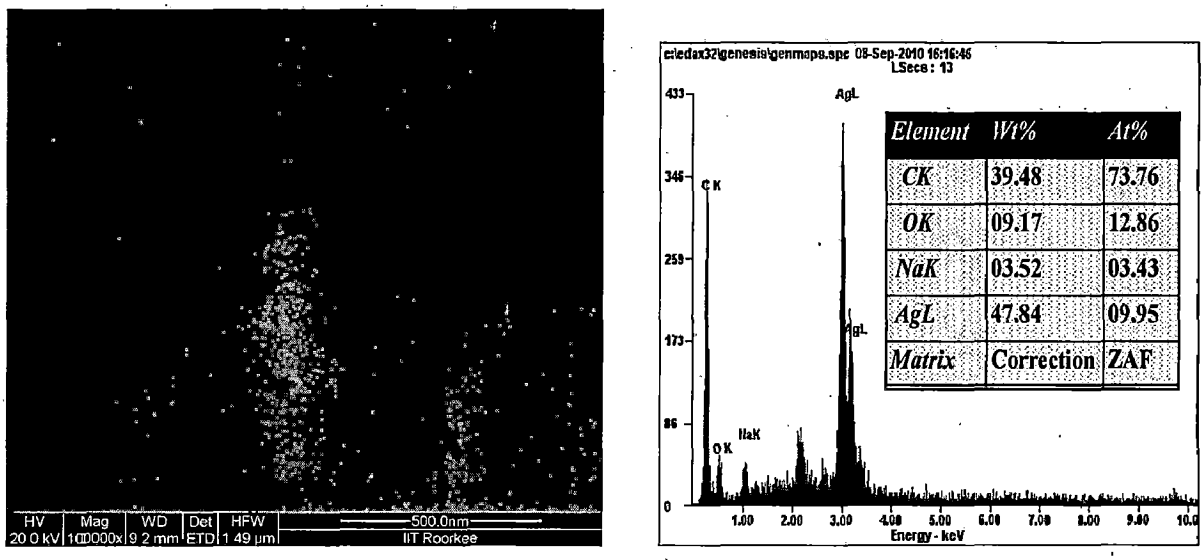

Element	Wt%	At%
CK	39.48	73.76
OK	09.17	12.86
NaK	03.52	03.43
AgL	47.84	09.95
Matrix	Correction	ZAF

Figure 81. FE-SEM image of silver nanoparticles and Corresponding EDAX

Aliquat 336 (0.3 M) (0.1 M HNO_3) , Ag (0.1M) (O.1M HNO_3)

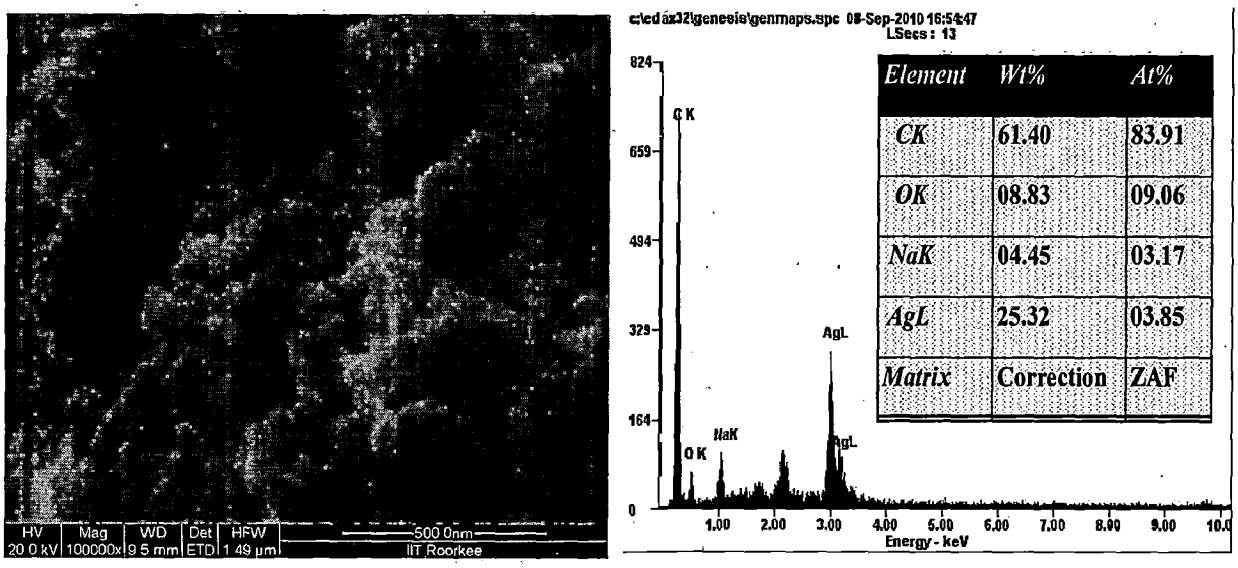

Figure 82. FE-SEM image of silver nanoparticles and Corresponding EDAX

Aliquat 336 (0.3 M) (0.1 M HNO_3), Ag (0.1M) (O.1M HNO_3)

3.6. HR-TEM Analysis of Silver - Aliquat 336 sample.

High-resolution transmission electron micrograph (HR-TEM) analysis was done to get a more accurate estimate of the particle size, to determine their internal structure, and to estimate the thickness of the particle.

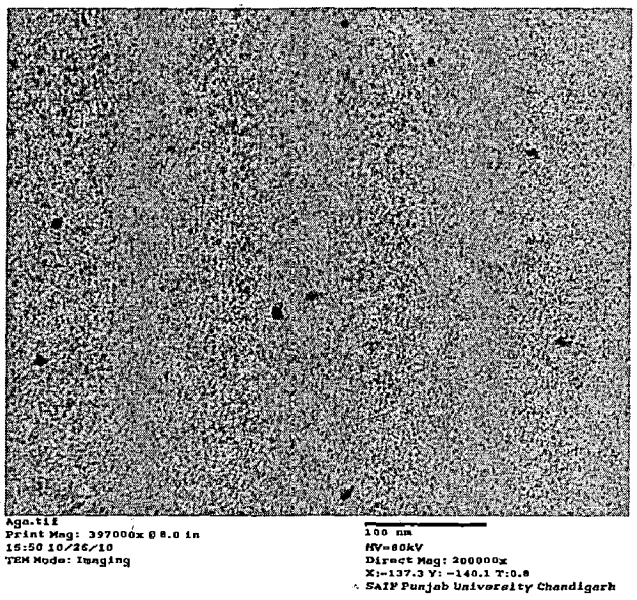

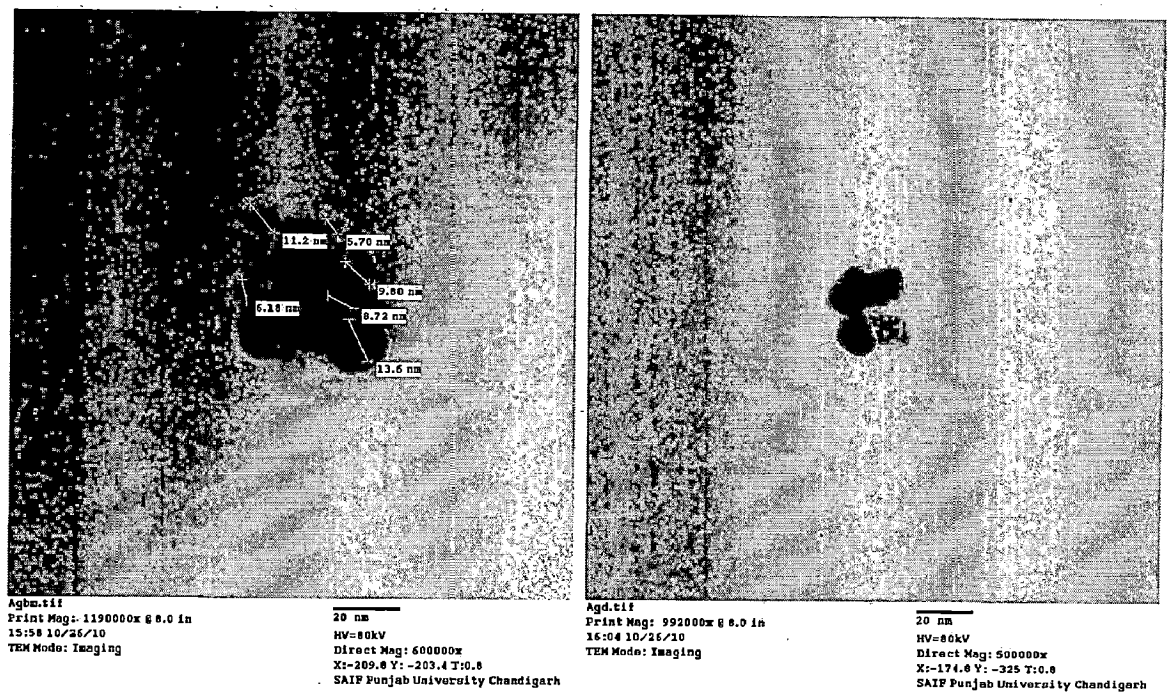

Figure 83. TEM image of Silver- Aliquate 336 Sample.

A 1µl drop of methanol with silver nanoparticles was put on a thin film of amorphous carbon that was supported by a copper grid. The methanol was evaporated leaving only the nanoparticles. TEM analysis was performed on Silver - Aliquat 336 sample. The Silver – Aliquate 336 nanoparticles were mostly spherical, multiple twinned. The diameter of obtained silver nanoparticle was around 6 to 16 nm which also correlates with XRD results. The particles were well dispersed and less aggregated.

CHAPTER 4

Conclusion

Chapter 4

Conclusion

The present work, **"Preparation of silver nanoparticles via solvent extraction route"** was performed by using different extractants such as Cyanex 923, Cyanex 471X and Aliquat 336. The AAS results revealed that in the case of cyanex 923 and cyanex 471X almost all the silver ions were transferred from aqueous phase to organic phase whereas, in the case of Aliquate 336 the percentage extraction was 67% only. Thus on the behalf of AAS results, it can be concluded that cyanex 923 and cyanex 471X are better extractants as compared to Aliquat 336. The FTIR results revealed that the Ag- extractant peak appears around 630 -650 cm^{-1} in the case of cyanex 923, 570-580 cm^{-1} in the case of cyanex 471X and 680 -740 cm^{-1} in the case of Aliquat 336. In all the cases the intensity of peak increases with the increasing concentration of the extractants. The AFM results revealed that the particle size of silver nanoparticles ranged between 9 and 63 nm with cyanex 923 as an extractant but with cyanex 471X the particle size was 4 to 23 nm. Thus with different extractants different size silver nanoparticles are obtained. However, with cyanex 471X small size nanoparticle are obtained as compared to cyanex 923. The XRD results revealed that the peaks observed in the spectra are consistent to Joint Committee on Powder Diffraction Standards (JCPDS-41-1402) data. The FE-SEM results revealed that particle size of silver nanoparticles were in the range of 50 to 100 nm but the particles are not well separated due to agglomeration. TEM analysis of Aliquat 336 shows particle size in the range of 6 to 13 nm.

The above results indicate that silver nanoparticles in the range of 10 -20 nm can be obtained using solvent extraction route (Extraction–Reduction method). The particles were well separated, less agglomerated and pure in the case of Aliquat 336. Results also suggest that these extractants act as both phase transferring agent and particle modifying agent. Some additional studies should have been carried out to optimise conditions for the preparation of well separated, pure, small silver nanoparticles but due to paucity of time further studies could not be carried out.

Due to lack of funds only one sample could be analysed by TEM. Aliquat 336 gave less agglomerated and relatively pure silver nanoparticle thus Silver- Aliquate sample was selected for TEM analysis.

Finally it can be concluded that out of the three extractants studied Aliquate 336 is most suitable for the synthesis of silver nanoparticles.

CHAPTER 5

References

1. C. Buzea, I. Pacheco and K. Robbie, Nanomaterials and Nanoparticles: Sources and Toxicity, *Biointerphases* **(2007),** 4, 17–71.
2. ASTM E 2456 – 06 Standard Terminologies Relating to Nanotechnology.
3. B. D. Fahlman, *Materials Chemistry*, Springer **(2007),** 1, 282–283.
4. http://en.wikipedia.org/wiki/Nanoparticle
5. S. P. Gubin, *Magnetic nanoparticles.* **(2009),** Wiley-VCH. ISBN 3527407901.
6. "Sunscreen". U.S. Food and Drug Administration. http://www.fda.gov/Radiation-EmittingProducts/RadiationEmittingProductsandProcedures/Tanning/ucm116445.html.
7. Best Practices Guide to Synthetic Nanoparticle Risk Management Report R-599, http://*www.irsst.qc.ca/files/documents/PubIRSST/**R-599**.pdf.*
8. A.J. Hoffman, G. Mills, H. Yee and M.R. Hoffman, Q-sized cadmium sulfide: synthesis, characterization, and efficiency of photo initiation of polymerization of several vinylic monomers, *Journal of Physical Chemistry* **(1992),** 96, 5546-5552.
9. V.L. Colvin, M.C. Schlamp and A.P. Alivisatos, Light-emitting diodes made from cadmium selenide nanocrystals and a semiconducting polymer, *Nature* **(1994),** 370, 354-357.
10. L.L. Beecroft and C.K. Ober, *Chemistry of Materials* **(1997),** 9, 1302-1317.
11. N. Toshima and T. Yonezawa, *New Journal of Chemistry* **(1998),** 22, 1179-1201.
12. H.S. Kim, J.H. Ryu, B. Jose, B.G. Lee, B.S. Ahn and Y.S. Kang, Langmuir **(2001),** 17, 5817-5820.
13. P. S. Rawson, *Ceramics.* **(1984)** University of Pennsylvania Press. ISBN 0812211561.
14. M. Faraday, Experimental relations of gold (and other metals) to light. *Philosophical Transaction of the Royal Society London* **(1857),** 147, 145–181.

15. G.T Beilby, The Effects of Heat and of Solvents on Thin Films of Metal. *Proceeding of Royal Society A* **(1903),** 72, 226-235.

16. T. Turner, Transparent Silver and Other Metallic Films. *Proceeding of Royal Society London A* **(1908),** 81 ,301-310.

17. X. Chen and H.J. Schluesener, Nanosilver: a nanoproduct in medical applications. *Toxicology Letters* **(2008),** 176, 1-12.

18. T.G. Dellwig, R. H. Unterhalt and H.J. Freund, Bridging the Pressure and Materials Gaps: High Pressure Sum Frequency Generation Study on Supported Pd Nanoparticles. *Physical Review Letter* **(2000),** 85, 776-779.

19. S. Stoeva, K.J. Klabunde, C.M. Sorensen and I Dragieva, Gram-Scale Synthesis of Monodisperse Gold Colloids by the Solvated Metal Atom Dispersion Method and Digestive Ripening and Their Organization into Two- and Three-Dimensional Structures. *Journal of the American Chemical Society* **(2002),** 124 , 2305-2311.

20. P. Smejkal, K. Siskova, B. Vlckova, J. Pfleger, I. Sloufova, M. Slouf and P. Mojzes, Characterization and surface-enhanced Raman spectral probing of silver hydrosols prepared by two-wavelength laser ablation and fragmentation. *Spectrochimica Acta A: Molecular and Biomolecular Spectroscopy* **(2003),** 2321-2329.

21. P.V. Krassimir, G.E. Zeger and A. Van Blaaderen, Synthesis and characterization of Large Colloidal Silver Particles. *Langmuir* **(2003),** 19, 1384-1389.

22. U. Kreibig and M. Vollmer, Optical Properties of Metal Clusters, *Materials Science*, **(1995),** 25 , 50-58.

23. Jr. D. D. Evanoff and G. Chumanov, *Journal of Physical Chemistry B* **(2004),** 108, 13957 – 13962.

24. http://www.springer.com/materials/book/978-1-4020-6119-6.

33 S. Lien-Chung Hsu, and R. Tarng Wu, Synthesis of contamination-free silver nanoparticle suspensions for micro-interconnects, *Materials Letters* **(2007),** *61*, 3719–3722.

34 A. Y. Olenin, A.Y. Krutyakov, A. A. Kudrinskii and G. V. Lisichkin, Formation of Surface Layers on Silver Nanoparticles in Aqueous and Water–Organic Media, *Colloid Journal* **(2008),** *70*, 71–76.

35 D. Seo , W. Yoon , S. Park , J. Kimb and J. Kima,, The preparation of hydrophobic silver nanoparticles via solvent exchange method , *Colloids and Surfaces A: Physicochemical and Engineering Aspects* **(2008),** *313*,158–161.

36 S. Navaladian, B. Viswanathan and T. K. Varadarajan, Microwave assisted rapid synthesis of anisotropic Ag nanoparticle by solid state transformation, Nanotechnology **(2008),** 19, 7-14.

37 A. Sarkar, R. Chadha, N. Biswas, T. Mukherjee and S. Kapoor, Phase-transfer and film formation of silver nanoparticles , *Journal of Colloid and Interface Science* **(2009),** *332*, 224–230.

38 F. Guo , L. Hongfei, Z. Zhang , S. Meng and L. Deqian , Synthesis of REF_3 (RE = Nd, Tb) nanoparticles via a solvent extraction route, *Materials Research Bulletin* **(2009),** *44*, 1565–1568.

39 C.W. Shen and T. Yu Size-fractionation of silver nanoparticles using ion-pair extraction in a counter-current chromatograph, *Journal of Chromatography A* **(2009),** *1216*, 5962–5967.